2011

Sub-Cooled Pool Boiling Enhancement with Nanofluids

Elliott Charles Rice
University of South Florida, e-rice@hotmail.com

Sub-Cooled Pool Boiling Enhancement with Nanofluids

by

Elliott Charles Rice

A thesis submitted in partial fulfillment
of the requirements for the degree of
Master of Science in Mechanical Engineering
Department of Mechanical Engineering
College of Engineering
University of South Florida

Major Professor: Frank Pyrtle III, Ph.D.
Muhammad M. Rahman, Ph.D.
Craig Lusk, Ph.D.

Date of Approval:
March 24, 2011

Keywords: heat flux, heat transfer coefficient, nanoparticles, phase change, comsol

Dedication

I would like to dedicate this thesis to my sister, Audrey. Thanks for always believing in me and showing me what it means to strive for academic excellence. Although a master's thesis cannot compare to a dissertation, I hope that while finishing your Ph.D. that this thesis somehow inspires you to complete your goal. I have no doubt that you will be successful in your studies. Love your little brother, or "monster" or "mickey dee's" or "numb-nut" or whatever other names you feel like calling me today.

Acknowledgements

First and foremost I would like to thank the God for His mercy and grace. This thesis is proof of Your everlasting Word, "Share you plans with the LORD and you will succeed." Proverbs 16:3 Contemporary English Version.

I would like to thank my parents Ella and Jerome Rice for always supporting their favorite "professional" student. Thank you for all your help and encouragement over the years. I would like to thank my research advisor Dr. Frank Pyrtle III for allowing me to join his research group and guiding me along the way to completion of this thesis. Also, thank you for allowing me work with you during the *Research Experience for Undergraduates* program. I would also like to thank Dr. Rahman and Dr. Lusk for being a part of my committee and supporting me during my time at USF. Thank you, Dr. Hess for allowing me to use your profilometer. Thank you times 10 to Bernard Batson for everything. Also a very special thank you to NSF Bridge to the Doctorate Florida Georgia Louis Stokes Alliance for Minority Participation (FGLSAMP) project award HRD #0217675. Thank you, Anca Mirsu-Paun, Ph.D. for listening to me. Thank you, Catherine Burton for all your help. I would like to thank my lab-mates. Thank you Ardit Agastra, for motivating me to finish and remaining calm at all times. Thank you John Shelton, for taking me under your wing, writing a million LabView programs for me, staying up late with me in the lab to ensure I finish and for saving my butt all of the time. Thank you Christian Martinez, for having the same "always be the best" drive as I do and helping me analyze my results. Well Christian, it looks like we are both finally 21!

Table of Contents

List of Tables

List of Figures

List of Symbols

Symbol	Meaning	Units
q	heat transfer rate	W
q''	heat flux	W/m^2
k	thermal conductivity	W/m K
A	cross sectional area normal to heat flux	m^2
T	temperature	^oC or Kelvin
T_∞	temperature at convective boundary	^oC or Kelvin
T_{sat}	saturation temperature	^oC or Kelvin
$\Delta T_{A..B}$	temperature difference between points A and B	^oC or Kelvin
ΔT_e	excess temperature	^oC or Kelvin
R_{th}	thermal resistance	$^oC/W$
$L_{A..B}$	distance between points A and B	m
h	convective heat transfer coefficient	W/m^2 K
D	diameter	m
Φ	diameter of copper hat	m
U	uncertainty associated with measurement	varies

Abstract

Phase-change heat transfer is an important process used in many engineering thermal designs. Boiling is an important phase change phenomena as it is a common heat transfer process in many thermal systems. Phase change processes are critical to thermodynamic cycles as most closed loop systems have an evaporator, in which the phase change process occurs. There are many applications/processes in which engineers employ the advantages of boiling heat transfer, as they seek to improve heat transfer performance. Recent research efforts have experimentally shown that nanofluids can have significantly better heat transfer properties than those of the pure base fluids, such as water.

The objective of this study is to improve the boiling curve of de-ionized water by adding aluminum oxide nanoparticles in 0.1%, 0.2%, 0.3% and 0.4% wt concentrations in a sub-cooled pool boiling apparatus. Enhancement to the boiling curve can be quantified in two ways: (i) the similar heat fluxes of de-ionized water at smaller excess temperature, indicating similar quantity of heat removal at lower temperatures and (ii) greater heat fluxes than de-ionized water at similar excess temperatures indicating better heat transfer at similar excess temperatures. In the same fashion, the secondary objective is to increase the convective heat transfer coefficient due to boiling by adding different concentrations of aluminum oxide nanoparticles.

Chapter 1

Introduction

1.1 Background and Motivation

Phase change heat transfer is a very effective process of removing thermal energy from a body. Processes that involve condensation and evaporation are extensively investigated phase change heat transfer processes. When a fluid in a gaseous state temperature falls below the saturation temperature, which itself is pressure dependent, the fluid condenses and returns to the liquid state. Inversely, in an evaporative process a fluid, in the liquid phase, is raised to a temperature above its saturation temperature and changes to the vapor phase. Evaporation occurs at the solid-liquid interface whereas a phase change that is driven by heat transfer from the solid surface to the liquid interface is termed boiling. This physical phenomenon can be explained by Newton's Law of Cooling

$$q_s'' = h\left(T_s - T_{sat}\right) = h\Delta T_e \tag{1}$$

where q_s'' is the heat flux (W/m^2), h is the heat transfer coefficient (W/m^2 * K) and T is the temperature (K). ΔT_e is also known as the excess temperature.

Boiling is classified as a convective heat transfer process since fluid motion occurs and consequently is a driving factor for heat transfer. However, boiling is unique as compared to other convective heat transfer processes because a phase change occurs

during the process. The phase change allows heat to be transferred to and from the surface without significantly affecting the fluid temperature, which can lead to large heat transfer rates that correspond to small temperature differences. The latter also leads to large heat transfer coefficients as compared to typical single phase convection processes.

Partially due to large heat transfer coefficients, which allow for greater heat transfer, boiling is a highly desirable heat transfer process to engineers. For example, boiling is critical to thermodynamic systems. In a power cycle, the working fluid is usually heated, until phase change occurs and the resulting vapor is used to drive a turbine or cylinder. In refrigeration cycles, evaporators absorb the heat until a phase change, due to boiling, occurs. The resulting vapor, flows into the condenser, and condenses back into the working fluid and the process begins again.

Boiling also plays a key role in the thermal management industry. Thermal management devices are critical to further development in the electronics industry, particularly microelectronics. As technology continues to increase, faster and smaller devices are being manufactured. These smaller devices produce significantly higher heat fluxes, are required to operate for longer periods in hazardous thermal environments, and are more sensitive to temperature in general. In order to increase operating temperatures, reduce burnout, and increase product life cycle it is essential that thermal management devices evolve and become more efficient. Boiling heat transfer is already used in the thermal management industry in heat sinks, through heat pipes, to effectively cool central processing units (CPUs) and graphical processing units (GPUs). Heat pipes work by taking advantage of phase change heat transfer. Inside the heat pipe there, is a working fluid, usually water or ammonia but sometimes mercury for high temperature operations

or liquid helium for low temperature heat transfer, which partially fills the pipe in liquid form. When the heat pipe absorbs the thermal energy dissipated from the device that it is cooling, all of the energy is used to boil the fluid, thus initiating a phase change from liquid to a vapor. The device is protected from burnout as the majority of the thermal energy released was used by the evaporation process which in turn provided a small temperature increase in the device.

In the manufacturing industry, engineers also take advantage of boiling heat transfer when it comes to metallurgy, in the form of spray cooling. Spray cooling is a heat transfer technique in which liquid fluid impinges, usually from a high pressure nozzle, and wets a surface. The wetted surface is cooled by the droplets of fluid as they absorb heat from the surface. In two-phase spray cooling, the kind in which a metallurgist would use, the wetted surface is at a temperature above the saturation temperature of the surface and the impinging droplets boil off the surface. Two phase heat transfer is the most desirable form of spray cooling because of the amount of heat removed from the surface, which is indicative to the effectiveness of boiling heat transfer.

Boiling heat transfer is a very complex process; successful characterization depends upon numerous parameters such as latent heat, nucleation sites, bubble formation, growth, size and detachment, buoyancy driven fluid forces, vapor formation, dynamics of liquid-bubble interactions, density variation between phases, fluid velocities, apparatus orientation, surface roughness and in some cases gravitational fields. Boiling heat transfer is also dependent on thermo-physical properties such as thermal conductivity and surface tension. Boiling can be classified by different modes: sub-cooled and saturated. During sub-cooled boiling the fluid temperature is below the

saturation temperature and bubbles formed at the heated surface can condense back into the fluid while during saturated boiling the fluid temperature is greater than the saturation temperature. In this mode bubbles formed at the heated surface are propelled through the fluid by buoyancy forces and, if a free surface is present, are free to escape to the environment.

Extensive research has been performed to reveal and understand the underlining mechanisms of boiling heat transfer, particularly in the area of pool boiling. Pool boiling occurs when a heated surface is inserted into a large, relative to the size of the heated surface, body of quiescent liquid, in which the motion of the fluid surrounding the surface is primarily driven by bubble formation and currents due to natural convection. If the bulk temperature of the liquid is below the saturation temperature of the fluid then it is termed sub-cooled pool boiling, hence the ability of the bubbles to condense back into the fluid. When the bulk temperature of the fluid is maintained at its saturation level, the process is considered saturated pool boiling. Shiro Nukiyama was the first to experimentally reveal different regimes of pool boiling in the 1930s [18]. Nukiyama gradually heated nichrome, nickel, iron and platinum wires, submerged and orientated horizontally, in saturated water at standard atmospheric pressure, to experimentally verify the maximum values of heat transfer for water in pool boiling. The results of the experiments for the maximum value of heat transfer turned out to be higher than previously believed at the time. Nukiyama's plot of the heat flux versus the excess temperature formed the basis of the boiling heat transfer curves used in the current study.

1.2 Regimes of Boiling Heat Transfer

The standard boiling heat transfer curve consists of four basic regimes: (i) free convection boiling, (ii) nucleate boiling, (iii) boiling transition and (iv) film boiling. Each regime has unique characteristics that identify it. Figure 1 shows a plot of the standard boiling heat transfer curve [19].

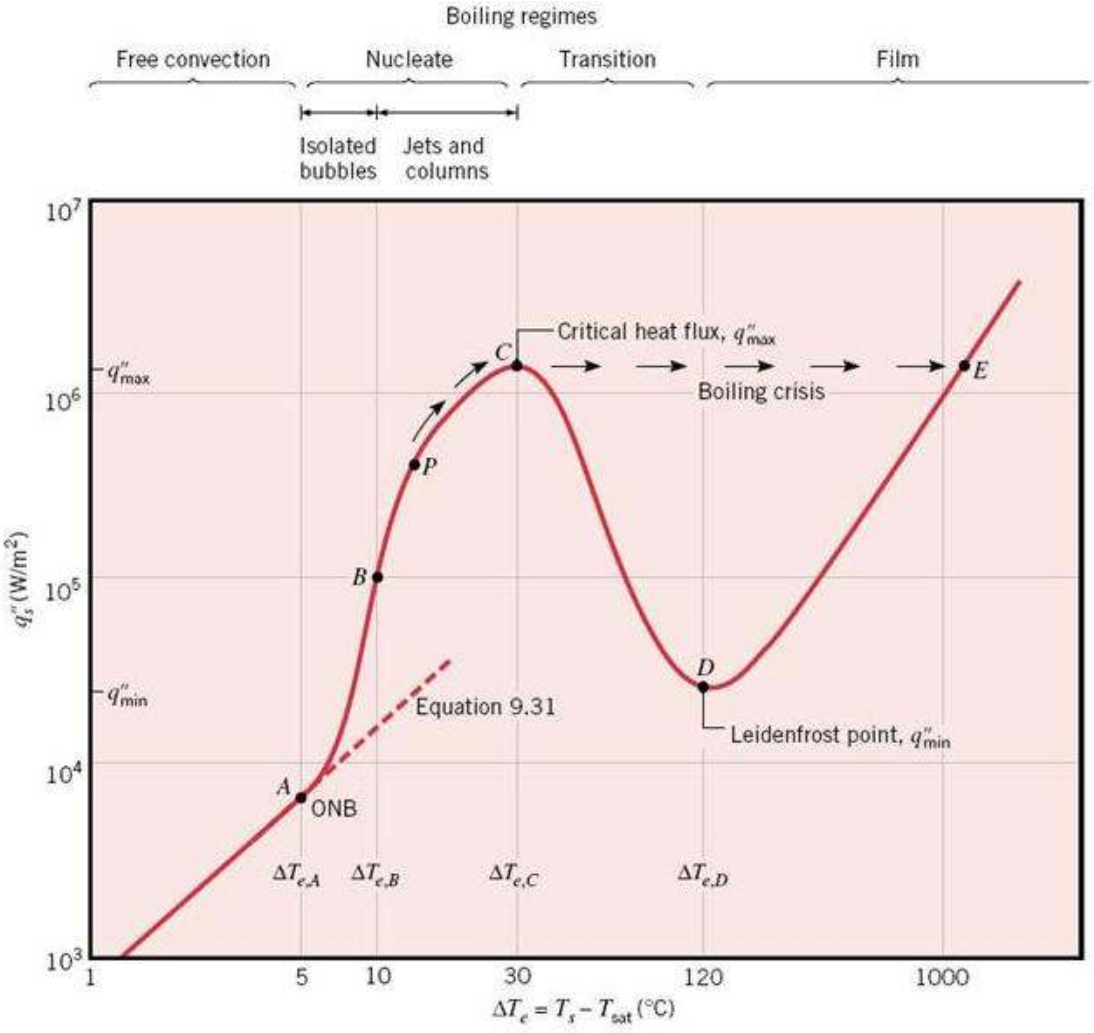

Figure 1: Boiling Heat Transfer Curve

In the free convection boiling regime, as shown from the origin to point A in Figure 1, heat is transferred from the surface by natural convection bubble formation at

the surface is yet to occur and consequently fluid motion is due to convection forces. The second regime, nucleate boiling (shown from point A to C), is when bubble formation first begins to occur. Bubbles begin to form and detach from the surface slowly at first, but then increase rapidly over time as more nucleation sites become active. This bubble detachment causes better mixing of the fluid than natural convection alone and heat transfer from the surface and surrounding fluid is increased. Heat transfer is enhanced until point C, considered the maximum heat flux or more commonly the critical heat flux, where the third regime, boiling transition begins. Transition boiling (shown from point C to D) is when the nucleation sites become so numerous that bubble formation and detachment begin to form a vapor surface around the surface, making it difficult for the liquid to wet the surface. Due to the vapor formed at the surface, the majority of the heat is forced to conduct through vapor, lowering the heat flux to a minimum at point D. Point D is often referred to as the Leidenfrost point. The final regime, film boiling, occurs when the surface is completely covered by vapor and heat transfer is dominated by conduction and radiation. Consequently, the heat flux will begin to increase with an increase in the excess temperature from this point forward. This is known as the boiling crisis because the heat flux will now continue to increase without a decrease as long as the excess temperature increases. It can be difficult to control the surface temperature. Point E is often referred to as the burnout point, however point E and C both represent the same heat flux, and as the boiling heat transfer curve illustrates to reach point E, the Leidenfrost point must be reached, which exists to due to poor heat transfer performance. The latter exhibits a waste of energy to achieve the same heat flux, therefore for practical

heat transfer applications the determination of point C, the critical heat flux, is the desired heat flux.

1.3 Emergence of Nanofluids

In the thermal sciences and engineering, significant amounts of research has been done studying various fluids. Particularly in heat transfer engineering, a plethora of research has been done examining the nature and performance of various fluids. As technology continues to advance, it is heat transfer that continues to play an increasingly important role in that advancement. In the electronic industry, particularly microelectronics, heat transfer is very important. Therefore the heat transfer applications of fluids are important. It has been shown that convective cooling solutions using gaseous fluids, such as air, can be more than adequate for devices such as a desktop computer. However, for more advanced devices such as computer servers, engines or advanced thermodynamic systems such as power plant operation, cooling systems involving liquid fluids are desirable. To meet the performance demands, engineers began to focus on different fluids and ways to enhance the performance of such fluids. One such way is a mix of two different phases of matter. Mixing phases of matter, lead to the idea to enhance fluids by adding particles of solids to a liquid creating a new fluid. In theory, this new fluid is to be the best of both worlds, by providing some of the performance benefits using solids while maintaining the ability to use fluids in apparatuses such as heat exchangers. In practice, this hybrid did provide an increase in performance as expected. However, clogging, sedimentation, and clumping of particles were some of the problems that prevented this idea from successful integration into heat transfer applications. Thus this idea was abandoned by many engineers and researchers.

It was not until the late 1990s did this idea resurface. In 1995 Choi coined the term "nanofluid" while trying to develop a new engineering fluid [3]. Choi's nanofluid contained nano-sized particles dispersed in a liquid. Through experimentation, it was demonstrated that the nanofluid had remarkably better heat transfer properties than the original fluid did. Previous problems with this type of mixture were overcome by the use of nano-sized particles. The first liquid-solid mixtures contained particles in the micro-scale and although small, particles of that size are difficult to keep in suspension. At the nano scale the particles are small enough to stay in suspension, and under the right conditions they can stay in suspension for an indefinite period. Permanent suspension has several advantages such as preventing aggregation and clogging. Explanation of the enhancement is still debated, but the scientific community is in accord on one thing: nanoparticles have been shown, experimentally, to greatly enhance the heat transfer properties of the original fluids by a very small addition of nanoparticles.

1.4 Objectives of the Current Study

It is clear that nanofluids can have better heat transfer properties than traditional fluids. The increases in thermal conductivity, critical heat flux, and heat transfer coefficients are not to be ignored but instead quantified and sought after to further enhancement. The purpose of the current study is to determine the effectiveness of alumina nanofluids in cooling a copper surface in a sub-cooled pool boiling experiment. The effectiveness of the alumina nanofluids are compared to de-ionized water. More specifically the objectives of the current study are as follows.

1) Improve the boiling curve of de-ionized water by adding aluminum oxide nanoparticles in various concentrations in a sub-cooled pool boiling apparatus.

2) Increase the convective heat transfer coefficient due to boiling by adding aluminum oxide particles in various concentrations in a sub-cooled pool boiling apparatus.

The primary and secondary objectives can both be observed with the same methodology. If the applied heat flux of nanofluids versus the excess temperature were plotted, and compared to de-ionized water, then an improvement in the boiling curve can be observed in several ways. One way to see enhancement is when similar heat fluxes at smaller excess temperature are observed, which indicates that comparable and/or the same quantity of heat is being removed at lower temperatures. Graphically this is represented by shifting the boiling heat transfer curve horizontally to the left. Another way to see enhancement is when greater heat fluxes are produced at similar and/or the same excess temperatures. The latter indicates better heat transfer at similar excess temperatures which is graphically indicated by shifting the boiling heat transfer curve vertically upwards. Enhancement in the convective heat transfer coefficient can be seen in the same way as the heat fluxes.

Chapter 2

Literature Review

2.1 Nanofluids

There are many different nanofluids and they are usually prepared depending on the need of the researcher. Basic preparation techniques are as follows: add a desired amount of nanoparticles on a mass or volume basis in relation to the total mass or volume of the fluid. Nanoparticles are usually dispersed into the fluid by a process known as ultrasonication for a situationally dependent amount of time. Ultrasonication is a process in which the creation of reciprocating high and low pressure waves are created in a liquid, causing small bubbles to form and burst. The latter is the basic principle of cavitation and the resulting fluid movement causes strong hydrodynamic shear forces which in turn can be used to thoroughly mix reactants.

Although most nanofluids contain nanoparticles dispersed by ultrasonication, keeping the particles in suspension for extended periods of time is still a challenge. The most widely used techniques to prevent sedimentation are by adding active surface agents and controlling the pH of the nanofluid. Some suspension techniques change the surface properties of the nanoparticles and reduce the tendency of the nanoparticles to conglomerate into clusters, which prevents uniform dispersion, which can have adverse effects on heat transfer.

2.1.1 Addition of Surface Agents to Nanofluids

The additions of surface agents, which are also referred to as surfactants, are selected depending on the properties of the base fluid and nanoparticles themselves. Y. Xuan *et al.* used oleic acid in addition to salt as surfactants to help with dispersion and suspension of copper nanoparticles in transformer oil and water. S.M.S Murshed *et al.* used oleic acid and cationic surfactant hexadecrltrimethlammonium bromide (CTAB) to keep Titanium Dioxide (TiO_2) nanoparticles in water based nanofluids. Y.J. Hwang *et al.* used sodium dodecyl sulfate (SDS) for water based MWCNT nanofluids.

Jin Huang *et al.* investigated the effect of using sodium dodecylbenzene sulfonate (SDBS) as a surfactant in aluminum oxide-water and copper-water nanofluids. Jin Huang *et al.* noticed that ultrasonication can have adverse effects on nanofluids after extended periods of time. The researchers prepared nanofluids in 150 *ml* beakers with 0.1% weight fractions of both aluminum oxide and copper nanoparticles. SDBS was added to the nanofluids and then the same nanofluid was prepared without SDBS. Both nanofluids were sonicated for an hour at a frequency of 40 *KHz*. After sonication the average particle size was measured. Nanofluids without SDBS had an average particle size of 5560 *nm* while the nanofluids containing SDBS had an average particle size of 130 *nm*, indicating better dispersion with surfactants.

X-Q Wang *et al.* states that although adding surfactants is intended as a method to suppress particle clusters from forming, surfactants can affect the heat transfer performance of nanofluids suggesting that excessive use of surfactants can deteriorate heat transfer performance.

2.1.2 Effect of pH on Nanofluids

The pH of the solution has been shown to affect the suspension time, so controlling the pH of the solution can be important. K.B. Anoop *et al.* performed research with 45 *nm* and 150 *nm* aluminum oxide nanoparticles creating nanofluids with weight concentrations of 1%, 2%, 4%, and 6%. The nanofluids had pH values of 6.5, 6, 5.5 and 5 respectively. K.B. Anoop *et al.*set aside 2.5 *l* of each concentration and noticed the nanoparticles stayed in suspension for several weeks. The rationale for the extended period of suspension is knowledge of the iso-electric point (IEP). The IEP corresponds to the point of zero zeta potential (ZZP). The zeta potential is the measurement of the stability of a colloidal system, a system in which matter in one of three phases, is finely dispersed in matter in a different phase, such as a nanofluid. At the ZZP the net charge between particles are at a maximum, wherein the attraction between particles is great enough to overcome the hydrodynamic forces surrounding the particle, causing the particles to conglomerate. K.B. Anoop *et al.* kept the nanofluid away from the ZZP, preventing the particles from clumping together.

Jin Huang *et al.* further investigated the effect of pH on nanofluids by observing the pH effects on nanofluids consisting of aluminum oxide and copper nanoparticles with water as the base fluid. The results of that research show that nanofluids can be kept in suspension for extended periods of time, and the pH corresponds to the absorbency and zeta-potential point, depending on the nanoparticle concentration. Jin Huang's research shows that aluminum oxide and copper nanoparticles both fall out of suspension rapidly when in water with a pH less than 2. Further investigation with adjusting the pH showed that the pH and absorbency and zeta potential to be directly related, such as for each

increase in pH, the zeta potential increases also. The optimum pH value for aluminum oxide nanoparticles in de-ionized water was found to be 7.5-8.9 and any pH value greater than or equal to 7.6 for copper nanoparticles.

2.2 Nanoparticles

The most common types of nanoparticles used in research are alumina oxide (Al_2O_3), copper II oxide (CuO), silica oxide (SiO_2), titanium dioxide (TiO_2), and zinc oxide (ZrO_2). Pure metallic nanoparticles such as gold, silver, iron, platinum, and copper are also being used in research. A few researchers have even begun to use carbon nanotubes in nanofluid research. However, the majority of nanoparticles are oxides; consequently they are primarily used in water based nanofluids. Non-oxides nanoparticles are used in water based nanofluids. For example, pure metallic nanoparticles have been used in aqueous solutions but difficulties associated with keeping the particles in suspension for extended periods of time, limit their usage. Instead, pure metallic nanoparticles are predominantly used in oils, like engine oil, or alcohols such as ethanol.

Nanoparticles are usually made by a synthesis technique, whereas a metal precursor, in the bulk, is heated to produce a vapor. Reactive gases are added to the newly formed vapor to create a new molecular structure. Next the vapor-reactive gas vapor is cooled at a controlled rate, causing nanoparticles to condense out of the process. Also nanoparticles are sometimes created from a more traditional chemical process in which an appropriate chemical solution is combined with reactants. Once reactants start the chemical reaction, nanoparticles precipitate out of the solution.

2.2.1 Aluminum Oxide

Aluminum oxide (Al_2O_3), or alumina is the most widely used nanoparticle since its thermal properties are well documented [5, 6, 8, 11, 14, 17]. Alumina can be acquired in sizes as low as 40 *nm*. Al_2O_3 comes in various shapes but are usually spherical, the thermal conductivity approximately 30 *W/m*K* depending on how pure the aluminum is. This particle is often used to increase the thermal conductivity of the base fluid. Alumina is often used in de-ionized water, ethylene glycol, and oil.

2.2.2 Copper II Oxide

Copper II Oxide (CuO) is another highly used nanoparticle for nanofluids [1, 3, 7, 11, 15]. The sizes and shapes depend on the manufacturer but some have been reported as small as 14 *nm*. The thermal conductivity of copper II oxide is approximately 20 *W/m*K*. Copper II oxide is often used in boiling tests and to increase the thermal conductivity of the base fluid. Nanofluids have been created with CuO nanoparticles added to de-ionized water, oil, ethylene glycol.

2.2.3 Silica Oxide

Silica oxide or silicon dioxide is another well used nanoparticle in nanofluid research [8]. Thermal conductivity is around 1.4 *W/m*K* and sizes as small as 22 *nm* have been achieved. Silica oxide is often used in boiling tests to examine the critical heat flux. Silica oxide nanoparticles have been added to oil, de-ionized water, and ethylene glycol to create nanofluids.

2.2.4 Titanium Dioxide

Titanium dioxide or titania is often used in boiling tests to study how it affects the critical heat flux [5, 8]. Sizes have been reported as low as 85 nanometers. The particles are usually spherically shaped. Titania nanoparticles have been added to ethylene glycol and de-ionized water to create nanofluids.

2.2.5 Zinc Oxide

Zinc oxide or zirconium oxide is another nanoparticle and is being one of the newest particles being studied [10, 14]. Most research is done using boiling tests to examine the CHF. Some manufacturers have reached sizes as small as 20 *nm*. The thermal conductivity is approximately 2 *W/m*K*. Zinc oxide nanoparticles have been used with base fluids of de-ionized water and ethylene glycol to create nanofluids.

2.2.6 Carbon Nanotubes

Carbon nanotubes are the strongest materials on earth, but in addition to their great strength they also have significant heat transfer properties. Theoretical calculations list the thermal conductivity of carbon nanotubes 6600 *W/m*K* at room temperature [23]. J Hone *et al.* states that in the when carbon nanotubes are aligned that thermal conductivity is greater than 200 *W/m*K* at room temperature. Carbon nanotubes come in two varieties: single walled carbon nanotubes (SWNT) and double walled carbon nanotubes (DWNT). SWNT have been manufactured as large as 1.25 *nm* in diameter [22]. Carbon nanotubes have been added to de-ionized water, ethylene glycol, oil, and decene.

2.3 Nanofluid Heat Transfer

Research has shown that nanofluids can have greater heat transfer properties than traditional fluids. Understanding and quantifying the superior properties is important, as such, much research is being done, however the majority of nanofluid research can be categorized into thermal conductivity enhancement, critical heat flux management, and pool boiling characterization. In addition to traditional heat transfer research some researchers are conducting nanofluid experiments which readily lend themselves to more traditional industry applications.

2.3.1 Thermal Conductivity Enhancement with Nanofluids

The thermal conductivity of a material is a unique transport property, defined as the proportionality constant, k [W/m*K], in Fourier's Law. The thermal conductivity is a heat transfer material property, which is most commonly used to quantify heat transfer effectiveness. Generally the higher the thermal conductivity, greater quantities of heat can be transferred at a faster rate through a material as compared to a material of lesser thermal conductivity.

It has been shown through experimentation that nanofluids have significantly increased thermal conductivity compared to their base fluids. Equally important are analytical models to predict the enhancement caused by nanoparticles addition. One such model, used by many researchers, is Maxwell's theoretical model for predicting the effective thermal conductivity of suspensions with spherical particles [1]. Maxwell's model for predicting the effective thermal conductivity of liquid-solid fluid suggests that as particle volume fraction increases so too does the effective thermal conductivity [1].

Hamilton and Crosser modified Maxwell's theoretical correlations to account for particle shape [1]. H.U. Kang et al. took the previous model and used it to predict the thermal conductivity of silica oxide using water as the base fluid and compared the results to the experimental thermal conductivity values acquired from using the transient hot wire method [1]. H.U. Kang et al results show that Hamilton and Crosser's model is indeed capable of predicting the thermal conductivity of nanoparticles. This point is significant in understanding thermal conductivity of nanofluids. Hamilton and Crosser's model was developed using Maxwell's model for effective thermal conductivity as the base model from which their work is based upon. Since Maxwell's model was not developed with nanofluids in mind, yet was sufficient enough develop nanofluid correlations, suggests thermal conductivity enhancement from micro sized particles gives good insight to enhancement from using nanoparticles. It also suggests that Maxwell's model is developed enough to use as a starting point to develop future nanofluid thermal conductivity models.

Yimin Xuan and Wilfried Roetzel conducted research to investigate nanofluid thermal conductivity. Yimin Xuan and Wilfried Roetzel reported that Hamilton and Crosser's model has been shown to satisfactorily predict the thermal conductivity of nanofluids whose ratio of conductivity of the solid/liquid phases is larger than 100. They believe that nanofluids behave like a single fluid for the most part but particle shape and sizes are not to be ignored and that model's such as H.U. Kang *et al.*, which incorporate these factors, are imperative to the understanding of thermal conductivity enhancement of nanofluids [4].

Another philosophy used to predict the thermal conductivity of nanofluids is based off of effective medium theory and the concept of fractal dimension for nanoparticle clusters while paying attention to nanoparticle clusters size and the particle size. B-Xuan *et al.* developed a fractal model that can predict the effective thermal conductive of a nanofluid. Effective medium theory has two models that can predict the thermal conductivity of nanofluids, the Maxwell-Grant correlations (MG) and Bruggeman model. For low particle concentrations both correlations provide the same results when compared to experimental results. However, for high volume fraction concentrations the Bruggeman model is the most accurate of the two. Therefore B-Xuan et al [3] used the latter to predict the effective thermal conductivity of nanoparticle clusters and MG to predict the thermal conductivity of the nanoparticle suspensions. By defining the necessary fractal indexes and with fractal theory, B-Xuan developed a fractal model by combining the MG and Bruggeman models. The thermal conductivity of copper II oxide nanofluids at mass concentrations of 0.02%, 0.04% and 0.06% were found experimentally and compared to those predicted from B-Xuan's fractal model. B-Xuan [3] model proved to be accurate but notes that when exceeding 0.5% mass concentrations deposition begins to occur. Nanoparticle deposition is beyond the assumptions used to develop the fractal model, hence it is no longer able to predict the thermal conductivity.

It is relevant to mention that nanofluids may have fluctuating thermal conductivity when used in certain apparatuses due to interactions with the device itself. For example, Dongsheng Wen discovered that when using nanofluids containing nanoparticles with a bulk thermal conductivity of 50 $W/m*K$ in a microchannel that

nanoparticles sometimes cluster at the walls or migrate in general. Therefore the local thermal conductivity of the fluid changes drastically with this increased non uniform particle distribution [12]. As the non-uniform particle distribution increases the constant thermal conductivity assumption becomes invalid [12].

It is very noteworthy to point out that the general method of creating nanofluids, the addition of nanoparticles to a specified base fluid, is not the only way to create nanofluids with high thermal conductivity. Min-Shen Liu *et al*. tried to increase the thermal conductivity of a base fluid with copper nanoparticles with the chemical reduction method [15]. Min-Shen Liu *et al*. added copper acetate to de-ionized water and mixed it slowly and uniformly while using hydrazine as a reducing agent [15]. Copper nanoparticles precipitated out of the solution. Volume concentrations produced, were below 0.2%. The chemical reduction caused the solution to turn from light brown to dark brown [15]. Three basic types of nanoparticles were produced; (i) spherical (ii) square shapes and (iii) needle assorted shapes. Min-Shen Liu *et al.* uses the ratio of the thermal conductivity of the nanofluid to the thermal conductivity of the base fluid to compare the various concentrations [15]. Also, spherical shape nanoparticles appear to cause the highest increases in thermal conductivity. The particles ranged in diameters from 50-100 *nm* and were produced in volume fraction concentrations of 0.05% to 0.02%. Min-Shen Liu *et al.* research demonstrated that the chemical reduction method can be used to produce a nanofluid that can effectively increase the thermal conductivity of the based fluid [15].

2.3.2 Critical Heat Flux Management with Nanofluids

Another highly researched topic is how nanofluids affect the critical heat flux (CHF). The CHF is the heat flux associated with the point in a heat transfer process whereas the heat transfer reaches a maximum effectiveness. That is, the maximum amount of heat is being removed from the heat transfer surface. Any future attempts to remove more heat are futile. Physically, for many convective processes such as spray cooling and pool boiling, the heated surface is at a temperature so great that all the fluid near the heated surface evaporates. This vapor forms a blanket between the heated surface and surrounding fluid, causing heat to conduct through vapor before reaching a liquid fluid. Vapors inherently are inferior conductors of thermal energy as compared to liquids. Having to dissipate heat through the vapor blanket first, significantly lowers the effectiveness of heat transfer. Thus knowledge of this phenomenon is important. In fact a higher CHF is often very desirable and nanofluids have been shown to affect the CHF in many experiments.

H Kim *et al.* performed comprehensive investigations to understand the phenomenon behind the enhanced CHF observed from the use of nanofluids. H Kim *et al.* looked at pool boiling of titania and alumina with diameters of 85*nm* and 47*nm* respectively. Previous experiments showed that that even small volume concentrations significantly increased the critical heat flux, so the experiment used concentrations ranging from 0.0001% to 1%. In the bath heaters were powered by NiCr 2 *mm* diameter wire and then by Ti 25 *mm* diameter wire. Each heater showed the same basic trend, significant increases in the CHF at small nanofluid concentrations when compared to pure water. Large increases in the CHF were observed in nanofluid with concentrations

up to 0.01%. Concentrations > 0.01% were characterized by smaller jumps in the CHF as nanofluid concentrations approach 1%. It is worth noting that the alumina fluid outperformed the titania fluid showing greater increases in the critical heat flux at the same concentrations. After the boiling tests surface conditions of the heaters were examined with a scanning electron microscope (SEM). The SEM showed that as particle concentrations increased so did the layer of nanoparticles deposited on the surface which suggests that the main reason for the enhanced CHF is indeed the layer of nanoparticles formed from boiling [5]. Then a pool boiling experiment measuring the CHF using a nanoparticle coated heater in pure water was compared to a nanoparticle coated heater in a nanofluid. The results of the pool boiling experiment show that the nanoparticle coated heater produced higher heat fluxes in nanofluids than the nanoparticle coated heater in pure water. It is important to point out that the nanoparticle coated heater used in the pure water pool boiling test produced higher heat fluxes than the smooth heater did in a pure water pool boiling test. This result supports H Kim *et al*. belief that the deposition of nanoparticles is the main contributor to the enhancement of the CHF. Those results give some insight on CHF behavior at lower concentrations. Particle deposition increased with particle concentrations which in turned increased the CHF. At higher concentrations a more dynamic layer of nanoparticles coated the heater revealing why no more enhancement to the heat flux occurred after a certain concentration.

In Cheol Bang *et al*. investigated the critical heat fluxes in pool boiling with alumina nanofluids using smooth heaters oriented in both the horizontal and vertical directions [6]. Results from that research show that regardless of the orientation of the heaters the CHF is increased by the addition of nanoparticles. Still, more dramatic

enhancement occurs in horizontal orientation with a 32% increase in the CHF compared to a 13% increase in the vertical orientation [6]. In Cheol Bang *et al.* suggests that the CHF enhancement is influenced by factors such as geometry, different nanoparticles, the surface roughness of the heaters, as well as the size of the nanoparticles [6].

Zhen-Hua Liu *et al.* investigated copper II oxide nanofluids and how the CHF would be affected using saturated and sub-cooled water as the base fluid with jet impingement on the heater surface. The results of that investigation demonstrated that using both saturated and sub-cooled water as a base fluid pool boiling experiments produced higher CHF than pure water. Also, the CHF enhancement gradually increases with particle concentration [7]. The CHF stopped increasing when the particle concentration exceeds 1 wt% (weight percentage), with the maximum increase of the CHF of 25% compared to pure water [7]. During jet boiling a sorption layer builds and continues to grow until a certain value at which point the CHF stops increasing.

Hyungdae Kim *et al.* performed research and compared the CHF of various nanofluids and examined how surface wet-ability, surface roughness, and maximum capillary wicking height of the nanoparticle coated surface affect the CHF [8]. The nanoparticles used were TiO_2, Al_2O_3 and SiO_2 at 85 *nm*, 47 *nm*, and 90 *nm* respectively. The experiment measured the critical heat fluxes and compared them to the values predicted by Zuber's correlations and pure water. The results were within 85% of the values predicted by Zuber's correlations and show that volume concentrations up to 0.01 % cause increase in the critical heat flux by up to 170% but at 0.1 % only SiO_2 showed improvement [8]. When nanofluid concentrations $\geq$ 1% were used no improvement in the CHF over pure water was generated. Hyungdae Kim *et al.* reported that surface wet-

ability, surface roughness and capillary wicking height all affect the CHF. Still, they do not account for the unusual CHF enhancement, but instead nanoparticle concentration is the largest factor involved in CHF enhancement [8].

2.3.3 Pool Boiling Characteristics with Nanofluids

Pool boiling is a process when a heated surface is submerged in a bath of fluid and the volume of the heated surface is much smaller than the volume of fluid, the heat surface is submerged in. The heated surface is heated to a temperature above the saturation temperature of the fluid and heat transfer occurs at the solid-liquid interface causing the liquid at the surface to form vapor, lowering its density, causing the vapor to rise further from the surface. As vapor travels through the fluid, the surrounding fluid replaces the vapor at the heated surface. When nanofluids are used as the working fluids in pool boiling experiments they have been known to significantly alter the pool boiling curve and the boiling heat transfer coefficient.

S.K. Das *et al*. investigated pool boiling characteristics of alumina nanofluids to understand how they would behave in a convective cooling situation, using smooth and rough heaters (caused by nanoparticle deposition) at volume fractions concentrations ranging from 1% to 4%. The ratio of the thermal conductivity of the nanofluid to the base fluid was calculated and shown to increase with temperature and was highest at 1% volume fraction and lowest at 4% volume fraction. Also, the surface roughness of the heaters was altered from experimentation, including the pre-coated heater. As boiling continued more nanoparticle deposition occurred. The nanoparticle deposition also caused the boiling point to increase with temperature, deteriorating the boiling properties

of the base fluid by lowering the heat transfer coefficient. However, it is noted that careful attention must be paid to the local heat fluxes as the pool boiling leaves the surfaces at a higher temperature than the base fluid, which could be undesirable [9].

Cheol Bang *et al.* also researched the boiling heat transfer performance in pool boiling of alumina nanofluids using smooth heaters oriented in both the horizontal and vertical directions [6]. The pool boiling heat transfer coefficients of the nanofluids are compared to that of pure water and the results show that the nanofluid coefficients were actually worse than that of pure water [6]. As particle concentration increased the boiling heat transfer coefficient decreased shifting the boiling curve to the right [6].

Manoj Chopkar *et al.* is currently researching zinc oxide nanofluids in boiling test and comparing the results to pure water and nanofluid using surfactants, which increase the boiling heat transfer, while looking at continued use of the same surface [10]. 0.005%, 0.01%, 0.02%, 0.5%, 0.07%, and 0.15% zinc oxide volume particle concentrations with 1% surfactant and average of three runs show results show that a decrease in boiling performance the more you run the experiment without cleaning the heater surface, degrading even to that point whereas boiling performance is below pure water [10]. Surfactants combined with nanofluids deteriorate the boiling heat transfer coefficient much more significantly than nanofluids without surfactants added [10]. Again, nanoparticle deposition appears to be the main cause of the deterioration of the boiling heat transfer coefficient [10].

2.3.4 Industry Related Applications of Nanofluids

Nanofluids are beginning to be researched in a variety of ways which can be readily related to industry applications. One such application has been done comparing the performance of nanofluids against engine oil. S.-C. Tzeng [11] used two distinct nanofluids in his research. One nanofluid consisted of copper II oxide particles, the other contained aluminum oxide particle nanofluids. Both nanofluids were created using automatic transmission oil as the base fluid. Automatic transmission oil with antifoam added, an additive used to prevent unwanted air from mixing with the oil, was compared to nanofluids in a 4-wheel drive transmission system. The engine has a four blade rotary system in which improvements in heat transfer could increase engine life and overall performance of the automobile. For this set up 40 grams of nanoparticles are added to 840 grams of automatic transmission fluid which was added to the oil cavity of the rotary blade coupling. Data collection was done for temperature placing sensors at 24 unique points on the rotary blades for measurement in both the axial and radial directions. The engine runs continuously for 60 minutes while a data recorder collects the data. Afterwards a temperature distribution is plotted showing the oil's performance over a period of time. The blades spin at 400, 800, 1200, and then 1600 RPMs during this 60 minute interval for each fluid. Tzeng's results are astounding, as they show that CuO performs the best with the lowest temperatures, therefore it transfers heat the most efficiently, regardless of the blade speed. Al_2O_3 comes in second while antifoam is the worst additive for heat transfer. In fact, antifoam is the worst as it degrades the quality of the oil at higher speeds. Both nanofluids outperform pure automatic transmission fluid.

Another industry related use of nanofluids is in the quenching industry. K. Narayan *et al.* performed comparative analysis of water and nanofluids in steel quenching tests [13]. The nanofluid, or nanoquenchant, consisted of Al_2O_3 particles no greater than 50 nm with water as the base fluid [13]. The parameter analyzed was surface wettability. Using FTA software and an image recorder, operating at 60 frames per second, the wetting behavior was examined. A furnace was used to heat the test specimen. The furnace was of tubular design and oriented vertically at both ends. Thermocouples were used to measure the furnace temperature. The test specimen was heated to 850 ^{O}C and quenched in 1500 mL of coolant [13]. Using lumped capacitance analysis, the heat transfer coefficient was calculated and results show that the boiling heat transfer coefficient is lower for the nanoquenchant than pure water. However the spreading of the nanofluid on the substrate continued for well over 1000 *ms* while it stopped at 200 *ms* for water. K. Narayan *et al.* suggests that results indicate that for industry applications there is a need for nanofluids various quench severity. Quench severity, is a term used by metallurgists to describe the cooling rates of various quench-ants. K. Narayan *et al.* suggest that nanofluids with low cooling severity would be ideal for thin sections of high quench sensitivity materials, while nanofluids with high cooling severity would be ideal for thick sections of low quench sensitivity materials [13].

C. Choi *et al*. investigated the use of nanofluids as a coolant by performing tests with three different nanofluids acting as coolants in an electrical transformer [14]. Spherical shaped Al_2O_3, AIN, and rod shaped Al_2O_3 with sizes of 13 *nm*, 50 *nm* 2 *nm*-20-200 *nm* respectively were added to transformer oil [14]. Ethylene alcohol and oleic acid were added to stabilize the nanofluids as an additive to prevent sedimentation. With

volume fractions up to 4%, all three nanofluids outperformed pure transformer oil, with greater thermal conductivity, convective heat transfer coefficients and convection properties [14]. One interesting resultant that came from C. Choi *et al.* research is that the spherical shaped Al_2O_3 oil based thermal conductivity was nearly double that of Al_2O_3 with water as the base fluid, showing enhancement greater than 20% at 4% volume fraction [14]. AIN nanofluid showed an increase in thermal conductivity of 8% and improvement in the heat transfer coefficient by 20%. It is important to mention that nanoparticles concentration could not be increased much higher. Higher nanoparticle concentrations would require the amount of additives used to increases, which in return increases the fluid viscosity causing chemical instability. Therefore, the particle concentration cannot be increased without end [14].

D.P. Kulkarni *et al.* investigated nanofluids in a diesel engine of electrical generators to improve performance [17]. D.P. Kulkarni *et al.* added 45 *nm* alumina nanoparticles to a 50-50 ethylene glycol-water mixture and compared that mixture to 2%, 4%, and 6% alumina nanofluids. D.P Kulkarni *et al*. measured the specific heat of the nanofluid using the correlations presented by Buongiorno [17]. Results show that as the particle concentration increases, the specific heat of the nanofluids decreases, implying that for higher particle concentrations, less heat input is required to increase the temperature of the nanofluid [17]. If the time required to heat reduces, and if the nanofluids are used as jacket water, the engine will heat up faster and may result in less emission to the environment, since higher concentration of pollutants are emitted during the engine warm-up [17]. After, replacing the jacket water with an alumina based nanofluid in the diesel engine; it was observed that as particle concentration increased,

the diesel engine cogeneration efficiency decreased [17]. The efficiency decrease may be attributed to a decrease in the specific heat associated with an increase in particle concentration [17]. However, the heat exchanger used in the system saw increases in efficiency with increasing particle concentrations, which could be beneficial if that excess heat is channeled away from the generator and used to heat buildings [17]. D.P. Kulkarni *et al.* suggests that future research should focus on measuring the thermophysical properties of different nanofluids as a function of temperature and concentration as the results could lead to heat exchangers designed specifically for nanofluids [17].

Chapter 3

Experimental Setup and Procedure

3.1 Nanofluid Preparation

In this investigation Al_2O_3 nanoparticles were chosen because of their well documented thermal properties, ease of dispersion in de-ionized water, and wide spread use in the research community. Aluminum Oxide nanoparticles were added to de-ionized water on a mass basis with concentrations of 0.1%, 0.2%, 0.3% and 0.4% wt. The nanoparticles were manufactured by the Alfa Aesar Corporation. The manufacturer provided specifications are:

Table 1: Properties of Aluminum Oxide Nanoparticles.

Avg. Particle Size	Purity	Formula Weight	Boiling Point	Melting Point	Specific Surface Area	Refractive Index
45 nm	99.5%	101.96	2980^o	2045^o	36 m^2/g	1.768

The feed water into the research facility was de-ionized using a water filtration system. The water filtration system used was the Barnstead E-pure ®, manufactured by the Barnstead International Corporation and the model number is D4641 120 VAC. The average resistivity of the de-ionized water was 18.0 megohm-cm. The mass of the de-ionized water was weighed on a digital scale. The digital scale was manufactured by the Ohaus Corporation and the model number is Adventurer Pro AV8108. At this point,

nanoparticles were added to the de-ionized water and then sonicated for a minimum of 12 hours using a Tabletop Ultrasonic Cleaner. The sonicator used was manufactured by the Fisher Scientific Corporation and the model number is FS-140H. During sonication, the temperature of the nanofluid is increased causing some evaporation. To avert the nanoparticle concentration from changing, a lid was placed on the beakers used to sonicate the nanofluid, therefore any changes to the mass concentration was considered to be negligible.

3.2 Boiling Apparatus

The device used to conduct the experiment for this investigation is considered to be a sub-cooled pool boiling apparatus. It consists of a cartridge heater inserted into a copper sleeve. The copper sleeve is connected to the boiling specimen, a copper hat, via thermal paste. The copper hat rests on top of a stainless steel plate. An open glass cylinder is fixated on top of the stainless steel plate, de-ionized water and nanofluids are stored in the cylinder. A lid was placed on top of the glass cylinder to prevent the majority of the fluid from evaporating. The lid has 2 shafts that allow vapor to escape. A rubber hose is connected to each shaft, a funnel is connected to one end of the hose and the other hose rests in the funnel, catching vapor which condenses back into the fluid. However, some vapor can still escape, the amount of which was considered insignificant. The boiling apparatus rests on top of 3 stands, each supporting the stainless plate. The copper sleeve is inverted below the stainless plate by a retention clamp to a stand. The height can be adjusted by sliding the heater up the stand and fixed at a desired location with a lock nut. The set up is shown in Figure 2.

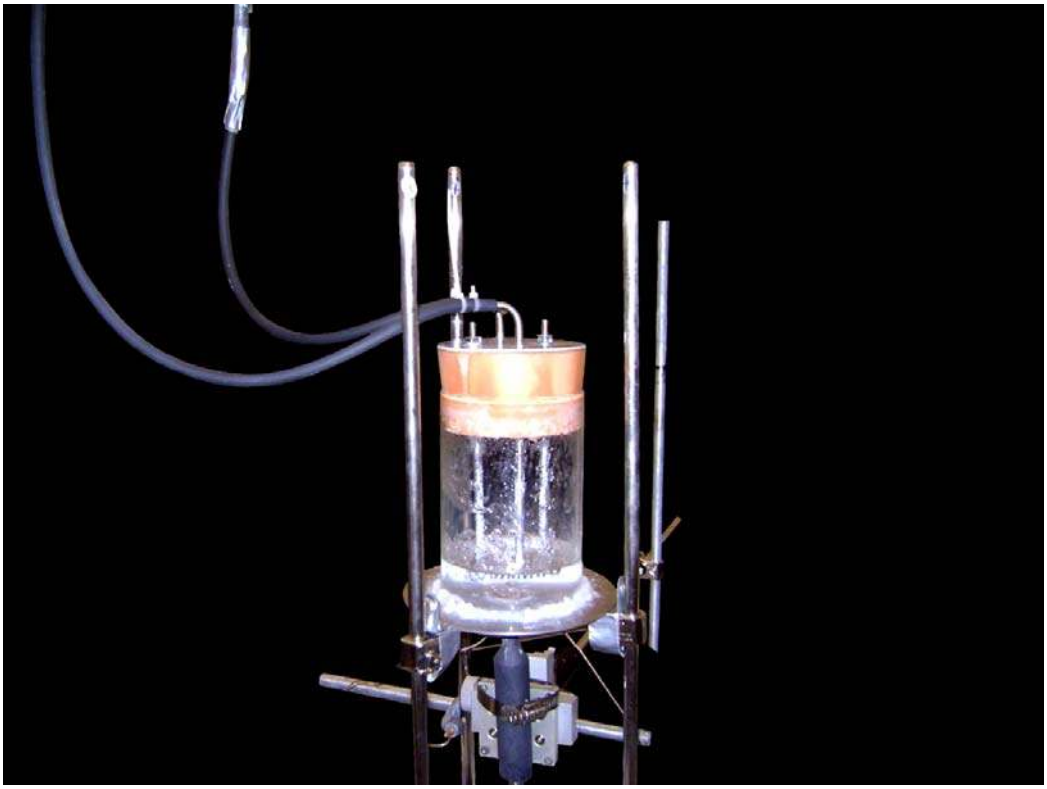

Figure 2: Boiling Apparatus.

3.2.1 Copper Sleeve

The copper sleeve is made from a single piece of tellurium copper. Tellurium copper was chosen in this investigation due to its high thermal conductivity (401 *W/mK*) and ease of machinability. The copper sleeve is 4 1/3" long, with different diameters at each end. At the bottom end the diameter is 1" and concentrically machined there is a hole drilled to depth of 2 2/3" with a diameter of 13 *mm*. The top end of the copper sleeve has a diameter of 12 *mm* and is 1 7/32" long. Three 1 *mm* holes are drilled at depth of 6mm into the upper portion of the copper sleeve for thermocouples. The first thermocouple hole is located 3 *mm* from the top surface, the second is located 13 *mm* from the top surface and is rotated 120^{o} from the first thermocouple, while the last

thermocouple hole is located 23 *mm* from the top surface and rotated 240^{o} from the first thermocouple. The copper sleeve is shown in Figure 3.

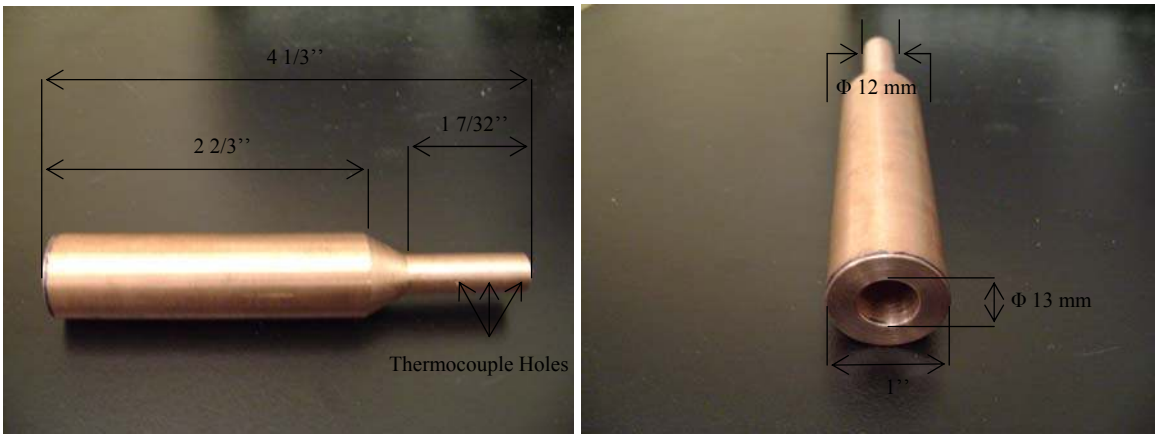

Figure 3: Copper Sleeve.

3.2.2 Cartridge Heater

The heater used in this investigation was a cylindrical cartridge heater manufactured by the OMEGA Corporation and the model number is CIR-30301/120V. The copper heater is rated for maximum wattage of 750 *W* and for 120 volts *AC*. The dimensions of the heater were measured using a digital caliper. The diameter was determined to be 12.6 *mm* and the length was determined to be 79 *mm*. Before insertion into the copper sleeve a thin layer of OmegaTherm ® thermal paste was applied to the body of the heater. The cartridge heater was connected to a variable autotransformer. The variable autotransformer was manufactured by the Staco Energy Products Corporation and the model number is 3PN1010B. The variable autotransformer has an input voltage of 120 volts, maximum output of 140 volts and a constant current load of 10 *A* maximum. The cartridge heater and variable autotransformer are shown in Figure 4.

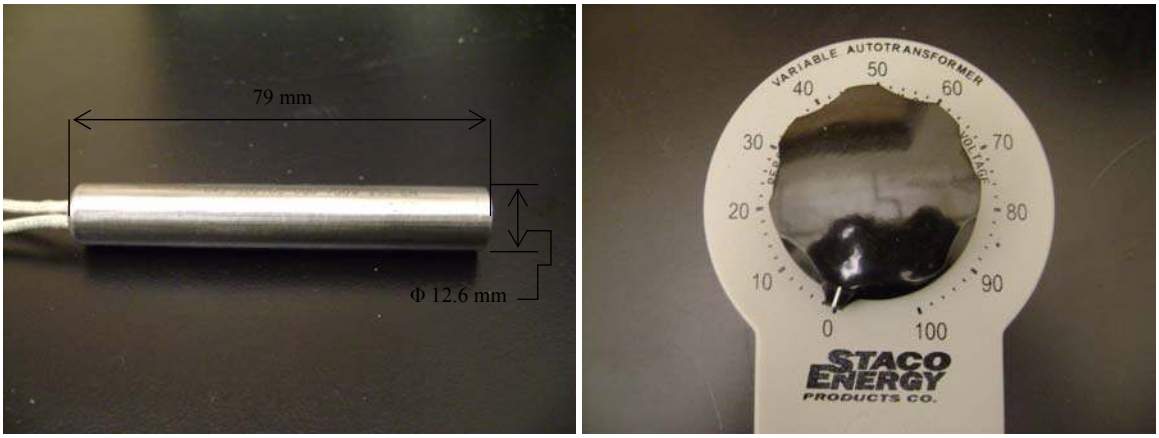

Figure 4: Cartridge Heater and Variable Autotransformer

3.2.3 Stainless Steel Plate

Stainless steel was chosen as a surface to balance the boiling apparatus on the stands but primarily for its low thermal conductivity (17.7 *W/m*K*) and thermal expansion properties, compared to copper. The coefficient of thermal expansion of stainless steel is 17 $*10^{-6}$ $in/in/^{o}C$ and the coefficient of thermal expansion of copper is 17.6 $*10^{-6}$ $in/in/^{o}C$. The idea is that over extended periods of time the copper hat would expand at a faster rate than the stainless steel plate, creating a tighter seal as temperatures increases. The outer diameter of the stainless steel plate is 6'' and the inner diameter is 12 *mm*. The plate has a thickness of 2 *mm* and is shown in Figure 5.

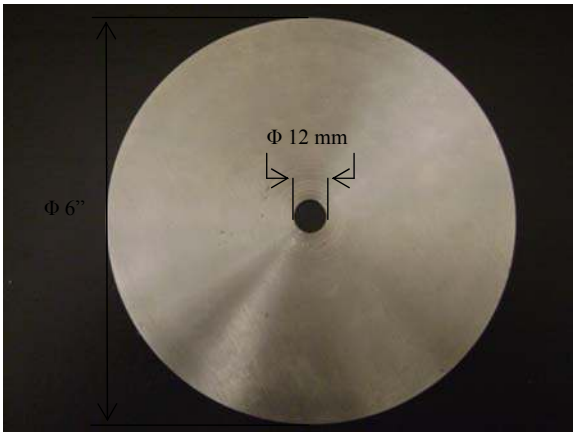

Figure 5: Stainless Steel Plate

3.2.4 Copper Hat

In the same fashion as the copper sleeve, the copper hat is made from a single piece of tellurium copper, due to its high thermal conductivity and machinability. The copper hat is has an outer diameter of 20 *mm* and inner diameter of 12 *mm*. The inner sleeve has a thickness of 2 *mm* while the outer sleeve has a thickness of 1 *mm*. The copper hat rests inside the stainless steel plate and was sealed to the plate by applying an adhesive to the outer sleeve. The adhesive used in this investigation was Silicone II © made by GE. Silicone II © is not water soluble and considered to be permanently flexible. The adhesive provided a water tight seal, which could be easily removed when needed. During experimentation the sealant had no noticeable adverse effects on the nanofluids.

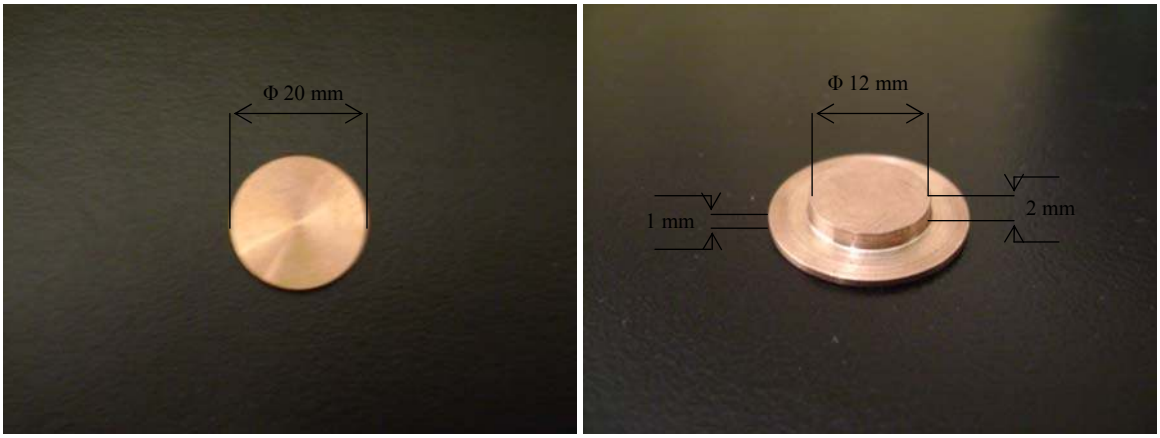

Figure 6: Copper Hat.

3.2.5 Glass Cylinder

During this investigation an open ended glass cylinder was used to hold the nanofluids. Glass was chosen primarily for visual observation and for its low thermal conductivity of 1.4 *W/m*K*. The glass cylinder has a diameter of 4", height of 5 3/4", and thickness of 2.5 *mm*. Silicone II © was used to adhere the glass cylinder to the stainless steel plate.

3.2.6 Thermocouple Wire

The thermocouple wire used in this investigation was type K and manufactured by Omega Engineering Inc. The part number is GG-K-30-SLE and has a nominal size of 0.037'' x 0.050''. The AWG number is 30, the conductor is insulated in glass wrap and the overall insulation is glass braid. The temperature range of the thermocouples is from -200 °*C* to 1350 °*C*, while the insulation is rated up to 482 °*C*. Before each experiment each thermocouple was cleaned with ArcticClean 1 © Thermal Material Remover and

ArcticClean 2 © Thermal Surface Purifier, then Arctic Silver 5 © was applied to the thermocouples before insertion into the copper sleeve.

3.3 Data Acquisition System

The research facility was equipped with a computer and data acquisition equipment made by National Instruments. All thermocouples were connected to a NI SCXI-1303 terminal block. The data acquisition software used was LabVIEW 7.1. A program was written to monitor and display all thermal couples using a waveform chart to illustrate the steady state condition.

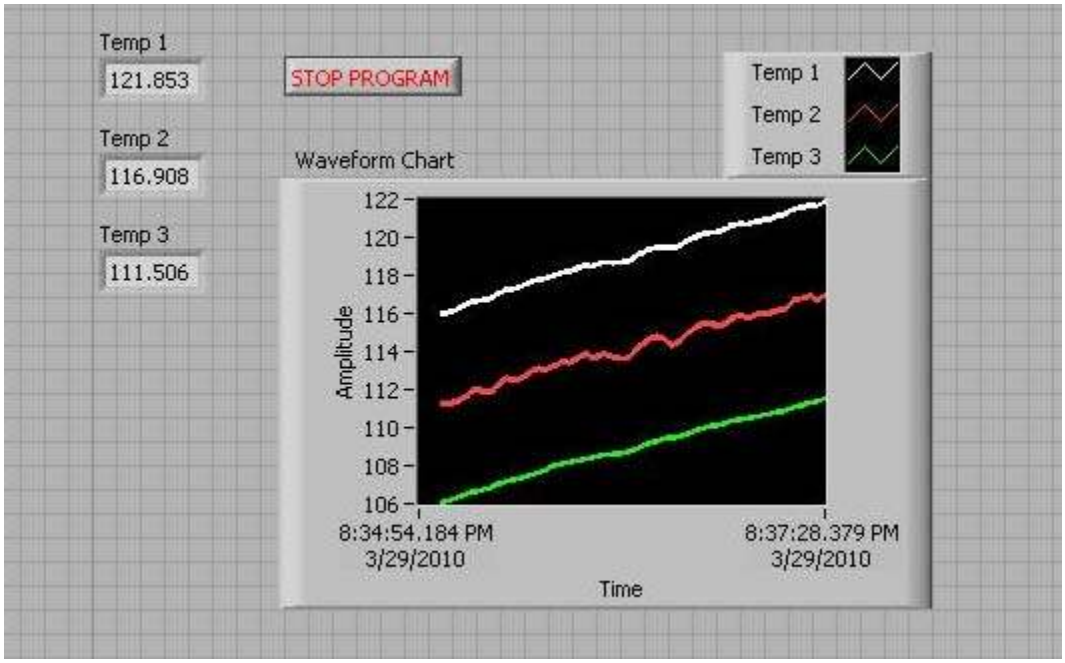

Figure 7: LabVIEW Front Panel Program

The waveform chart shown in Figure 7 is a temperature versus time graph. The chart displays temperatures as a function of time over a 2 minute interval. When the temperature gradient had a slope approximately equal to zero, it was used as a visual

indicator of the steady state condition. The corresponding block diagram for the LabVIEW program is shown in Figure 8.

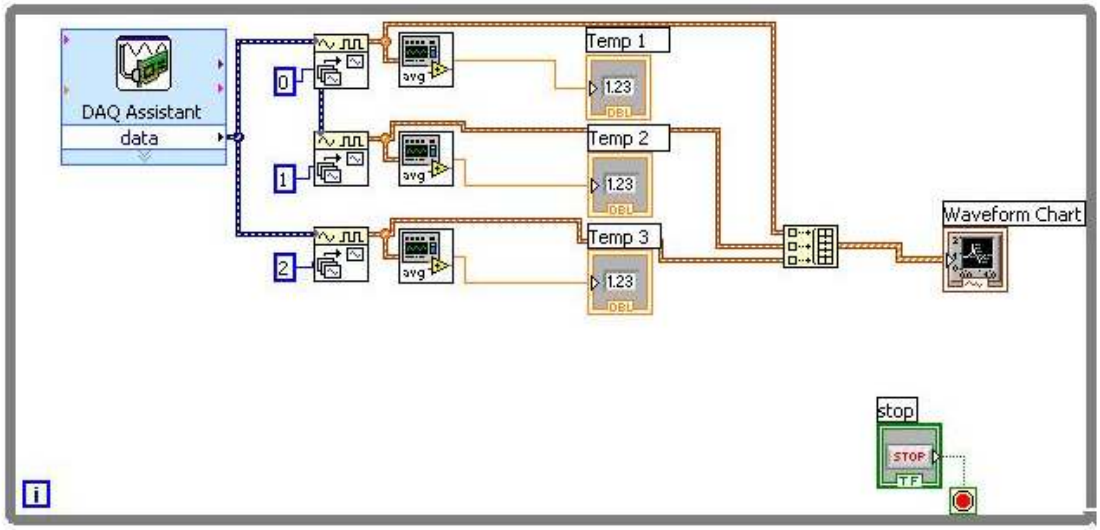

Figure 8: LabVIEW Block Diagram

3.4 Boiling Surface Preparation

Before and after each experiment the top of the copper sleeve and bottom of the copper hat was cleaned. Arctic Clean 1® Thermal Material Remover was used first to remove any containments and previous thermal paste with a lint free cloth. Next, Arctic Clean 2® Thermal Surface Purifier was used to prepare the surfaces for thermal paste; again the excess fluid was removed with a lint free cloth. The boiling surface, the top of the copper hat, was prepared without using any chemicals. Prior experimentation using M-Prep Conditional MCA1 and M-Prep Neutralizer MN5A-1 caused an adverse effect on the nanofluids, causing the nanoparticles to fall out of suspension once in contact with the boiling surface. Therefore, the copper hat was wet lapped with 320 grit sandpaper and de-ionized water 10 times in one direction, then 10 times in a direction perpendicular to

the latter. This process was repeated again for a total of 20 laps in each direction after each experiment.

3.5 Surface Roughness Measurement

To investigate the effects of pool boiling with nanofluids on the boiling surface, the surface roughness was taken as a means to quantify the surface. A profilometer was used to take the roughness profile. The profilometer used was the Surtronics 3P, which contains a diamond tip stylus of 5 μm. A cutoff length of 0.8 *mm* was used for the copper hat. Thus any deviation greater than 0.8 *mm* could not be detected by the profilometer.

3.6 COMSOL Model

Before the investigation began, a COMSOL model was developed for the investigation. A model was used because it was difficult to insulate the copper sleeve, thus none was used. The lack of insulation was a concern since a 1-D conduction model would be used for analysis, so COMSOL was used to quantify the amount of heat lost to the environment, and to illustrate if surface temperatures of 100 ^{o}C or greater could be reached.

The COMSOL model used was a 3-D Multiphysics →Heat Transfer →Conduction →Steady State Analysis. The material properties for copper, stainless steel, and water were loaded from COMSOL's material database. The thermal paste layer was specified to have a thermal conductivity value of 8.89 *W/m*K*, based on the thermal properties presented for Artic Silver ® 5 from the manufacturer. Inside the copper sleeve the cartridge heater was modeled as a generating cylinder with a diameter of 13 mm and height of 2 2/3''. The generation rate, *q'''*, was determined by

$$q''' = P_R \times \left(\frac{V_A}{V_R} \right)^2 \times \frac{1}{\lambda_C} \quad (2)$$

where P_R is the rated wattage, V_A is the actual voltage applied to the cartridge heaters, V_R is the rated voltage of the cartridge heaters, and λ_C is the circumferential volume of the heater. Figure 9 shows the path of heat flow with a generation rate of 4,758,644.021 W/m^3, the boiling apparatus exposed to air at 293 K with a heat transfer coefficient of 30 W/m^2*K.

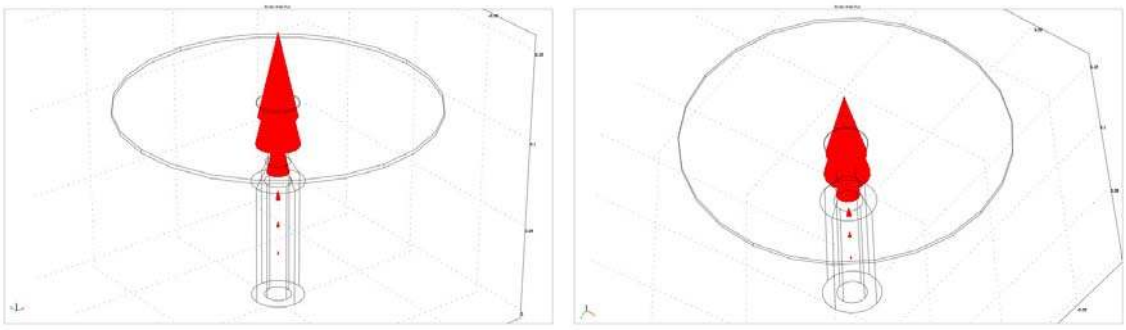

Figure 9: Path of Heat Flow

Figure 9 shows that although the copper sleeve is not insulated the majority of the heat flows upwards to copper hat and shows little heat flow outward into the stainless steel plate. Figure 10 shows the boiling apparatus's boundary temperature profile. The boiling apparatus is exposed to the same boundary conditions as Figure 9.

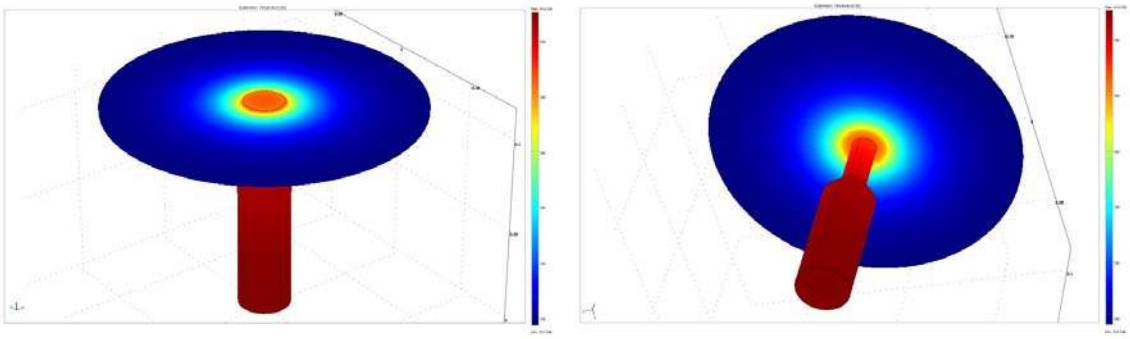

Figure 10: Boiling Apparatus Temperature Profile.

Figure 10 shows that there is very little spreading of the heat from the copper hat to the surrounding stainless steel. So the embedded cartridge heater is more than adequate to cause the copper hat to reach temperatures necessary for boiling. Figure 11 shows the boiling apparatus with water on the top surface. A slice plot was taken to show the temperatures through the water.

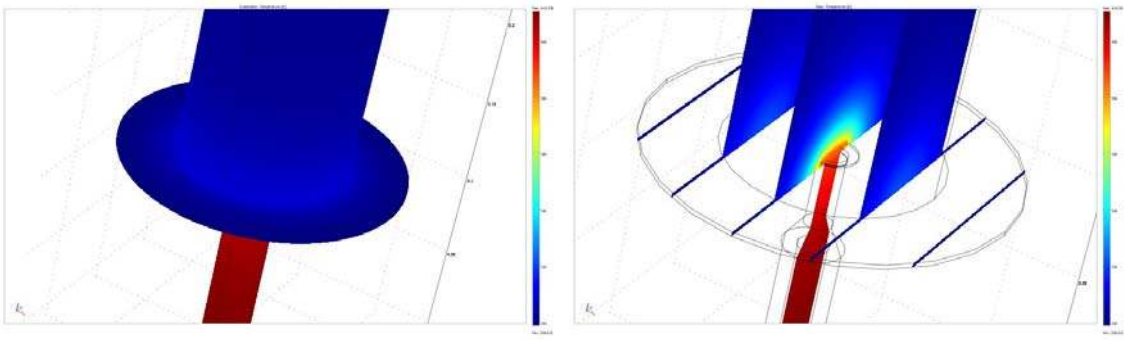

Figure 11: Water Temperature Profile.

Figure 11 shows that the water near the copper hat is hot enough to boil. However, the water around the stainless plate and above the copper hat is at a lower temperature than

the water near the copper hat, illustrating that this experiment produces the conditions associated with sub-cooled pool boiling adequately.

3.7 Thermocouple Calibration Procedure

Before the investigation was started, the thermocouples were checked for accuracy and variation. All 3 thermocouples were simultaneously placed in the same water bath of constant temperature for 10 minutes. During a 10 minute interval, the temperatures were monitored and $T_1 = 21.7673\ ^oC$, $T_2 = 21.9611\ ^oC$, $T_3 = 21.6149\ ^oC$. Since T_3 is closest to the surface, it was taken as absolute, thus $0.1524\ ^oC$ was subtracted from all temperatures recorded at T_1 and $0.3462\ ^oC$ from all temperatures recorded at T_2.

3.8 Experimental Procedure

Voltage was applied to the cartridge heater energizing it. The energized heater heated the copper sleeve resulting in the heating of the fluid. During the heating process, the temperatures were monitored by the thermocouples at the specified locations. When the temperatures reached steady state, they were recorded. Then the voltage applied to the heaters was increased again and the temperatures were monitored until steady state was again reached. The initial voltage applied to the cartridge heater was approximately 40 volts, and increased incrementally by approximately 3 volts. This process was repeated until 16 data points were captured, at which point the experiment was considered to be completed. Steady state was considered to be a two minute interval during which the temperatures of the thermocouples did not increase by more than $1\ ^oC$. The equipment was allowed to cool until safe to begin another experiment. A surface roughness measurement was taken of the boiling surface after each experiment. Using

the temperatures and the thermal resistances along the copper sleeve and copper hat, the heat transfer rates, then heat fluxes were calculated. The heat flux at the surface was plotted versus the excess temperature. Next using the Newton's Law of Cooling, the boiling heat transfer coefficient was calculated. A plot of the boiling heat transfer coefficient versus the heat flux was created. For each nanofluid concentration, two experiments were done and the results analyzed.

Chapter 4

Results and Discussion

4.1 Heat Transfer Calculations

For this investigation a one-dimensional conduction analysis was performed, using the principles of thermal circuits and thermal resistance to calculate the heat flux, surface temperature, and heat transfer coefficient on the boiling surface. Fourier's Law states that the one-dimensional heat transfer rate conducted through a solid is

$$q = -kA\frac{dT}{dx} \tag{3}$$

For a 1-D steady state analysis, equation (3) can be expressed as:

$$q = kA\frac{\Delta T_{A..B}}{L_{A..B}} \tag{4}$$

Where q is the heat transfer rate, k is the thermal conductivity, A is the cross sectional area normal to the direction of heat flow, $L_{A..B}$ is the distance heat travels, and $\Delta T_{A..B}$ is the temperature difference between points A and B. Equation (4) suggest a similar analogy between electrical energy and resistance, leading to the definition of thermal resistance

$$R_{th} \equiv \frac{\Delta T_{A..B}}{q} \tag{5}$$

For conduction, equation (5) becomes:

$$R_{cond} \equiv \frac{L_{A..B}}{kA} \tag{6}$$

Using equation (4), the thermal resistance between each thermocouple was calculated along the copper sleeve up until the copper hat. The 1-D thermal circuit analysis is for a constant cross sectional area, as you analyze the copper hat from top to bottom, the cross sectional area changes, negating the use of equation (6) to find the thermal resistance of the copper hat. However, equation (5) reveals that if a heat transfer rate was applied to a specimen and the resulting temperature difference was calculated between the surfaces where the heat transfer rate enters and leaves the specimen the thermal resistance can be calculated. Using COMSOL the above procedure was applied to the copper hat to determine its thermal resistance.

The copper hat was modeled to exact physical dimensions and insulated along the sides of the specimen. A convective heat transfer coefficient of 2500 W/m^2K was applied through a convective boundary condition to the top surface and a heat transfer rate was applied to the bottom of the copper hat. Figure 12 illustrates the copper hat modeled in COMSOL.

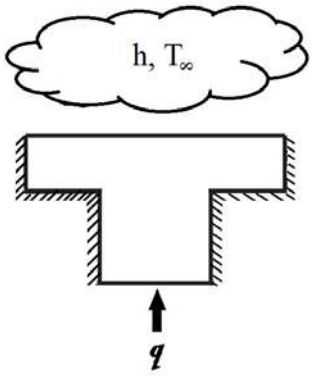

Figure 12: COMSOL Copper Hat Boundary Conditions

The COMSOL model used was a 3-D multiphysics, steady-state, conduction heat transfer analysis. All material properties were loaded from COMSOL's material database. Using COMSOL's post processing boundary integration function and the surface area of the specimen, the average temperature across the top and bottom surfaces were calculated for a particular heat transfer rate. The following Figures show the temperature profile on the copper hat with a heat transfer rate of 100 *W*.

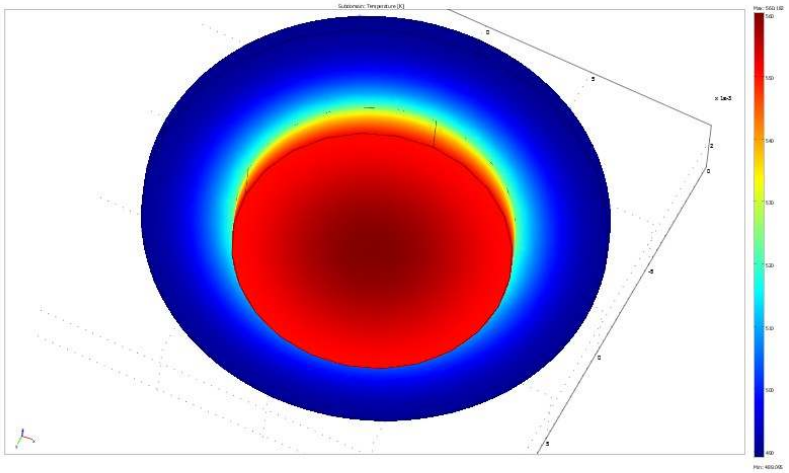

Figure 13: Boundary Temperature Profile at Bottom of Copper Hat.

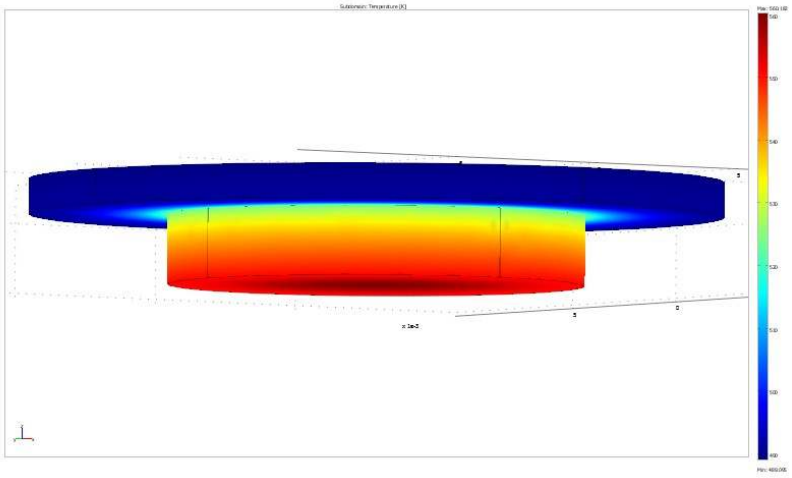

Figure 14: Boundary Temperature Profile at Side View of Copper Hat.

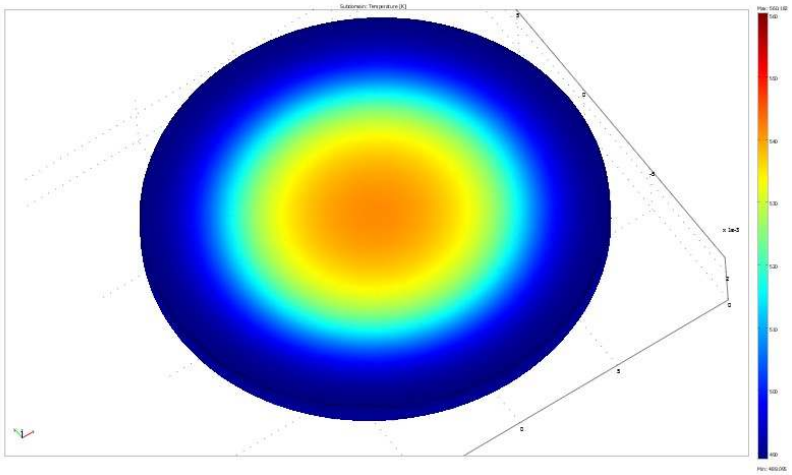

Figure 15: Boundary Temperature Profile at Top of Copper Hat.

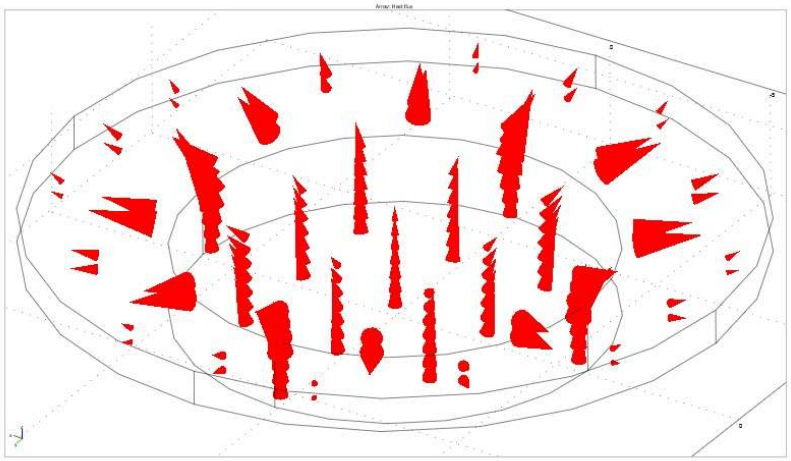

Figure 16: Heat Flux Path through Copper Hat.

Thermal resistance is a material and geometric property, where the value is constant regardless of specimen boundary conditions. However, since the temperatures used in equation (4) as T_A and T_B are actually the average temperature across the surfaces of the copper hat, the thermal resistance calculated will vary somewhat due to boundary conditions. To quantify the variation, the thermal resistance was calculated for a range of heat transfer rates from experimental data. The thermal resistance as a function of the heat transfer rate is shown in the Figure 17.

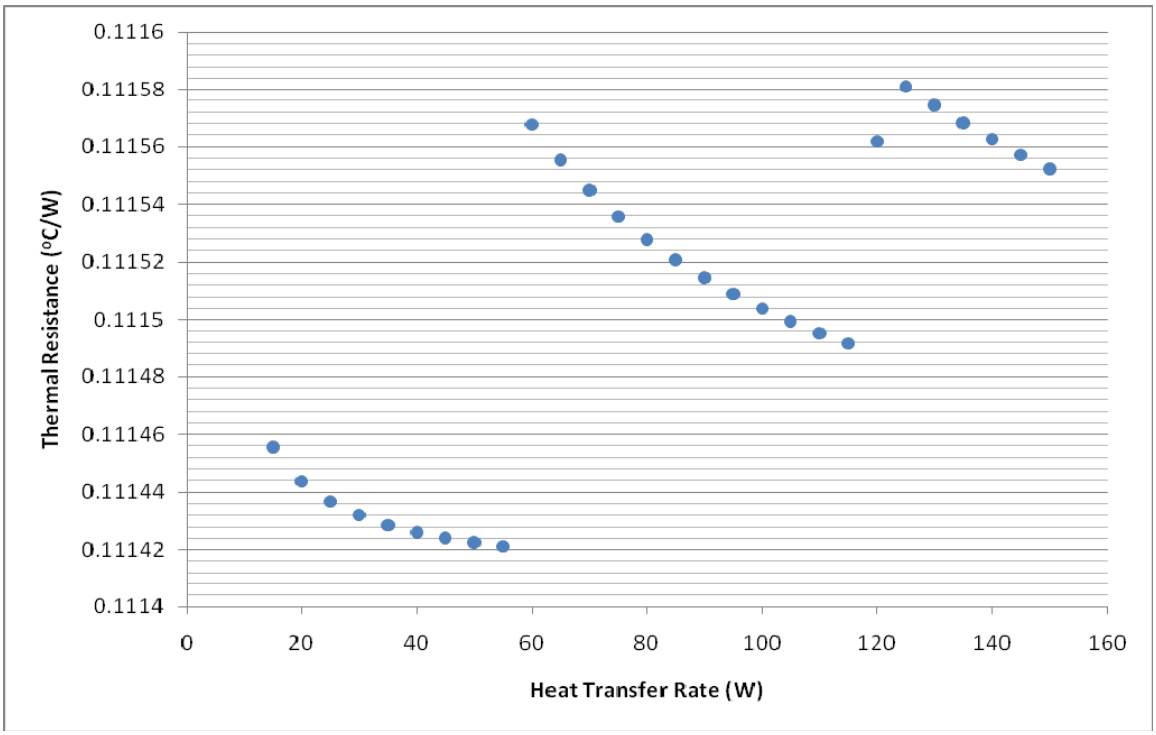

Figure 17: COMSOL Calculated Thermal Resistances

Figure 17 illustrates that the calculated thermal resistance of the copper hat, does indeed vary with the heat transfer rate. Analyzing the calculated thermal resistance in table 2, illustrates that although variation occurs with increasing heat transfer rate, the thermal resistance values does not begin to change until the fourth significant digit, located in the ten thousandths place, which will provide little change in any temperature or fluxes calculated using the calculated thermal resistance of the copper hat. Refer to appendix F for all data used in the COMSOL calculated thermal resistances.

Table 2: COMSOL Calculated Thermal Resistances

q (W)	R_{th} ($^oC/W$)	q (W)	R_{th} ($^oC/W$)	q (W)	R_{th} ($^oC/W$)	q (W)	R_{th} ($^oC/W$)
15	0.1114556	50	0.1114226	85	0.1115208	120	0.1115617
20	0.1114438	55	0.1114213	90	0.11151456	125	0.1115811
25	0.1114368	60	0.1115676	95	0.11150898	130	0.1115744
30	0.111432	65	0.1115554	100	0.11150395	135	0.1115683
35	0.1114287	70	0.1115449	105	0.11149941	140	0.1115626
40	0.1114261	75	0.1115358	110	0.11149527	145	0.1115572
45	0.1114242	80	0.1115278	115	0.1114915	150	0.1115523

Taking the variation of the calculated thermal resistance into account, the value of the calculated thermal resistance used in further calculations were chosen based on the following methodology: each experimental heat transfer rate ($q_{\exp}$) has a value between each heat transfer rate in Table 2 (q_L, q_H). If $q_{\exp} - q_L < 2.5W$ then $R_{th\_\exp} = R_{th\_L}$ and if $q_H - q_{\exp} \geq 2.5W$ then $R_{th\_\exp} = R_{th\_H}$.

With the thermal resistance of the copper hat determined the heat flux, excess temperature, and the heat transfer coefficient at the surface could now be calculated using thermal circuits.

In order to calculate the heat flux, excess temperature, and heat transfer coefficient at the boiling surface, the surface temperature at the boiling surface must be first calculated. Figure 18 is a suitable schematic for this investigation where T_1, T_2, T_3, are the temperatures at the thermocouples 23 *mm*, 13 *mm*, and 3 *mm* from the surface of the copper sleeve respectively. T_4 and T_5 are the temperatures at the bottom and top of the thermal paste layer between the copper sleeve and copper hat, while T_s is the temperature at the top of the copper hat. The surface temperature T_s, is determined by using the thermal circuit shown in Figure 18.

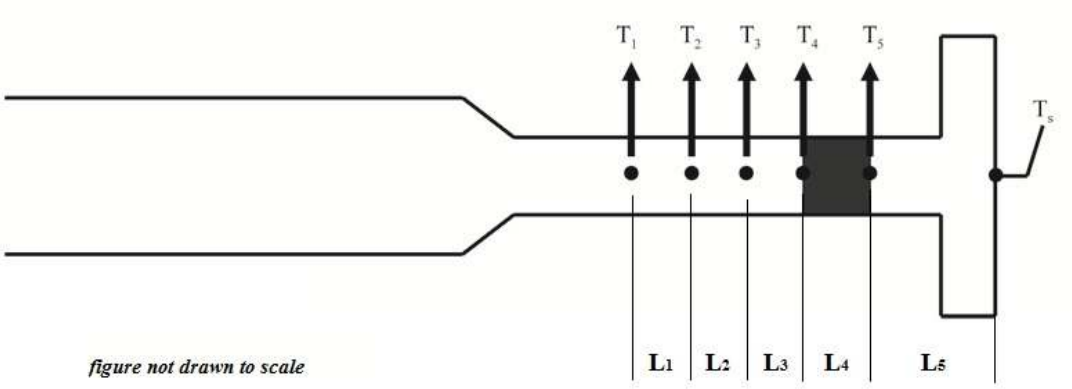

Figure 18: Thermal Circuit Schematic

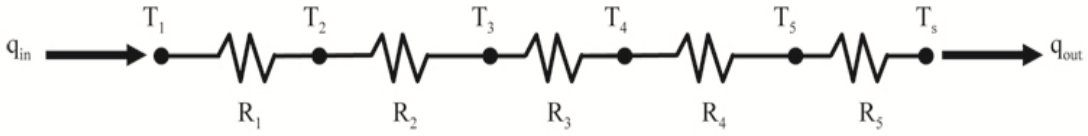

Figure 19: Thermal Circuit

The appropriate thermal circuit for this investigation is shown in Figure 19, where q_{in} is the heat transfer rate along the neck of the copper sleeve, generated from the embedded cartridge heater, and q_{out} is the heat transfer rate which is conducted out of the copper hat into the nanofluid. Arctic Silver®5 was used as thermal paste in this investigation and has a thermal conductivity value of *8.89 W/m*K* per 0.001 inch layer. As shown in Figure 18, *L* is the distance between thermocouples, where $L_1 = L_2 = 10\ mm$, $L_3 = 3\ mm$, and $L_4 = 0.0254\ mm$. As illustrated in Figure 19, *R* is the thermal resistance for each segment of the circuit. From equation (4) $R_1 = \frac{L_1}{k_1 \cdot A_1}$, $R_2 = \frac{L_2}{k_2 \cdot A_2}$, $R_3 = \frac{L_3}{k_3 \cdot A_3}$, $R_4 = \frac{L_4}{k_4 \cdot A_4}$ and $R_5 = R_{th\_comsol}$.

The method of thermal circuits applies to composite systems, in which equation (5) becomes

$$\sum R_{A..B} = \frac{\Delta T_{A..B}}{q} \tag{7}$$

Thermal resistances add like electrical resistances and for this investigation the thermal resistances are in series. Solving equation (7) for the heat transfer rate yields.

$$q = \frac{\Delta T_{A..B}}{\sum R_{A..B}} \tag{8}$$

Taking the heat transfer rate and dividing it by the cross sectional area normal to the direction of heat flow, defines the heat flux, q'' from a heated surface. The heat flux is expressed as

$$q'' = \frac{q}{A} \tag{9}$$

In this investigation, all calculations are based on the assumption that the heat transfer rate between the second and third thermocouple is equal to the heat transfer rate between the third thermocouple and the surface of the copper hat as shown in equation (10).

$$q_{2..3} = q_{3..S} \tag{10}$$

Thus, from Figure 19 and equation (10), equation (7), becomes

$$\sum R_{3..5} = \frac{\Delta T_{3..S}}{q_{2..3}} \tag{11}$$

Solving equation (11) for T_S yields

$$T_S = T_3 - (q_{2..3} \times \sum R_{3..5}) \tag{12}$$

Revisiting and using equation (7) to define the heat transfer rate between the first and second thermocouple yields

$$q_{2..3} = \frac{\Delta T_{2..3}}{R_2} \tag{13}$$

From equation (9) the heat flux at the copper surface is calculated to be

$$q''_s = \frac{q_{2..3}}{A_{copper\_hat}} \tag{14}$$

Finally, from equation (1) and (14), the heat transfer coefficient is determined to be

$$h = \frac{q''_s}{\Delta T_e} \tag{15}$$

4.2 Uncertainty Analysis

In the current investigation, the heat fluxes and the heat transfer coefficient for experimental data were reported. The uncertainty of those calculated values are presented.

Combining equation (5) and (9) defines the heat flux as

$$q'' = \frac{\Delta T_{A..B}}{R_{th} \cdot A} \tag{16}$$

Equation (16) indicates that the heat flux is a function of the temperature difference between the thermocouples ΔT, thermal resistance R_{th}, and cross sectional area normal to

the flow of heat transfer, A. Thus the uncertainty of the heat flux is calculated by the following equation

$$U_{q''} = q'' \times \sqrt{\left(\frac{U_{\Delta T_{A..B}}}{\Delta T_{A..B}}\right)^2 + \left(\frac{U_{R_{th}}}{R_{th}}\right)^2 + \left(\frac{U_A}{A}\right)^2} \tag{17}$$

The temperature change between thermocouples, thermal resistance, and area all have uncertainties associated with them which are $U_{\Delta T_{A..B}}$, $U_{R_{th}}$ and U_A respectively. The uncertainty associated with temperature difference is determined as follows. First, recall that

$$\Delta T_{A..B} = T_A - T_B \tag{18}$$

From equation (18) the uncertainty of the temperature difference is calculated to be

$$U_{\Delta T_{A..B}} = \sqrt{\left(U_{T_A}\right)^2 + \left(U_{T_B}\right)^2} \tag{19}$$

Since all temperatures were measured with type K thermocouples, the uncertainty for $U_{T_A} = U_{T_B} = 0.4\%$ of the temperature reading.

The uncertainty of the thermal resistance, $U_{R_{th}}$, can be calculated by first reevaluating equation (6) and it is clear that the thermal resistance is a function of the distance, L, between thermocouples, thermal conductivity, *k*, and cross sectional area, A, then the uncertainty of the thermal resistance is

$$U_{R_{th}} = R_{th} \times \sqrt{\left(\frac{U_L}{L}\right)^2 + \left(\frac{U_k}{k}\right)^2 + \left(\frac{U_A}{A}\right)^2} \tag{20}$$

The uncertainty of L is associated with the instrument used to measure the distance L. In this investigation L was measured with a digital caliper. The uncertainty of the digital caliper is taken to be half of the resolution of the measuring device, which is $U_L = \frac{1}{2}(0.00001m)$. The value of the thermal conductivity, *k*, is taken to be a constant material property therefore $U_k = 0$. The uncertainty associated with the area is determined by first defining the area. In this investigation the cross sectional area normal to the heat flux is

$$A = \frac{\pi D^2}{4} \tag{21}$$

From equation (21) the area is a function of the diameter therefore the uncertainty of the area calculation is

$$U_A = 2A \times \left(\frac{U_D}{D} \right) \tag{22}$$

where U_{D_c} is the uncertainty associated with measurement of the diameter of the test specimens. The same digital calipers used to measure the distance L, were used to measure the diameter of the copper hat, thus $U_D = U_L = \frac{1}{2}(0.00001m)$. With all the parameters of equation (17) defined, the uncertainty of the heat flux calculation can be readily determined. Refer to appendix C for heat flux uncertainty analysis data.

Revisiting equation (15), the heat transfer coefficient is a function of the heat flux at the heated surface, q'' and excess temperature ΔT_e. Therefore, the uncertainty of the heat transfer coefficient is determined to be

$$U_h = h \times \sqrt{\left(\frac{U_{q''}}{q''}\right)^2 + \left(\frac{U_{\Delta T_e}}{\Delta T_e}\right)^2} \tag{23}$$

where, $U_{q''}$ is calculated from equation (17). In order to find $U_{\Delta T_e}$, one must look at the following equation, derived from equation (1)

$$\Delta T_e = T_S - T_{sat} \tag{24}$$

From equation (24) the uncertainty of the excess temperature is

$$U_{\Delta T_e} = \sqrt{\left(U_{T_S}\right)^2 + \left(U_{T_{sat}}\right)^2} \tag{25}$$

where $U_{T_S} = 0.4\%$ of the temperature reading and $U_{T_{sat}} = 0$. For a detailed list of the heat transfer coefficient uncertainty data refer to appendix D. Using the formulae above, the uncertainty of each data point was calculated and plotted using error bars in the experimental results section.

4.3 Surface Roughness Measurement Results

As stated in chapter 1, there are several factors that influence boiling heat transfer. Of them, the number of nucleation sites might be the most important. In this investigation, surface roughness measurements were made to characterize the surface. More specifically surface roughness is defined as the measurement of vertical deviation

of a real surface from its ideal surface. There are several roughness parameters that can be used to report this deviation. The most common parameter, which is used in this investigation, is the Ra value. The Ra value is defined as the arithmetic average of the vertical deviation from the mean line established in a surface roughness measurement and has units of length, usually μm.

Table 3: Surface Roughness Data

	Initial Ra value	Ra value after experiment	Ra value after cleaning	% of Initial Ra value
H_2O	1.25 (μm)	1.25 (μm)	1.25 (μm)	-
0.1% wt NF	1.25 (μm)	1.09 (μm)	1.21 (μm)	96.80%
0.2% wt NF	1.21 (μm)	1.01 (μm)	1.18 (μm)	97.52%
0.3% wt NF	1.18 (μm)	0.95 (μm)	1.13 (μm)	95.76%
0.4% wt NF	1.13 (μm)	0.85 (μm)	1.06 (μm)	93.81%

As presented in the literature review of chapter 2, the use of nanofluids in convective heat transfer experimentation has a direct effect on the heated surface, usually leaving a smoother surface at the end of experimentation compared to pre-experimentation. Table 3 shows that this phenomenon also occurred in this investigation, as the surface of the copper hat became smoother, indicated by a lower Ra value after experimentation. The reason the surface becomes smoother is that the nanoparticles are several magnitudes smaller than the surface roughness of the copper hat. When the nanofluid evaporates at the boiling surface, it leaves behind nanoparticles that adhere to the boiling surface. This build up of nanoparticles on the boiling surface introduces a

new contact resistance, reducing heat transfer. Since aluminum oxide nanoparticles were used in this investigation which has a considerably lower thermal conductivity value than copper, the nanoparticle layer further reduces heat transfer performance. Also, a smoother surface reduces nucleation site density, the physical locations at which the boiling process begins.

It is clear that the build up on nanoparticles on the boiling surface must be addressed. A cleaning procedure, outlined in section 3.4 was used to address the nanoparticles deposited on the boiling surface after experimentation. Table 3 shows that the cleaning procedure restored most of the surface's initial roughness. Therefore the copper hat continues to serve as a baseline specimen for this investigation.

4.4 Experimental Heat Flux Results

For this investigation, each nanofluid concentration and de-ionized water pool boiling experiment was conducted twice. Before applying any voltage to the heater, the fluid level was marked on the glass container. Once the experiment started, vapor began to escape slowly. When the nanofluid level dropped 2 *mm* below the initial fluid level de-ionized water was added through the rubber tubing in an effort to keep the nanofluid concentration consistent. At approximately 73 volts, or after 12 data points were taken, it became clear that no matter how much de-ionized water was added to the nanofluid, significant vapor was escaping. Therefore, the true concentration of the nanofluids from approximately 73 volts and above, cannot be reported with the same level of confidence as with lower voltages.

In this investigation, boiling heat flux and convective heat transfer coefficient curves using de-ionized water were generated and compared to curves generated from nanofluids with 0.1%, 0.2%, 0.3%, and 0.4% wt concentrations under the same conditions. The results of this investigation are presented below. Unfortunately, during the 0.1% wt nanofluid experiments, the thermocouples malfunctioned at 67 volts causing an error in the recorded temperatures from that point forward. Therefore, only the first ten data points of each experiment are used to compare and analyze the results. For a complete representation using all sixteen data points, please refer to appendices A and B.

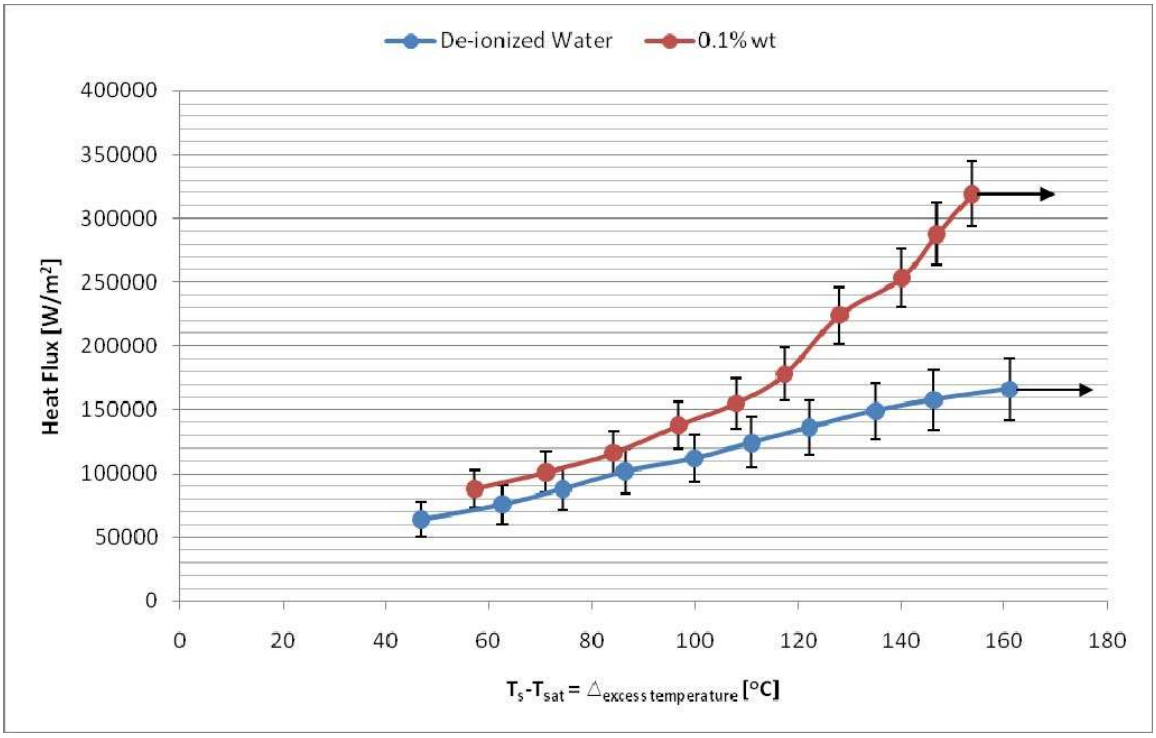

Figure 20: Heat Flux Curve of De-Ionized Water vs 0.1% wt Nanofluid

The data shows a noticeable increase in the heat flux generated at the copper hat's boiling surface when using 0.1% wt nanofluid versus de-ionized water. In general, the heat flux increased by an average of 52.9%. The highest heat flux generated by using

0.1% wt nanofluids is 319,234.82 W/m^2 compared to de-ionized water at 166,097.73 W/m^2 which corresponds to an increase in the heat flux by 92.2%. The minimum generated heat flux for 0.1% wt nanofluids is 88,114.46 W/m^2, whereas the lowest value for de-ionized water is 63,991.9 W/m^2, corresponding to a 37.7% increase in the generated heat flux. The data also reveals a slow, steady increase in the nanofluid generated heat flux, compared to water, followed by a sudden dramatic 43.2% to 64.7% increase in the heat flux from the sixth data point to the seventh. Afterward, the heat flux continues to increase at a steady rate for the remainder of the experiment. One possible reason for the sudden increase could be related to nanoparticle deposition. As evident by table 3 and the photos in Appendix D, nanoparticles adhere to the boiling surface during experimentation, which suggest that nanoparticles may fall out of suspension during experimentation. It is possible that when a certain heat flux is reached, there is enough fluid movement and there now exists convection currents strong enough to prevent further nanoparticle deposition on the heated surface. The sudden dramatic increase in the heat flux might correspond to this reaching this unique heat flux.

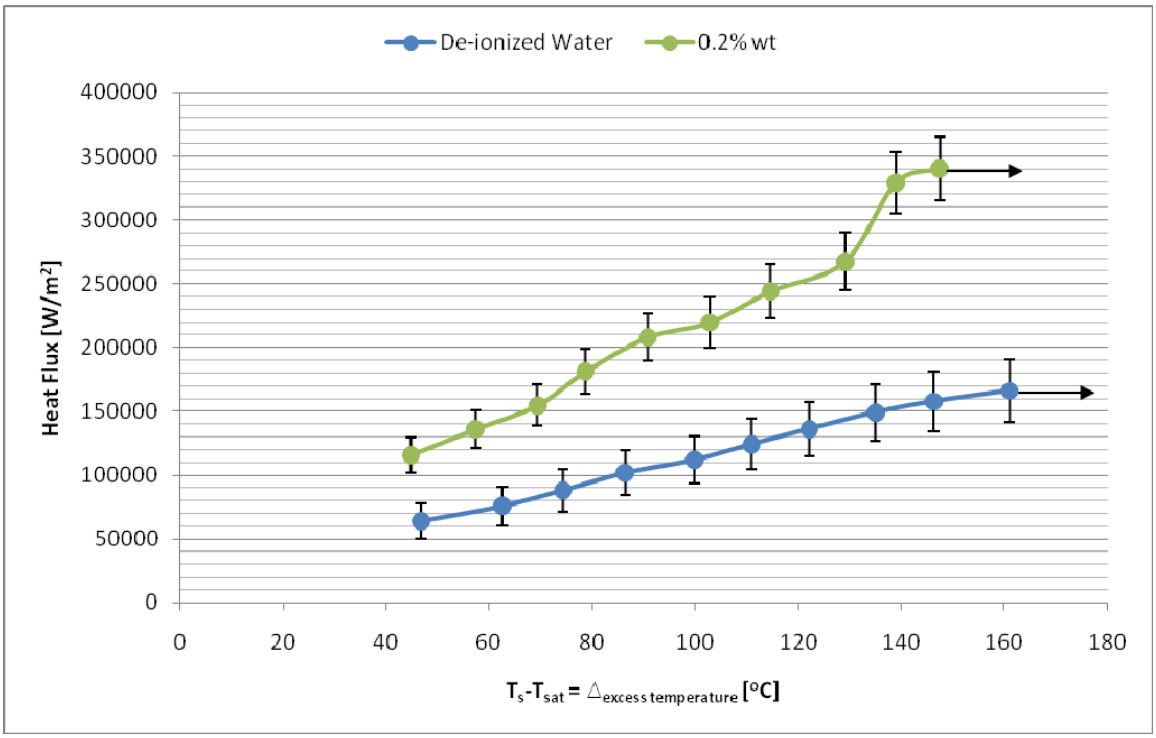

Figure 21: Heat Flux Curve of De-Ionized Water vs 0.2% wt Nanofluid

The data shows an even more noticeable increase in the heat flux generated at the copper hat's boiling surface when using 0.2% wt nanofluid versus de-ionized water than compared to 0.1% wt nanofluid. In general, the heat flux increased by an average of 85%. The maximum generated heat flux from 0.2% wt nanofluid is 340,412.42 W/m^2 which is a 105% increase when compared to the maximum heat flux generated using de-ionized water. Similarly the minimum generated heat flux from using 0.2% wt nanofluid is 116,004.81 W/m^2 which is an 81.3% increase when compared to de-ionized water. Also, akin to the generated heat flux curve from 0.1% wt nanofluid, there is a sudden dramatic increase in the generated heat flux from 79.3% to 108.9%. However, unlike the 0.1% wt nanofluid, the sudden increase in the generated heat flux occurred at a much higher heat flux, which corresponds to greater input power from the variable

autotransformer used to heat the copper hat. One possible explanation for the latter is again related to nanoparticle deposition. As evident in table 3, the surface roughness decreased by a greater amount than it in did when compared to 0.1% wt nanofluid. Thus a thicker layer of nanoparticles were deposited on the boiling surface. It is possible that more thermal energy was required to reach the fluid state related to the dramatic increase in the heat flux first seen in the 0.1% wt nanofluid experiment.

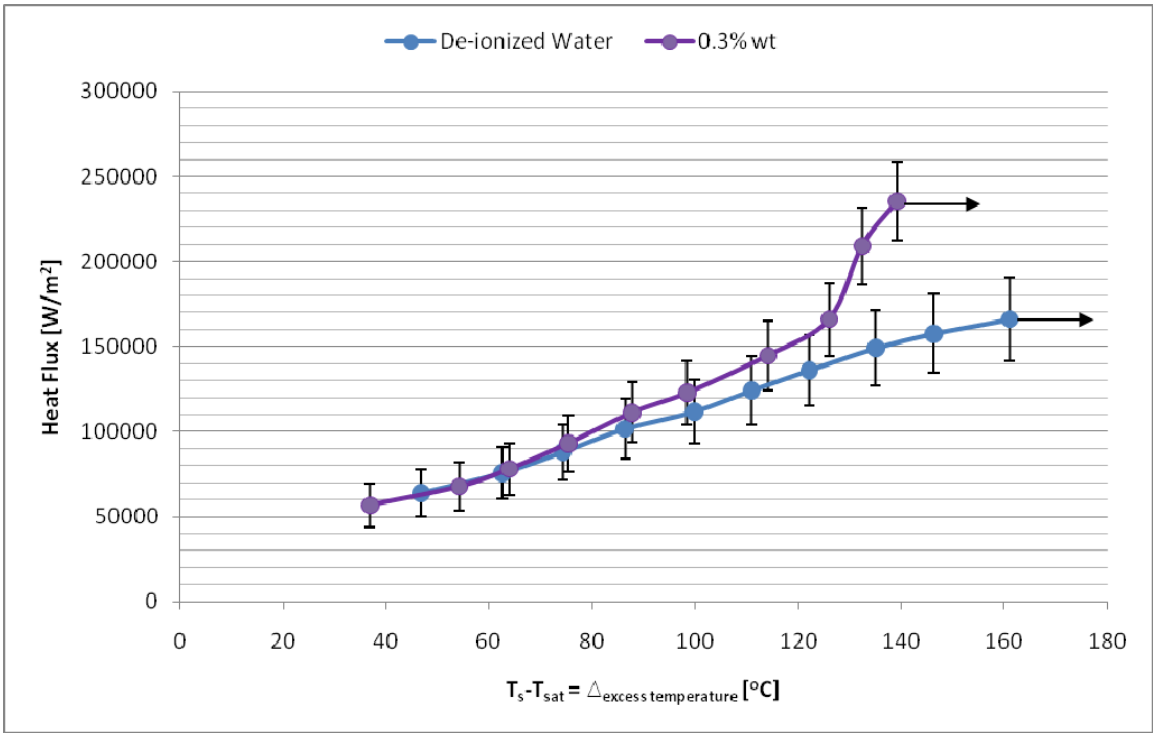

Figure 22: Heat Flux Curve of De-Ionized Water vs 0.3% wt Nanofluid

Unlike the generated heat fluxes from 0.1% and 0.2% wt nanofluid the enhancement from using 0.3% wt nanofluid over de-ionized water is not as remarkable. The average increase in the generated heat flux is 4.84%, which is a 48% decrease in the effectiveness of the use of nanofluids when compared to 0.1% wt nanofluid and an 80% decrease compared 0.2% wt nanofluid. The minimum generated heat flux from using

0.3% wt nanofluid is 56,773.9 W/m^2 which is a decrease of 11.3% when compared to de-ionized water. Despite the initial decrease in the generated heat flux, the data does show a steady increase in the heat flux versus de-ionized water as more power is supplied to the boiling apparatus via the autotransformer. The greatest generated heat flux was 235,491.59 W/m^2 which is 41.8% greater than the maximum generated heat flux using de-ionized water. Identical in behavior to 0.1% wt and 0.2% wt nanofluid experimental data, there is a sudden dramatic increase in the generated heat flux near the end of data collection. The sudden dramatic increase in the generated heat flux for 0.3% wt nanofluid is from 11.3% to 32.6%. It is clear however, that heat flux enhancement from using 0.3% wt nanofluids is not as great as 0.1% and 0.2% wt nanofluids. One possible reason the enhancement is not as great as the lower nanofluid concentrations is that, as evident by table 3, the surface roughness value decreased by an even greater amount than previous experiments. Perhaps the thickness of this nanoparticle layer deposited on the surface is significant enough to reduce heat transfer performance. Another possible reason for lesser heat flux enhancement is that perhaps the nanoparticles began to fall out of suspension during the pool boiling experiment. In this investigation, nothing was done to keep the nanoparticles in suspension besides ultrasonication. Ultrasonication may not be enough to keep the particles in suspension for the duration of the experiment for this particular concentration of nanoparticles. Although evidence of the nanoparticles falling out of suspension was not easily observed during experimentation, the duration of the experiment increased with each increase in nanofluid concentrations as it took longer to reach steady state for each data point.

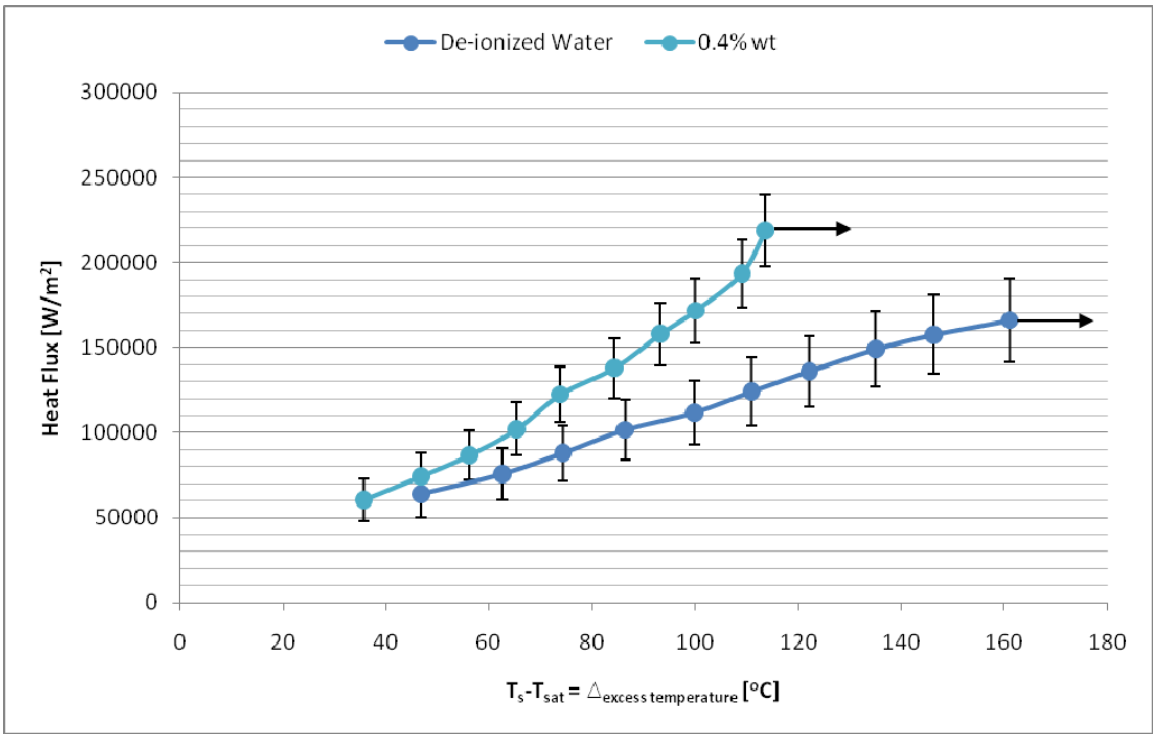

Figure 23: Heat Flux Curve of De-Ionized Water vs 0.4% wt Nanofluid

The 0.4% wt nanofluid performed similarly to 0.3% wt nanofluids when compared to the generated heat fluxes from 0.1% and 0.2% wt nanofluids, with an average heat flux enhancement of 9.81%, a decrease in effectiveness of 43.1% from 0.1% wt nanofluid and 79.2% from 0.2% wt nanofluid, compared to heat fluxes generated from using de-ionized water. The minimum heat flux generated was 60,585 W/m^2, a 5.3% decrease in the heat flux when compared to the de-ionized water at the same applied wattage from the autotransformer. Nevertheless, the data did show an increase in the generated heat flux as the experiment continued as the highest heat flux generated was 218,716.95 W/m^2, 31.7% higher than the maximum heat flux generated from de-ionized water. For this particular nanofluid concentration, it there is not a sudden dramatic increase in the heat flux compared to the previous experiments of this investigation. The

greatest increase is again at the end of data collection with an increase in the heat flux from 22.8% to 31.7%. This 8.9% increase is not as significant when compared to the sudden dramatic increase in the heat flux of lower concentrations, all of which have been characterized by an increase of at least 21.2%. Interestingly, the heat fluxes generated from 0.4% wt nanofluid, although greater than de-ionized water, are lower than then the heat fluxes generated from 0.3% wt nanofluid. This decrease in the heat flux possibly suggests that the nanoparticles might be falling out of suspension. The more concentrated nanofluid might have allowed for a greater amount of nanoparticles to fall out suspension. Also the 0.4% wt nanofluid pool boiling experiment took the longest to complete. The latter reasons, combined with a thicker nanoparticle layer deposited on the copper hat, as evident by Table 3, might explain why the 0.4% wt nanofluid produced lesser heat fluxes than the 0.3% wt nanofluid.

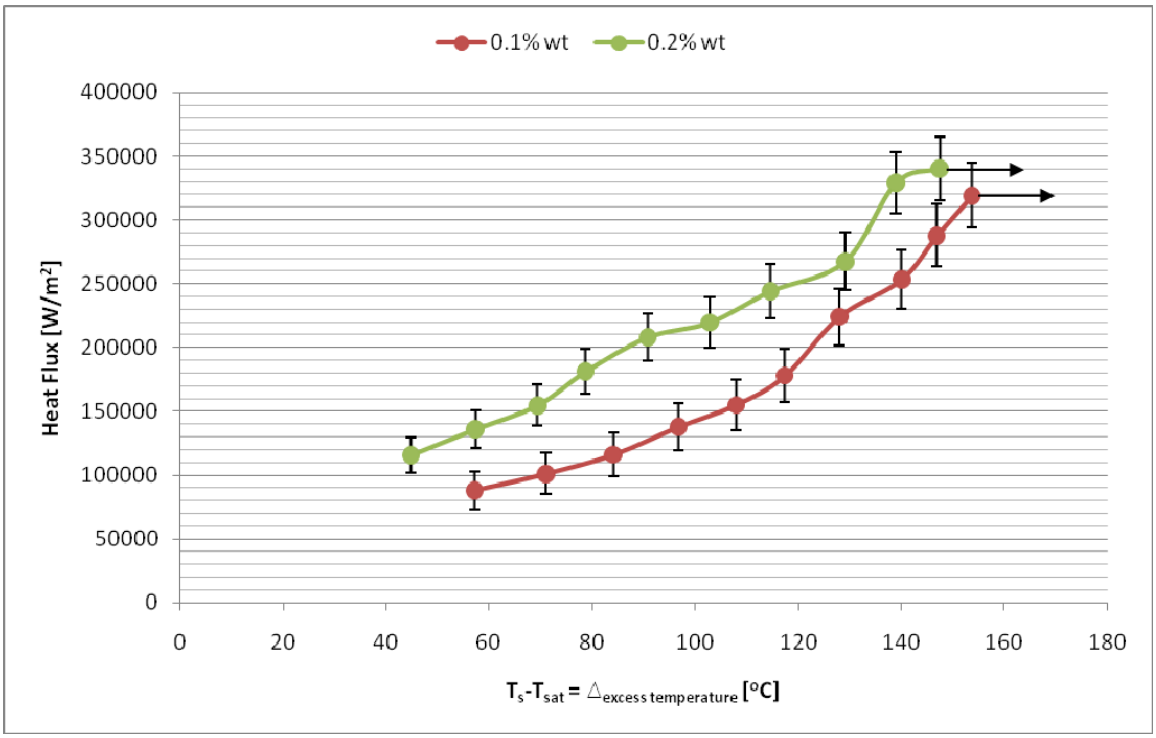

Figure 24: Heat Flux Curve 0.1% wt vs 0.2% wt Nanofluid

As evident from Figures 20-23, the 0.2% wt nanofluid showed the greatest heat flux enhancement. Figure 24 compares 0.2% to 0.1% wt nanofluid. The 0.2% wt generated heat fluxes an average of 22.4% greater than 0.1% wt nanofluid. The difference in performance between nanofluids cannot be characterized by a constant factor as one might presume. Initially, the 0.2% wt nanofluid heat flux enhancement is nearly a constant 31% for 60% of the data points. The remaining 40% of data points show a near constant enhancement of about 8.8%. Varying enhancement suggest that pool boiling with nanofluids might be best described by transient-like condition as first suggested by Kwark, *et al.* It also suggests that nanofluid enhancement is a function of several unique variables as opposed to a single mechanism.

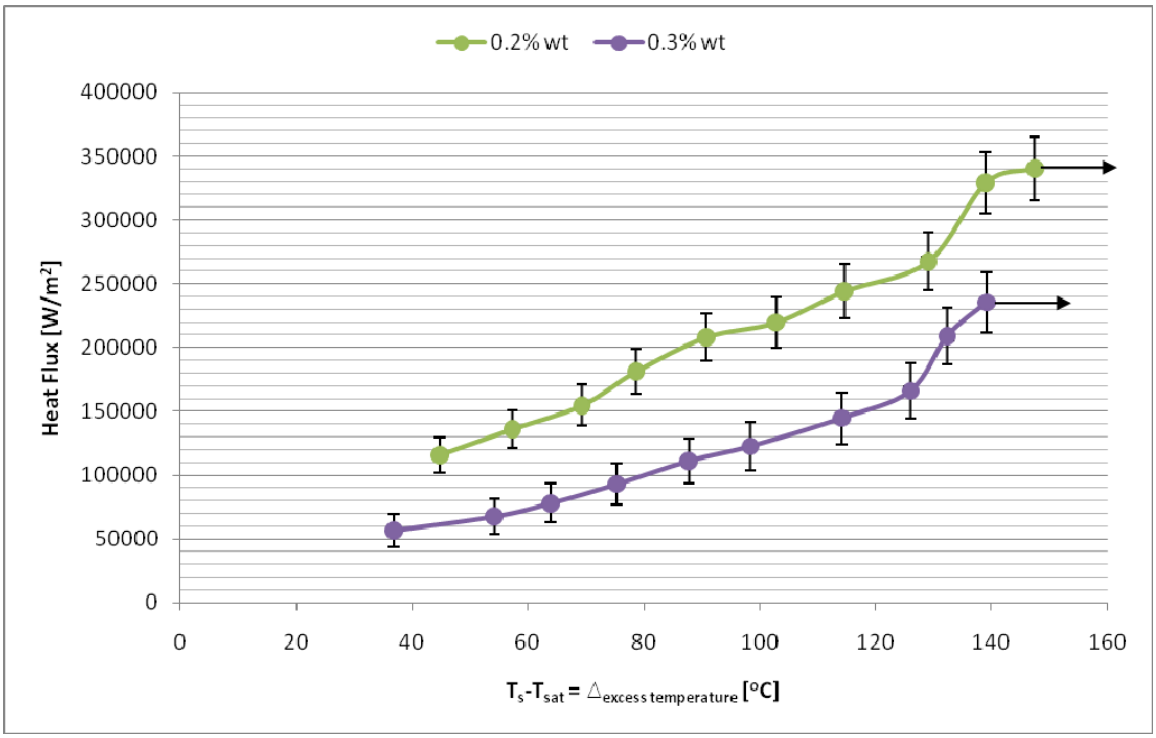

Figure 25: Heat Flux Curve 0.2% wt vs 0.3% wt Nanofluid

Figure 25 compares the boiling performance of 0.2% wt to 0.3% wt nanofluid. On average, the 0.2% wt nanofluid provided heat fluxes 79% greater than 0.3% wt nanofluid. Heat flux enhancement varied from point to point, again suggesting transient characteristics, and decreased from 104.3% to 44.6% from beginning of experimentation to the end. The shapes of the boiling curves are nearly identical, which might suggest that the nanofluid concentrations are close to an optimum value as the transient conditions are parallel. Analogous transient boiling characteristics also suggest that the optimum concentration is between 0.2% and 0.3%. The 0.3% wt nanofluid can be almost be classified as a downwards shift of the 0.2% wt nanofluid curve. This possibly suggests that a single mechanism may be responsible for the deterioration of the boiling curve. The increase in the thickness of the nanoparticle layer deposited on the boiling

surface may be the main cause of the deterioration as the contact resistance introduced by nanoparticle deposition became significant enough to affect heat transfer performance.

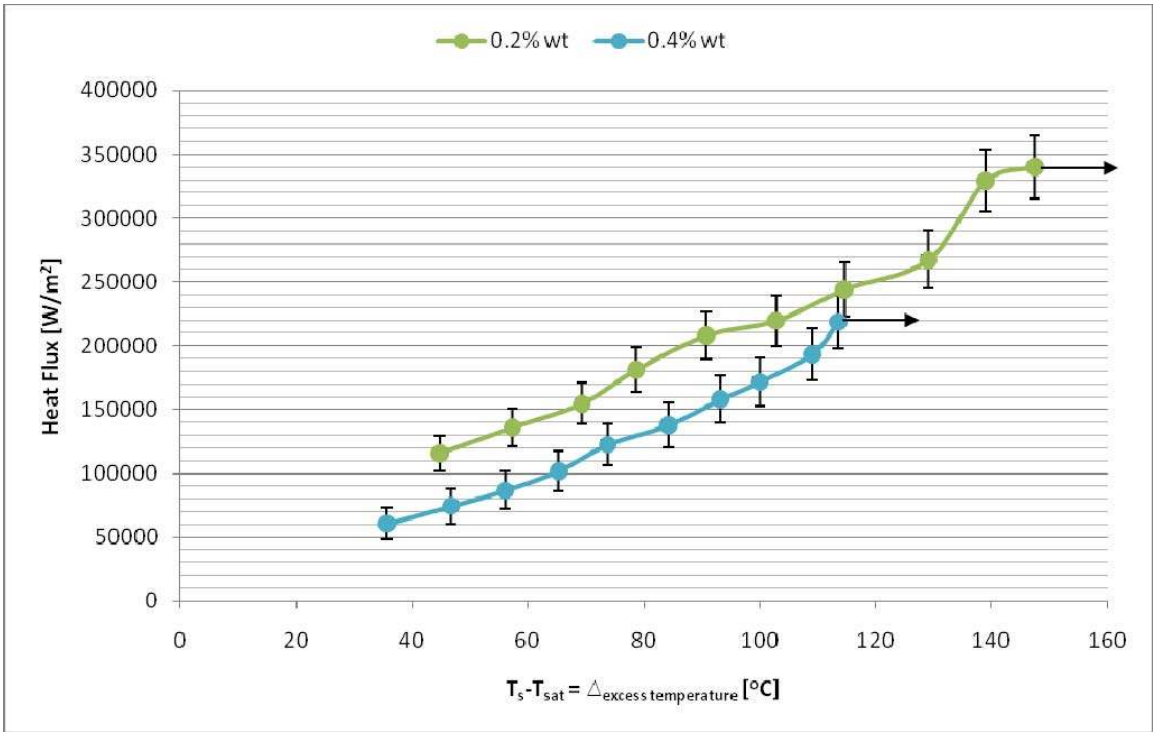

Figure 26: Heat Flux Curve 0.2% wt vs 0.4% wt Nanofluid

Figure 26 compares the boiling performance of 0.2% wt nanofluid to that of 0.4% wt nanofluid. In Figure 26 it is clear that 0.2% wt nanofluid has more significant heat flux enhancement over 0.4% wt nanofluid with an average enhancement of 69.5%. Also, the boiling characteristic of the curve changed significantly when compared to previous nanofluid concentrations which suggest that a significant change in the mechanism of enhancement has occurred. The change of surface roughness might possibly be the most direct cause for the change in shape of the boiling curve, as the surface roughness decreased the most during the 0.4% wt nanofliud experiment. Interestingly, the heat fluxes generated for the 0.4% wt nanofluid were the lowest of all nanoparticle

concentrations. Smaller heat fluxes may be attributed to this concentration having the greatest decrease in the surface roughness. A decrease in the surface roughness corresponds to an increase in the nanoparticle layer deposited on the surface. 0.4% wt nanofluid had the greatest decrease in the surface roughness; hence it had the thickest nanoparticle build up on the surface, which creates a greater thermal resistance for heat to conduct though at the boiling surface. This particular nanoparticle layer might have completely changed the characteristics of the boiling curve. It is worth noting that the 0.4% wt nanofluid had the lowest excess temperatures of all nanofluids, meaning that the boiling surface reached steady state at lower temperatures. This phenomenon can become important when dealing with devices or equipment with low melting temperatures. However, the goal of this investigation is to solely increase the boiling heat flux and boiling heat transfer coefficient. Addressing and quantifying the excess temperatures enhancement is outside the scope of this investigation.

Overall, the addition of aluminum oxide nanoparticles had a positive effect on the boiling curve for de-ionized water as nanofluids generated higher heat fluxes for the same applied input power. The results of this investigation are agreement with the findings of Kwark *et al*. Kwark *et al.* suggest that a possible reason for nanofluid heat flux enhancement is that during pool boiling experimentation, with very small nanoparticle concentrations, a layer of nanopaticles are deposited on the boiling surface. The nanoparticle layer which is created, increases the wettability of the surface by improving the contact angle of the fluid flowing across the surface. The deposited nanoparticles also create a porous sorportion layer which is characterized by cavities on the order of μm. Fluids flowing though the sorportion layer become trapped in the micro sized

cavities; therefore fluids are kept in contact with the boiling surface longer, effectively removing more heat. However, as nanoparticle concentration increases, the sorportion layer deposited on the boiling surface becomes characterized by cavities on the order of nm. Fluid flow is hindered by the nm sized cavities and heat transfer begins to deteriorate. Additionally, the sorportion layer becomes thicker, creating a new thermal interface layer which introduces a greater contact resistance, further reducing heat transfer performance. Kwark *et al.* suggest that there must exist an optimum nanoparticle concentration that corresponds to maximum heat flux enhancement and minimal thermal resistance effects. This rationale possibly explains why the 0.3% and 0.4% wt nanofluid showed inferior performance to 0.1% and 0.2% wt nanofluids. Perhaps the optimum nanoparticle concentration is closer to 0.2%, and if concentrations > 0.4% were used, the heat flux enhancement might become inferior to de-ionized water.

4.5 Experimental Heat Transfer Coefficient Results

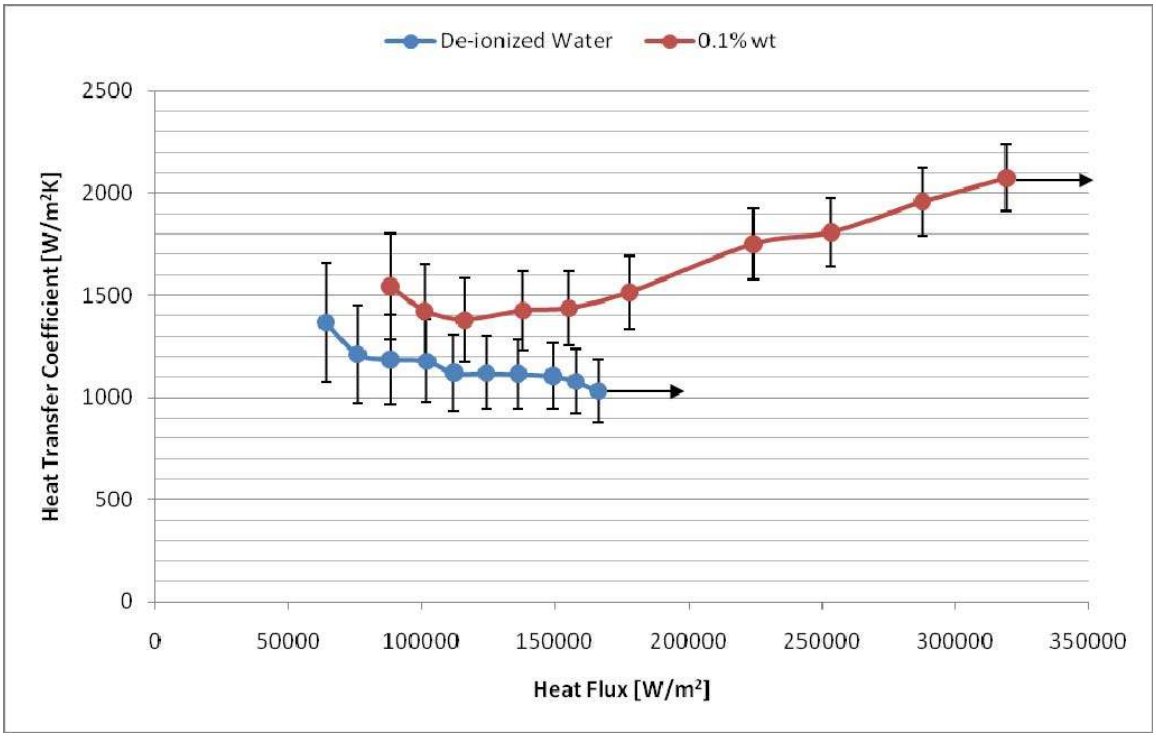

Figure 27: Heat Transfer Coefficient Curve of De-Ionized Water vs 0.1% wt Nanofluid

Figure 27 compares the heat transfer coefficient curves of de-ionized water to that of 0.1% wt nanofluid. Comparatively speaking, the heat transfer coefficient of 0.1% wt nanofluid was on average 43.5% greater than that of de-ionized water. De-ionized water produced lower heat transfer coefficients as the heat flux increased. Conversely, 0.1% wt nanofluids, after an initial decrease, generated increasingly higher heat transfer coefficients as the heat flux increased. The initial increase in the heat flux was 12.8%, but increased to 101.3% by the end of data collection. The reason for the increase is that the heat flux was increasing at a greater rate than the excess temperature, producing high heat transfer coefficients. The de-ionized water heat transfer coefficient decreased because the excess temperatures were increasing at a greater rate than the heat fluxes.

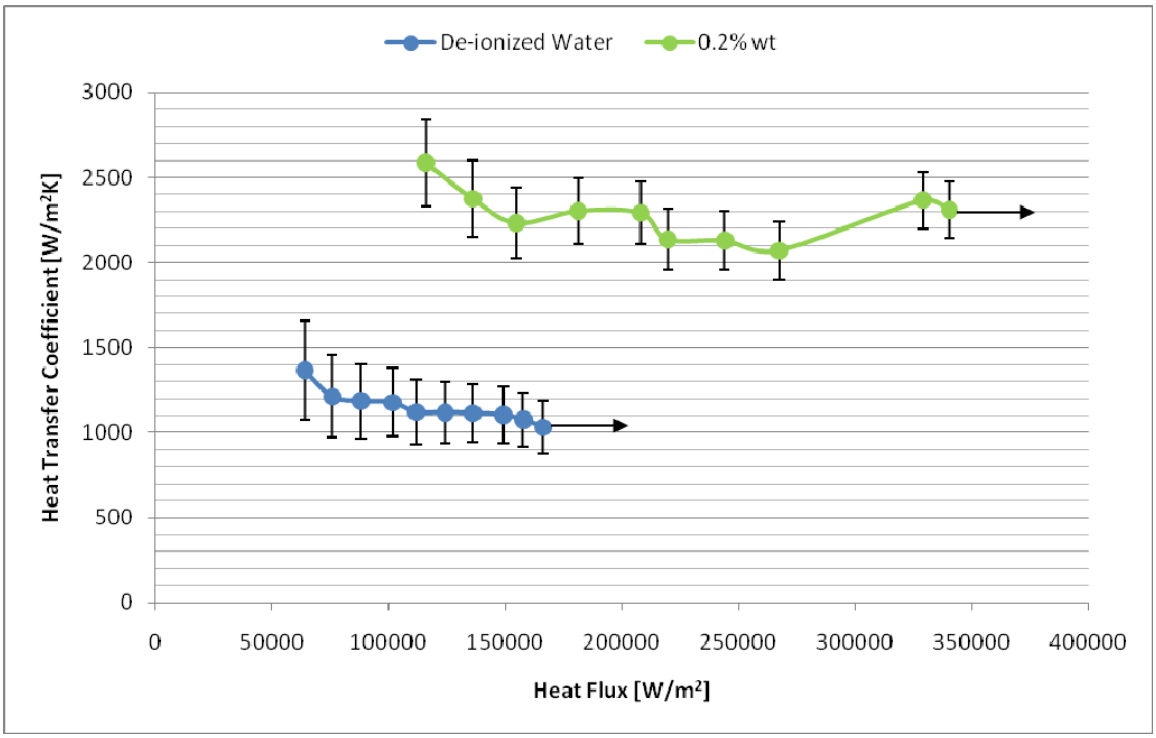

Figure 28: Heat Transfer Coefficient Curve of De-Ionized Water vs 0.2% wt Nanofluid

Figure 28 compares the heat transfer coefficients of de-ionized water to those of 0.2% wt nanofluid. It is clear that the heat transfer coefficients from the 0.2% wt nanofluids are significantly higher than those of de-ionized water with an average increase of 98.6%, more than twice that of 0.1% wt nanofluid. Also, excluding 30% of the initial data points, the heat transfer coefficients of 0.2% wt nanofluid were nearly constantly. This means that the generated heat fluxes and excess temperatures were increasing at an almost equal rate.

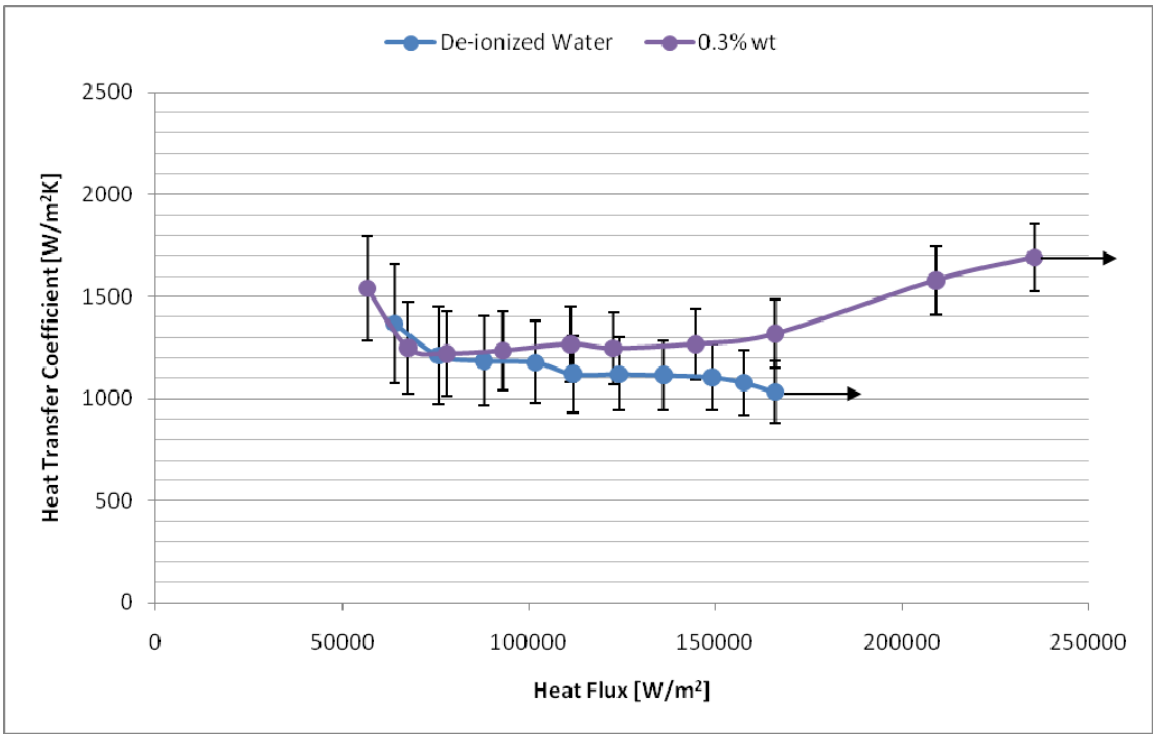

Figure 29: Heat Transfer Coefficient Curve of De-Ionized Water vs 0.3% wt Nanofluid

Figure 29 compares the heat transfer coefficients of de-ionized water to those of 0.3% wt nanofluid. The heat transfer coefficients of 0.3% wt nanofluid were greater than those of de-ionized water for all data points. The average increase in the heat transfer coefficient was 19.2%. This percentage is somewhat misleading as the last 2 data points indicate remarkable enhancement of 46.5% and 64%, while in actuality 70% of the data show an enhancement in the heat transfer coefficient of 8.8%. This small enhancement shows that this particular nanofluid concentration had little effect on the heat transfer coefficient for heat fluxes in this range. The last two data points suggest that 0.3% wt nanofluids may be more effective in heat fluxes above 150,000 W/m^2. Also, the heat transfers coefficients were mostly uniform for most of the data collection indicating that both the heat fluxes and excess temperatures increased at a nearly the same rate.

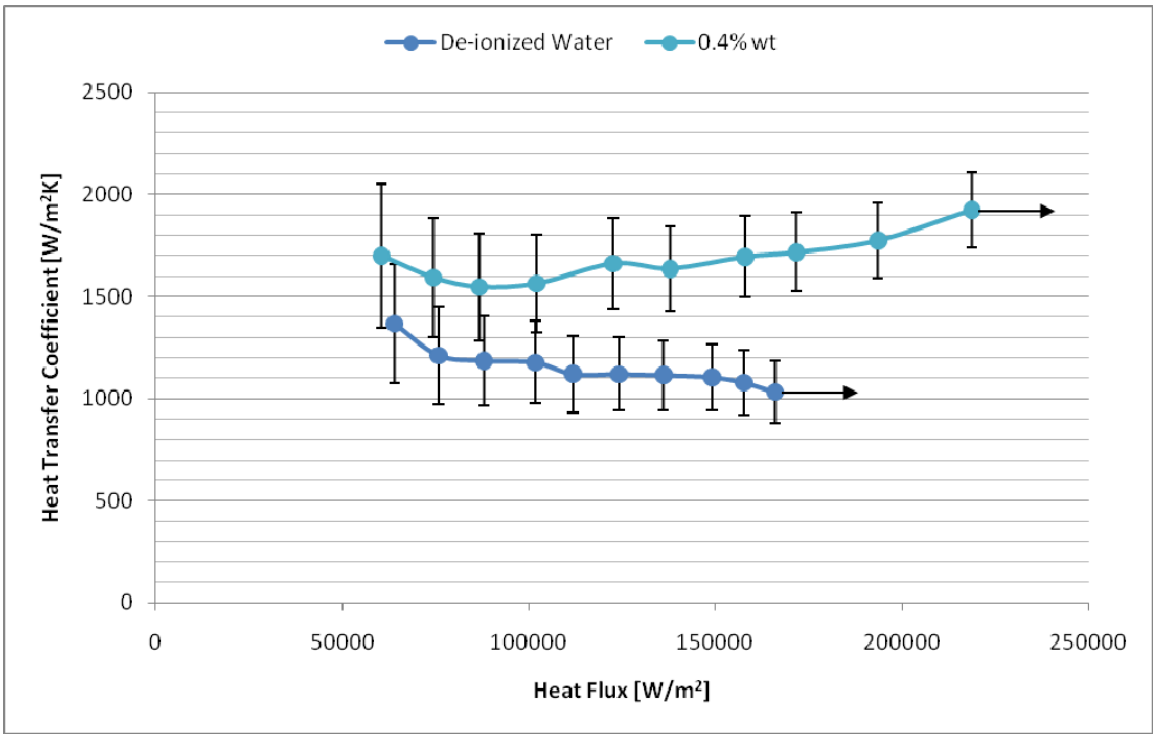

Figure 30: Heat Transfer Coefficient Curve of De-Ionized Water vs 0.4% wt Nanofluid

Figure 30 compares the heat transfer coefficients of de-ionized water to those of 0.4% wt nanofluids. The average increase in the heat transfer coefficient is 47.2%. Unlike 0.2% and 0.3% wt nanofluid concentrations, where the heat transfer coefficients were nearly constant for the duration of experimentation, the 0.4% wt concentration was shown to be increasing linearly throughout data collections. Although, 0.2% wt nanofluid showed the most significant enhancement overall, the trend of the 0.4% wt data is arguably more significant as it represents the ideal heat transfer scenario. The increasing heat transfer coefficient is due to the fact that the heat flux is increasing at a greater rate than the excess temperatures. A greater amount of heat is being removed per increase in excess temperatures, which is wholly significant in real world applications whereas surface temperatures of high heat flux apparatus must always be considered.

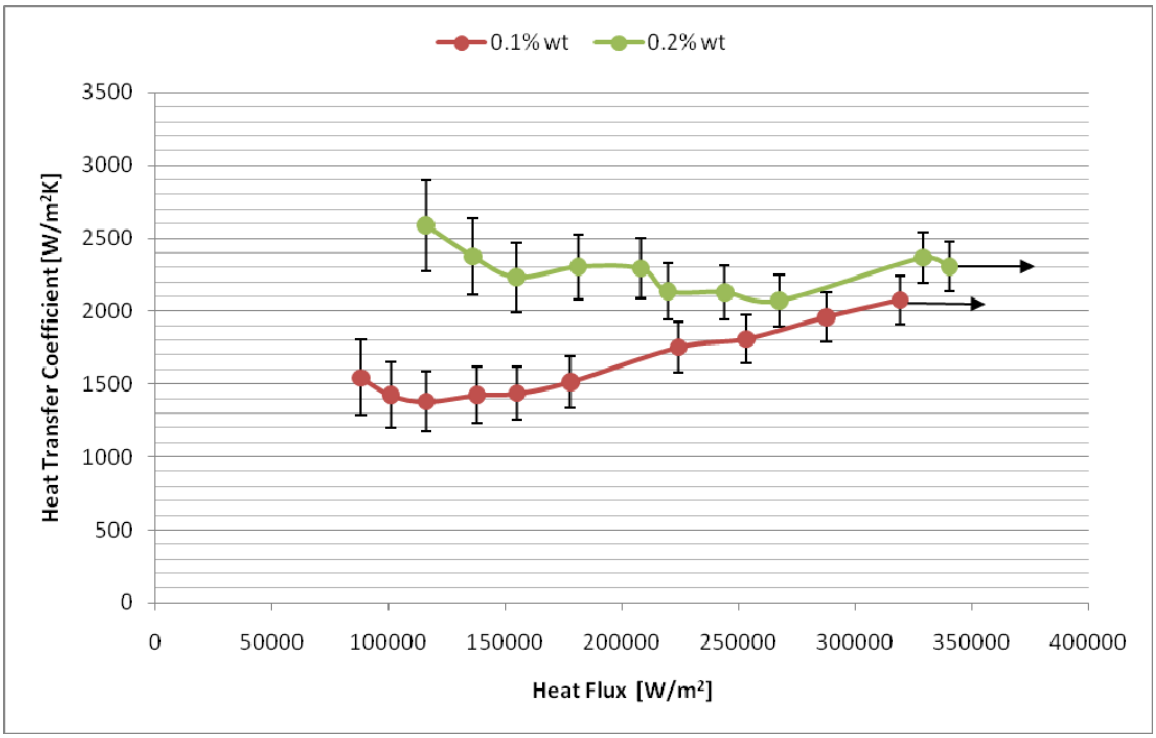

Figure 31: Heat Transfer Coefficient Curve 0.1% wt vs 0.2% wt Nanofluid

Figure 31 compares the heat transfer coefficients of 0.1% wt nanofluid to those of 0.2% wt nanofluid. As evident in the Figure, 0.2% performed better overall with an average enhancement over 0.1% of 42.7%. However, it also clear that the percentage increase is steadily decreasing over time as the increase dropped from 67.7% to 11.2%. It is entirely possible that if more experimentation were to occur the heat transfer coefficient of 0.1% wt nanofluid might begin to become greater than 0.2% wt. These trends suggest that although the concentrations used are differentiated by a factor of only 2, they still readily affect the boiling performance of the nanofluids.

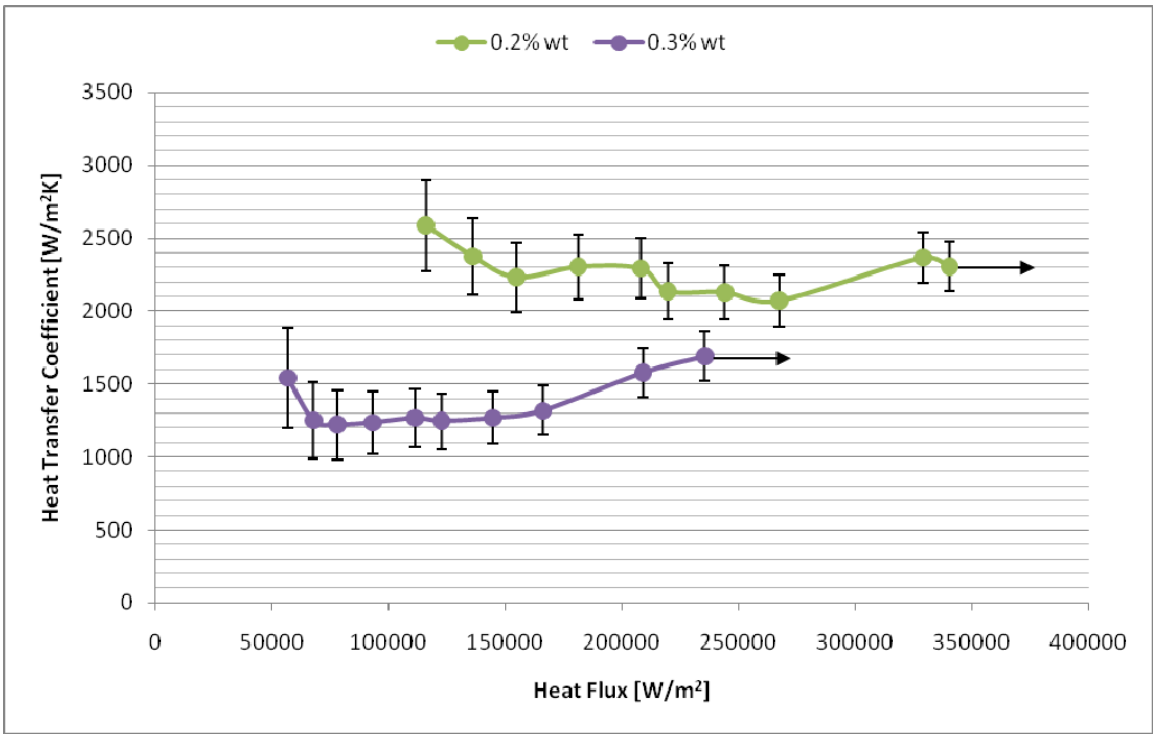

Figure 32: Heat Transfer Coefficient Curve 0.2% wt vs 0.3% wt Nanofluid

Figure 32 compares the heat transfer coefficients generated from 0.2% wt nanofluids to those of 0.3% wt nanofluid. The 0.2% wt heat transfer coefficients were on average 69.1% greater than those of 0.3% wt nanofluid. This percentage of enhancement is more representative of the physical processes that occurred during experimentation, as both 0.2% and 0.3% wt nanofluid produced nearly constant heat transfer coefficients for the length of experimentation. It is possible that since both concentrations produced nearly constant heat transfer coefficient, that both concentrations are affecting the same mechanism of heat transfer enhancement.

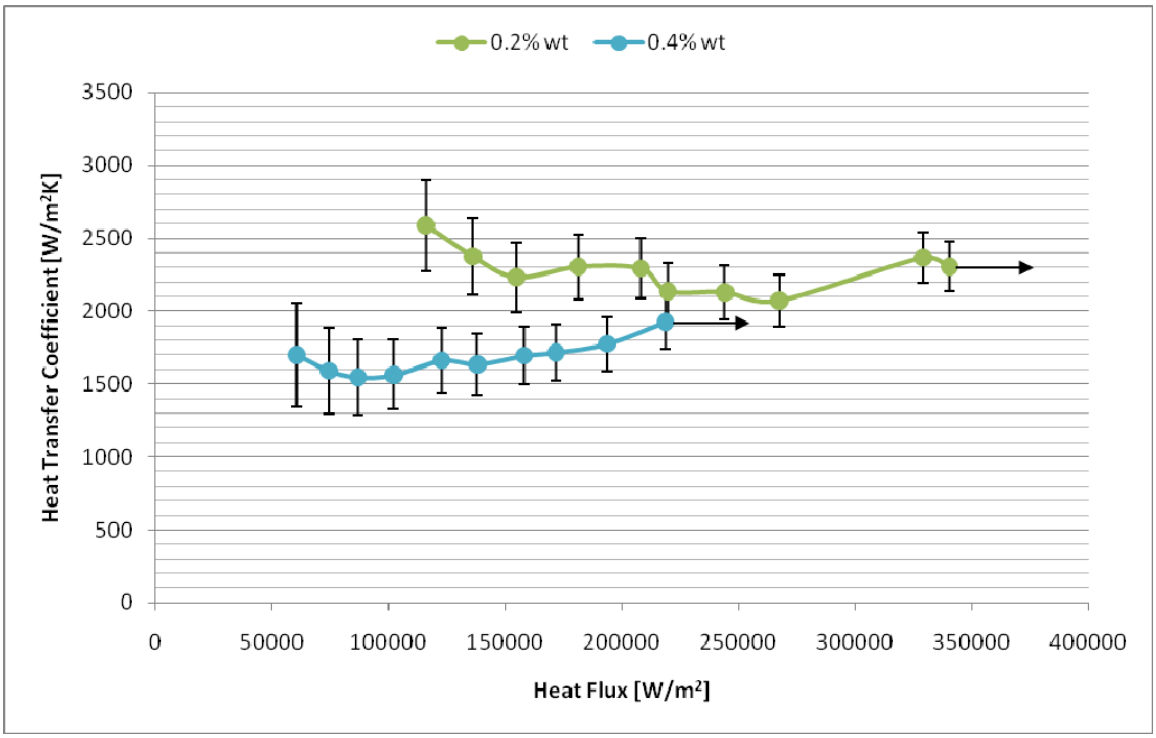

Figure 33: Heat Transfer Coefficient Curve 0.2% wt vs 0.4% wt Nanofluid

Figure 33 compares the heat transfer coefficients of 0.2% wt nanofluid to those of 0.4% wt. The 0.2% wt nanofluid showed an average increase of 36.1% when compared to the heat transfer coefficients from 0.4% wt nanofluid. This percentage is 1.9 times less than the enhancement determined from 0.2% wt heat flux enhancement versus 0.4% heat flux generation. Perhaps heat flux and heat transfer coefficient nanofluid enhancement are inversely related. Additionally, the 0.4% wt nanofluid heat transfer curve is similar in behavior to 0.1% wt nanofluid, with increasing heat transfer coefficients over time. If the trend of the data continues, it is possible that if higher heat fluxes were generated, then 0.4% wt might surpass 0.2% wt nanofluid heat transfer coefficients. Figures 27-33 do not readily point towards an optimum concentration, as Figures 20-26 do with nanofluid heat flux enhancement.

Chapter 5

Conclusions and Recommendations

5.1 Conclusions

In conclusion, the additions of aluminum oxide nanoparticles to de-ionized water were able to improve the boiling curve of de-ionized water. Nanofluids with concentrations of 0.1%, 0.2%, 0.3%, and 0.4% on mass basis created with a base fluid of de-ionized water, were used in this investigation. All of the nanofluids provided better performance compared to de-ionized water. The greatest heat flux enhancement was observed from the 0.2% wt nanofluid, which produced an average increase in the heat flux of 85%, followed by 0.1% wt with an average heat flux increase of 53%. Next was 0.4% wt with an average increase in the heat flux of 9.8%, and lastly 0.3% wt nanofluid with an average enhancement of 4.8%. One possible reason for nanofluid heat flux enhancement is that the nanoparticles deposited on the boiling surface change the surface characteristics of the surface, improving the wettability of the boiling surface. The improved wettability of the boiling surface allows the nanofluild to stay in contact longer with the surface, effectively removing more heat.

The addition of aluminum oxide nanoparticles to de-ionized water also increased the boiling heat transfer coefficients of de-ionized water. The 0.2% wt nanofluid performed the best, with an average increase in the heat transfer coefficient of 98.6%, followed by 0.4% with average increase of 47.2%. Next was 0.1% with an average

increase of 43.5% and lastly was 0.3% with average an increase of 19.2%. The order of the enhancement due to different concentrations changed when comparing heat flux enhancement and heat transfer coefficient enhancement. This observation suggests that their respective mechanisms of enhancement are affected differently. Therefore, it is better to choose a specific nanofluid to enhance either the heat flux or heat transfer coefficient, unlike in this investigation, whereas a single nanofluid was used to simultaneously enhance both the heat flux and heat transfer coefficient.

5.2 Recommendations

In investigations similar to the current study, it would be important to design a complete closed loop system that quickly causes the escaping vapor to condense, in order to maintain the nanoparticle concentrations. Specifically, for this investigation, a condenser could be added to prevent condensation of the fluid around the surrounding glass, but instead on the condenser, allowing the fluid to drop directly back in the liquid.

Also it would be important to use a single piece of copper as the boiling surface, to minimize the effects of contact resistance, allowing the researcher to get better estimation of heat fluxes, heat transfer coefficients, and surface temperatures. For this investigation, a single piece of copper was insufficient, due to leakage problems from the inability to seal the copper sleeve to the stainless steel plate. A single piece of copper that overcomes the sealant issues presented in this investigation will provide a better test specimen.

Thermal paste was used in this investigation. Although great care was taken to use the same amount for each experiment, the fact that the thermal paste came in tubular

form, made it difficult to apply the same amount in a uniform thickness each time. Since the thermal paste layer resistance is critical to heat transfer calculations, thermal pads could make a better choice due to more uniform dimensions.

Also, the orientation of the boiling surface could be changed. The current investigation has the boiling surface upwards facing allowing bubble formation to develop, detach and flow away from the surface. If the boiling surface was inverted or orientated on its side then direction of bubble flow and convection currents become more important. Different orientations can provide insight to how boiling would occur under different conditions.

In this investigation, the effects of surface roughness were reported. The average roughness value was measured before and after experimentation, then cleaned before another experiment, if nanofluids were used in a closed device such as a heat pipe, surface cleaning would not be possible. In the future one could investigate the pool boiling if the boiling surface was not cleaned to determine boiling performance, as surface roughness increases or decreases over time.

Increasing the nanoparticles concentration beyond 0.3% starts to deteriorate the boiling curve. Any future efforts to enhance the boiling curve should explore concentrations closer to 0.2% with an upper concentration limit of 0.25%. Also, future efforts to improve the boiling heat transfer coefficients should be done with nanofluid concentrations close to 0.1% and 0.4% as both concentrations showed promise to surpass 0.2 % at heat fluxes higher than those achieved in this investigation. Therefore, a future boiling apparatus should be designed to allow for much greater applied heat fluxes.

References

1. H.U. Kang, S.H. Kim, J.M. Oh, Estimation of Thermal Conductivity of Nanofluid using Experimental Effective Particle Volume, Experimental Heat Transfer 19 (2006) 181-191.

2. P. Keblinski, S.R. Phillpot, S.U.S. Choi, J.A. Eastman, Mechanisms of Heat Flow in Suspensions of Nano-sized Particles (nanofluids), Int. Journal of Heat and Mass Transfer. 45 (2002) 855-863.

3. B-X. Wang, L-P. Zhou, X-F. Peng, A Fractal Model for Predicting the Effective Thermal Conductivity of Liquid with Suspension of Nanoparticles, Int. Journal of Heat and Mass Transfer. 46 (2003) 2665-2672.

4. Y. Xuan, W. Roetzel, Conceptions for Heat Transfer Correlation of Nanofluids, Int. Journal of Heat and Mass Transfer. 43 (2000) 3701-3707.

5. H. Kim, J. Kim, M.H. Kim, Effect of Nanoparticles on CHF Enhancement in Pool Boiling of Nano-fluids, Int. Journal of Heat and Mass Transfer. 49 (2006) 5070-5074.

6. I.C. Bang, S.H. Chang, Boiling Heat Transfer Performance and Phenomena of Al2O3-Water Nano-fluids from a Plain Surface in A Pool, Int. Journal of Heat and Mass Transfer. 48 (2005) 2407-2419.

7. Z-H. Liu, Y-H Qiu, Boiling Heat Transfer Characteristics of Nanofluids Jet Impingement on a Plate Surface, Heat Mass Transfer. 43 (2007) 699-706.

8. H. Kim, M. Kim, Experimental Study of the Characteristics and Mechanism of Pool Boiling CHF Enhancement using Nanofluids, Heat Mass Transfer.

9. S.K. Das, N. Putra, W. Roetzel, Pool Boiling Characteristics of Nano-fluids, Int. Journal of Heat and Mass Transfer. 46 (2003) 851-862.

10. M. Chopkar, A.K. Das, L. Manna, P.K. Das, Pool Boiling Heat Transfer Characteristics of ZrO2-Water Nanofluids from a Flat Surface in a Pool, Heat Mass Transfer.

11. S-C. Tzeng, C-W. Lin, K.D. Huang, Heat Transfer Enhancement of Nanofluids in a Rotary Blade Coupling of Four-Wheel-Drive Vehicles, Acta Mechanica. 179 (2005) 11-23.

12. D. Wen, Y. Ding, Effect of Particle Migration on Heat Transfer in Suspensions of Nanoparticles Flowing through Minichannels, Microfluid Nanofluid. 1 (2005) 183-189.

13. K. Narayan Prabhu, Peter Fernades, Nanoquenchants for Industrial Heat Treatment, Journal of Materials Engineering and Performance, (2007).

14. C. Choi, H.s. Yoo, J.M. Oh, Preparation and Heat Transfer Properties of Nanoparticles –in-Transformer Oil Dispersions as Advanced Energy-Efficient Coolants, Current Applied Physics. (2007).

15. Min-Shen Liu, Mark Ching-Cheng Lin, C.Y. Tsai, Chi-Chuan Wang, Enhancement of Thermal Conductivity with Cu for Nanofluids using Chemical Reduction Method, Int. Journal of Heat and Mass Transfer. 49 (2006) 3028-3033.

16. R.J. Goldstein, W.E Ibele, S.V. Patankar, T.W. Simon, T.H. Kuehn, P.J. Strykowski, K.K. Tamma, J.V.R Herberlein, J.H. Davidson, J. Bischof, F.A. Kulacki, U. Kortshangen. S. Garrick, V. Srinivasan, Heat Transfer- A review of 2003 Literature, Int. Journal of Heat and Mass Transfer. 49 (2006) 451-534.

17. D.P. Kulkarni, R.S. Vajjha, D.K. Das, D. Oliva, Application of Aluminum Oxide Nanofluids in Diesel Electric Generator as Jacket Water Coolant, Applied Thermal Engineering (2007).

18. Shiro Nukiyama, The Maximum and Minimum Values of the Heat Q Transmitted from Metal to Boiling Water under Atmospheric Pressure, Japan Society of Mechanical Engineers. 37 (1934) 367-374.

19. Incropera, Frank P., Dewitt David P., "Modes of Pool Boiling" Introduction to Heat Transfer, 4th edition John Wiley & Sons (2002) 560-563.

20. J. Haung, X. Wang, Influence of pH on the Stability Characteristics of Nanofluids, Photonics and Optoelectronics (2009).

21. K.B. Anoop, T. Sundaraajan, Sarit K. Das, Effect of Particle Size on the Convective Heat Transfer in Nanofluid in the Developing Region, International Journal of Heat and Mass Transfer (2009).

22. J. Hone, M.C. Llaguno, M.J. Biercuk, A.T. Johnson, B. Batlogg, Z. Benes, J.E. Fischer, Thermal Properties of Carbon Nanotubes and Nanotube-Based Materials,l Applied Physics. 74 (2002) 339-343.

23. S. Berber, Y.K. Kwon, D. Tomanek, Physical Review Letters 84, (2000) 4613.

24. Xiang-Qi Wang, Arun S.Mujumdar, Heat Transfer Characteristics of Nanofluids: A Review, International Journal of Thermal Sciences. 46 (2007) 1-19.

25. Y. Xuan, Q. Li, Heat Transfer Enhancement of Nanofluids, International Journal of Heat and Fluid Transfer. 21 (2000) 58-64.

26. S.M.S. Murshed, K.C. Leong, C Yang, Enhanced Thermal Conductivity of TiO_2-Water Based Nanofluids, International Journal of Thermal Sciences 44. (2005) 367-373.

27. Y.J. Hwang, Y.C. Ahn, H.S. Shin, C.G. Lee, G.T. Kim, H.S. Park, J.K. Lee, Investigation on Characteristics of Thermal Conductivity Enhancement of Nanofluids, Current Applied Physics, in press.

28. S. M. Kwark, R. Kumar, G. Moreno, J. Yoo, S. M. You, Pool Boiling Characteristics of Low Concentration Nanofluids, International Journal of Heat and Mass Transfer. 53 (2010) 972-981.

Appendices

Appendix A: Heat Flux, Heat Transfer Coefficient Calculations

Table A: De-Ionized Water Data Calculations

De-ionized Water												
P_R	V_A	V_R	P_A	q	L_1	L_2	L_3	L_4	L_5	k_1	k_2	k_3
750	40.4	120	85.00833	85.00833	0.01	0.01	0.003	2.54E-05	0.003	401	401	401
750	43.4	120	98.10208	98.10208	0.01	0.01	0.003	2.54E-05	0.003	401	401	401
750	45.9	120	109.7297	109.7297	0.01	0.01	0.003	2.54E-05	0.003	401	401	401
750	48.9	120	124.5422	124.5422	0.01	0.01	0.003	2.54E-05	0.003	401	401	401
750	52.2	120	141.9188	141.9188	0.01	0.01	0.003	2.54E-05	0.003	401	401	401
750	55.1	120	158.1255	158.1255	0.01	0.01	0.003	2.54E-05	0.003	401	401	401
750	58.3	120	177.0255	177.0255	0.01	0.01	0.003	2.54E-05	0.003	401	401	401
750	61.4	120	196.3521	196.3521	0.01	0.01	0.003	2.54E-05	0.003	401	401	401
750	64.1	120	214.0005	214.0005	0.01	0.01	0.003	2.54E-05	0.003	401	401	401
750	67.2	120	235.2	235.2	0.01	0.01	0.003	2.54E-05	0.003	401	401	401
750	71	120	262.5521	262.5521	0.01	0.01	0.003	2.54E-05	0.003	401	401	401
750	73	120	277.5521	277.5521	0.01	0.01	0.003	2.54E-05	0.003	401	401	401
750	76.2	120	302.4188	302.4188	0.01	0.01	0.003	2.54E-05	0.003	401	401	401
750	79.2	120	326.7	326.7	0.01	0.01	0.003	2.54E-05	0.003	401	401	401
750	82.1	120	351.063	351.063	0.01	0.01	0.003	2.54E-05	0.003	401	401	401
750	85.3	120	378.963	378.963	0.01	0.01	0.003	2.54E-05	0.003	401	401	401

Appendix A: (continued)

Table A: (continued)

De-ionized Water (cont)											
k_4	k_5	A_1	R_1	R_2	R_3	R_4	R_5	T_1	T_2	T_3	$T_{1\,cal}$
8.89	401	0.000113	0.220497	0.220497	0.066149	0.025263	0.111444	160.613	155.629	150.85	160.4606
8.89	401	0.000113	0.220497	0.220497	0.066149	0.025263	0.111437	178.768	172.992	167.393	178.6156
8.89	401	0.000113	0.220497	0.220497	0.066149	0.025263	0.111432	193.11	186.382	179.934	192.9576
8.89	401	0.000113	0.220497	0.220497	0.066149	0.025263	0.111432	207.933	200.263	192.87	207.7806
8.89	401	0.000113	0.220497	0.220497	0.066149	0.025263	0.111429	223.56	215.045	206.95	223.4076
8.89	401	0.000113	0.220497	0.220497	0.066149	0.025263	0.111426	237.374	227.816	218.866	237.2216
8.89	401	0.000113	0.220497	0.220497	0.066149	0.025263	0.111424	251.624	240.594	230.818	251.4716
8.89	401	0.000113	0.220497	0.220497	0.066149	0.025263	0.111424	266.973	255.205	244.528	266.8206
8.89	401	0.000113	0.220497	0.220497	0.066149	0.025263	0.111423	279.955	267.584	256.317	279.8026
8.89	401	0.000113	0.220497	0.220497	0.066149	0.025263	0.111423	296.449	283.495	271.643	296.2966
8.89	401	0.000113	0.220497	0.220497	0.066149	0.025263	0.111421	309.566	295.747	282.767	309.4136
8.89	401	0.000113	0.220497	0.220497	0.066149	0.025263	0.111568	319.545	304.565	290.941	319.3926
8.89	401	0.000113	0.220497	0.220497	0.066149	0.025263	0.111555	331.858	316.076	301.383	331.7056
8.89	401	0.000113	0.220497	0.220497	0.066149	0.025263	0.111536	343.739	327.295	310.313	343.5866
8.89	401	0.000113	0.220497	0.220497	0.066149	0.025263	0.111528	356.527	338.58	321.107	356.3746
8.89	401	0.000113	0.220497	0.220497	0.066149	0.025263	0.111528	367.947	349.008	330.574	367.7946

Appendix A: (continued)

Table A: (continued)

De-ionized Water (cont)											
$T_{2\ cal}$	$T_{3\ cal}$	q_{1-2}	q_{2-3}	q_{3-4}	% q_{lost}	q_{4-5}	T_4	T_5	$q_{3\text{-surface}}$	A_2	$q''_{3\text{-surface}}$
155.2828	150.85	23.48237	20.10365	20.10365	76.35097	20.10365	149.5202	149.0123	20.10365	0.000314	63991.9
172.6458	167.393	27.07426	23.82252	23.82252	75.71661	23.82252	165.8172	165.2153	23.82252	0.000314	75829.42
186.0358	179.934	31.39177	27.6729	27.6729	74.78084	27.6729	178.1035	177.4044	27.6729	0.000314	88085.58
199.9168	192.87	35.66393	31.95867	31.95867	74.33908	31.95867	190.756	189.9486	31.95867	0.000314	101727.6
214.6988	206.95	39.49618	35.14238	35.14238	75.23767	35.14238	204.6254	203.7376	35.14238	0.000314	111861.7
227.4698	218.866	44.22639	39.01998	39.01998	75.32341	39.01998	216.2849	215.2991	39.01998	0.000314	124204.5
240.2478	230.818	50.90221	42.76606	42.76606	75.84187	42.76606	227.9891	226.9087	42.76606	0.000314	136128.6
254.8588	244.528	54.24919	46.85228	46.85228	76.13864	46.85228	241.4288	240.2451	46.85228	0.000314	149135.4
267.2378	256.317	56.98392	49.52805	49.52805	76.85611	49.52805	253.0408	251.7895	49.52805	0.000314	157652.7
283.1488	271.643	59.62794	52.18114	52.18114	77.81414	52.18114	268.1913	266.873	52.18114	0.000314	166097.7
295.4008	282.767	63.55089	57.29685	57.29685	78.17696	57.29685	278.9769	277.5294	57.29685	0.000314	182381.5
304.2188	290.941	68.81627	60.21752	60.21752	78.30406	60.21752	286.9577	285.4364	60.21752	0.000314	191678.3
315.7298	301.383	72.4535	65.06565	65.06565	78.48491	65.06565	297.079	295.4352	65.06565	0.000314	207110.4
326.9488	310.313	75.4558	75.44673	75.44673	76.90642	75.44673	305.3223	303.4163	75.44673	0.000314	240154.4
338.2338	321.107	82.27221	77.67352	77.67352	77.87477	77.67352	315.969	314.0067	77.67352	0.000314	247242.5
348.6618	330.574	86.77113	82.03185	82.03185	78.3536	82.03185	325.1477	323.0753	82.03185	0.000314	261115.5

Appendix A: (continued)

Table A: (continued)

De-ionized Water (cont)		
$T_{surface}$	Δ_{excess}	$h_{boiling}$
146.7719	46.77186	1368.171
162.5606	62.56064	1212.095
174.3207	74.32072	1185.209
186.3874	86.38738	1177.575
199.8217	99.8217	1120.615
210.9513	110.9513	1119.451
222.1435	122.1435	1114.497
235.0247	135.0247	1104.505
246.271	146.271	1077.812
261.0589	161.0589	1031.286
271.1453	171.1453	1065.653
278.7181	178.7181	1072.518
288.1768	188.1768	1100.616
295.0013	195.0013	1231.553
305.344	205.344	1204.041
313.9265	213.9265	1220.585

Appendix A: (continued)

Table B: 0.1% wt Nanofluid Data Calculations

0.1% wt Nanofluid												
P_R	V_A	V_R	P_A	q	L_1	L_2	L_3	L_4	L_5	k_1	k_2	k_3
750	40.6	120	85.85208	85.85208	0.01	0.01	0.003	2.54E-05	0.003	401	401	401
750	43	120	96.30208	96.30208	0.01	0.01	0.003	2.54E-05	0.003	401	401	401
750	46.2	120	111.1688	111.1688	0.01	0.01	0.003	2.54E-05	0.003	401	401	401
750	49.2	120	126.075	126.075	0.01	0.01	0.003	2.54E-05	0.003	401	401	401
750	52.2	120	141.9188	141.9188	0.01	0.01	0.003	2.54E-05	0.003	401	401	401
750	54.9	120	156.9797	156.9797	0.01	0.01	0.003	2.54E-05	0.003	401	401	401
750	58.4	120	177.6333	177.6333	0.01	0.01	0.003	2.54E-05	0.003	401	401	401
750	61.8	120	198.9188	198.9188	0.01	0.01	0.003	2.54E-05	0.003	401	401	401
750	64.6	120	217.3521	217.3521	0.01	0.01	0.003	2.54E-05	0.003	401	401	401
750	67.2	120	235.2	235.2	0.01	0.01	0.003	2.54E-05	0.003	401	401	401
750	70.3	120	257.4005	257.4005	0.01	0.01	0.003	2.54E-05	0.003	401	401	401
750	73.2	120	279.075	279.075	0.01	0.01	0.003	2.54E-05	0.003	401	401	401
750	76.4	120	304.0083	304.0083	0.01	0.01	0.003	2.54E-05	0.003	401	401	401
750	79.1	120	325.8755	325.8755	0.01	0.01	0.003	2.54E-05	0.003	401	401	401
750	82.2	120	351.9188	351.9188	0.01	0.01	0.003	2.54E-05	0.003	401	401	401
750	85.2	120	378.075	378.075	0.01	0.01	0.003	2.54E-05	0.003	401	401	401

Appendix A: (continued)

Table B: (continued)

0.1% wt Nanofluid (cont)											
k_4	k_5	A_1	R_1	R_2	R_3	R_4	R_5	T_1	T_2	T_3	$T_{1\,cal}$
8.89	401	0.000113	0.220497	0.220497	0.066149	0.025263	0.111432	175.501	169.18	162.73	175.3486
8.89	401	0.000113	0.220497	0.220497	0.066149	0.025263	0.111432	191.848	184.78	177.433	191.6956
8.89	401	0.000113	0.220497	0.220497	0.066149	0.025263	0.111429	208.176	199.878	191.495	208.0236
8.89	401	0.000113	0.220497	0.220497	0.066149	0.025263	0.111424	224.845	215.397	205.506	224.6926
8.89	401	0.000113	0.220497	0.220497	0.066149	0.025263	0.111423	239.277	228.914	217.825	239.1246
8.89	401	0.000113	0.220497	0.220497	0.066149	0.025263	0.111421	252.588	241.398	228.728	252.4356
8.89	401	0.000113	0.220497	0.220497	0.066149	0.025263	0.111545	269.705	258.139	242.262	269.5526
8.89	401	0.000113	0.220497	0.220497	0.066149	0.025263	0.111528	286.14	274.106	256.209	285.9876
8.89	401	0.000113	0.220497	0.220497	0.066149	0.025263	0.111515	296.434	285.49	265.218	296.2816
8.89	401	0.000113	0.220497	0.220497	0.066149	0.025263	0.111504	308.222	296.592	274.132	308.0696
8.89	401	0.000113	0.220497	0.220497	0.066149	0.025263	0.111528	321.117	309.238	290.915	320.9646
8.89	401	0.000113	0.220497	0.220497	0.066149	0.025263	0.111528	333.92	323.715	305.912	333.7676
8.89	401	0.000113	0.220497	0.220497	0.066149	0.025263	0.111536	350.022	338.397	321.164	349.8696
8.89	401	0.000113	0.220497	0.220497	0.066149	0.025263	0.111521	366.915	355.035	336.212	366.7626
8.89	401	0.000113	0.220497	0.220497	0.066149	0.025263	0.111515	382.608	370.471	350.543	382.4556
8.89	401	0.000113	0.220497	0.220497	0.066149	0.025263	0.111509	399.922	387.042	365.988	399.7696

Appendix A: (continued)

Table B: (continued)

0.1% wt Nanofluid (cont)											
$T_{2\ cal}$	$T_{3\ cal}$	q_{1-2}	q_{2-3}	q_{3-4}	% q_{lost}	q_{4-5}	T_4	T_5	$q_{3\text{-surface}}$	A_2	$q''_{3\text{-surface}}$
168.8338	162.73	29.54594	27.68197	27.68197	67.7562	27.68197	160.8989	160.1995	27.68197	0.000314	88114.46
184.4338	177.433	32.93374	31.75005	31.75005	67.03078	31.75005	175.3328	174.5307	31.75005	0.000314	101063.5
199.5318	191.495	38.51204	36.44852	36.44852	67.21334	36.44852	189.084	188.1632	36.44852	0.000314	116019.2
215.0508	205.506	43.72752	43.28761	43.28761	65.66519	43.28761	202.6426	201.549	43.28761	0.000314	137788.7
228.5678	217.825	47.87723	48.72078	48.72078	65.66995	48.72078	214.6022	213.3713	48.72078	0.000314	155083.1
241.0518	228.728	51.62785	55.89094	55.89094	64.39607	55.89094	225.0309	223.6189	55.89094	0.000314	177906.4
257.7928	242.262	53.33308	70.43533	70.43533	60.34791	70.43533	237.6028	235.8234	70.43533	0.000314	224202.6
273.7598	256.209	55.45556	79.59644	79.59644	59.98545	79.59644	250.9438	248.9329	79.59644	0.000314	253363.3
285.1438	265.218	50.51219	90.36755	90.36755	58.42343	90.36755	259.2403	256.9573	90.36755	0.000314	287648.8
296.2458	274.132	53.62334	100.2906	100.2906	57.35945	100.2906	267.4979	264.9643	100.2906	0.000314	319234.8
308.8918	290.915	54.7526	81.52844	81.52844	68.32623	81.52844	285.522	283.4623	81.52844	0.000314	259513.1
323.3688	305.912	47.16067	79.17013	79.17013	71.63123	79.17013	300.675	298.6749	79.17013	0.000314	252006.4
338.0508	321.164	53.60066	76.58507	76.58507	74.80823	76.58507	316.098	314.1632	76.58507	0.000314	243777.8
354.6888	336.212	54.75714	83.79604	83.79604	74.28587	83.79604	330.669	328.552	83.79604	0.000314	266731.1
370.1248	350.543	55.92268	88.80744	88.80744	74.76479	88.80744	344.6685	342.4249	88.80744	0.000314	282682.9
386.6958	365.988	59.29234	93.91408	93.91408	75.15993	93.91408	359.7757	357.4031	93.91408	0.000314	298937.8

Appendix A: (continued)

Table B: (continued)

0.1% wt Nanofluid (cont)		
$T_{surface}$	Δ_{excess}	$h_{boiling}$
157.1149	57.11488	1542.758
170.9927	70.9927	1423.577
184.1018	84.10176	1379.51
196.7257	96.72571	1424.531
207.9427	107.9427	1436.716
217.3915	117.3915	1515.497
227.9667	127.9667	1752.039
240.0557	140.0557	1809.018
246.88	146.88	1958.393
253.7815	153.7815	2075.899
274.3696	174.3696	1488.293
289.8452	189.8452	1327.431
305.6212	205.6212	1185.567
319.207	219.207	1216.8
332.5216	232.5216	1215.727
346.9309	246.9309	1210.613

Appendix A: (continued)

Table C: 0.2% wt Nanofluid Data Calculations

0.2% wt Nanofluid												
P_R	V_A	V_R	P_A	q	L_1	L_2	L_3	L_4	L_5	k_1	k_2	k_3
750	40.3	120	84.58802	84.58802	0.01	0.01	0.003	2.54E-05	0.003	401	401	401
750	43.3	120	97.65052	97.65052	0.01	0.01	0.003	2.54E-05	0.003	401	401	401
750	46.5	120	112.6172	112.6172	0.01	0.01	0.003	2.54E-05	0.003	401	401	401
750	49.2	120	126.075	126.075	0.01	0.01	0.003	2.54E-05	0.003	401	401	401
750	52.3	120	142.463	142.463	0.01	0.01	0.003	2.54E-05	0.003	401	401	401
750	55.3	120	159.2755	159.2755	0.01	0.01	0.003	2.54E-05	0.003	401	401	401
750	58.8	120	180.075	180.075	0.01	0.01	0.003	2.54E-05	0.003	401	401	401
750	61.9	120	199.563	199.563	0.01	0.01	0.003	2.54E-05	0.003	401	401	401
750	35.5	120	65.63802	65.63802	0.01	0.01	0.003	2.54E-05	0.003	401	401	401
750	68.3	120	242.963	242.963	0.01	0.01	0.003	2.54E-05	0.003	401	401	401
750	71.2	120	264.0333	264.0333	0.01	0.01	0.003	2.54E-05	0.003	401	401	401
750	74.5	120	289.0755	289.0755	0.01	0.01	0.003	2.54E-05	0.003	401	401	401
750	77.3	120	311.213	311.213	0.01	0.01	0.003	2.54E-05	0.003	401	401	401
750	80.2	120	335.0021	335.0021	0.01	0.01	0.003	2.54E-05	0.003	401	401	401
750	83.4	120	362.2688	362.2688	0.01	0.01	0.003	2.54E-05	0.003	401	401	401
750	86.2	120	387.0021	387.0021	0.01	0.01	0.003	2.54E-05	0.003	401	401	401

Appendix A: (continued)

Table C: (continued)

0.2% wt Nanofluid (cont)											
k_4	k_5	A_1	R_1	R_2	R_3	R_4	$R_{5\ comsol}$	T_1	T_2	T_3	$T_{1\ cal}$
8.89	401	0.000113	0.220497	0.220497	0.066149	0.025263	0.111429	167.328	160.609	152.227	167.1756
8.89	401	0.000113	0.220497	0.220497	0.066149	0.025263	0.111424	182.956	175.765	165.988	182.8036
8.89	401	0.000113	0.220497	0.220497	0.066149	0.025263	0.111423	199.346	190.272	179.204	199.1936
8.89	401	0.000113	0.220497	0.220497	0.066149	0.025263	0.111421	213.279	203.103	190.204	213.1266
8.89	401	0.000113	0.220497	0.220497	0.066149	0.025263	0.111555	229.053	218.807	204.044	228.9006
8.89	401	0.000113	0.220497	0.220497	0.066149	0.025263	0.111545	245.136	232.413	216.847	244.9836
8.89	401	0.000113	0.220497	0.220497	0.066149	0.025263	0.111536	261.548	247.448	230.195	261.3956
8.89	401	0.000113	0.220497	0.220497	0.066149	0.025263	0.111521	280.559	265.013	246.143	280.4066
8.89	401	0.000113	0.220497	0.220497	0.066149	0.025263	0.111499	295.703	283.123	259.986	295.5506
8.89	401	0.000113	0.220497	0.220497	0.066149	0.025263	0.111499	307.499	293.123	269.196	307.3466
8.89	401	0.000113	0.220497	0.220497	0.066149	0.025263	0.111491	323.912	309.738	283.552	323.7596
8.89	401	0.000113	0.220497	0.220497	0.066149	0.025263	0.111581	342.506	327.652	299.616	342.3536
8.89	401	0.000113	0.220497	0.220497	0.066149	0.025263	0.111574	358.607	342.956	313.524	358.4546
8.89	401	0.000113	0.220497	0.220497	0.066149	0.025263	0.111568	376.061	359.62	329.658	375.9086
8.89	401	0.000113	0.220497	0.220497	0.066149	0.025263	0.111515	391.853	374.176	353.648	391.7006
8.89	401	0.000113	0.220497	0.220497	0.066149	0.025263	0.111504	404.117	384.761	362.021	403.9646

Appendix A: (continued)

Table C: (continued)

0.2% wt Nanofluid (cont)											
$T_{2\ cal}$	$T_{3\ cal}$	q_{1-2}	q_{2-3}	% q_{lost}	q_{3-4}	q_{4-5}	T_4	T_5	$q_{3\text{-surface}}$	A_2	$q''_{3\text{-surface}}$
160.2628	152.227	31.35095	36.44399	56.9159	36.44399	36.44399	149.8163	148.8956	36.44399	0.000314	116004.8
175.4188	165.988	33.49157	42.77059	56.20034	42.77059	42.77059	163.1588	162.0783	42.77059	0.000314	136143
189.9258	179.204	42.03136	48.62554	56.82227	48.62554	48.62554	175.9875	174.759	48.62554	0.000314	154779.9
202.7568	190.204	47.02915	56.9295	54.84474	56.9295	56.9295	186.4382	185	56.9295	0.000314	181212.2
218.4608	204.044	47.34661	65.38312	54.1052	65.38312	65.38312	199.719	198.0672	65.38312	0.000314	208120.9
232.0668	216.847	58.58031	69.02488	56.66322	69.02488	69.02488	212.2811	210.5373	69.02488	0.000314	219713
247.1018	230.195	64.82529	76.67577	57.42009	76.67577	76.67577	225.123	223.1859	76.67577	0.000314	244066.6
264.6668	246.143	71.38319	84.0092	57.90343	84.0092	84.0092	240.5859	238.4636	84.0092	0.000314	267409.6
282.7768	259.986	57.93178	103.3609	-57.4711	103.3609	103.3609	253.1488	250.5376	103.3609	0.000314	329008
292.7768	269.196	66.077	106.9437	55.98354	106.9437	106.9437	262.1218	259.4201	106.9437	0.000314	340412.4
309.3918	283.552	65.16089	117.1887	55.61593	117.1887	117.1887	275.8001	272.8396	117.1887	0.000314	373023.4
327.3058	299.616	68.24483	125.5789	56.55846	125.5789	125.5789	291.3091	288.1366	125.5789	0.000314	399730
342.6098	313.524	71.85939	131.91	57.61424	131.91	131.91	304.7983	301.4659	131.91	0.000314	419882.6
359.2738	329.658	75.4422	134.3137	59.90662	134.3137	134.3137	320.7733	317.3801	134.3137	0.000314	427533.7
373.8298	353.648	81.04771	91.52856	74.73462	91.52856	91.52856	347.5935	345.2812	91.52856	0.000314	291344.5
384.4148	362.021	88.66231	101.5604	73.75714	101.5604	101.5604	355.3029	352.7372	101.5604	0.000314	323276.9

Appendix A: (continued)

Table C: (continued)

0.2% wt Nanofluid (cont)		
$T_{surface}$	Δ_{excess}	$h_{boiling}$
144.8347	44.83468	2587.39
157.3126	57.31258	2375.448
169.3411	69.34106	2232.154
178.6568	78.65681	2303.834
190.7734	90.77337	2292.753
202.8379	102.8379	2136.498
214.6338	114.6338	2129.097
229.0948	129.0948	2071.42
239.0129	139.0129	2366.744
247.4959	147.4959	2307.945
259.774	159.774	2334.694
274.1244	174.1244	2295.658
286.7481	186.7481	2248.391
302.395	202.395	2112.373
335.0744	235.0744	1239.371
341.4128	241.4128	1339.104

Appendix A: (continued)

Table D: 0.3% wt Nanofluid Data Calculations

0.3% wt Nanofluid												
P_R	V_A	V_R	P_A	q	L_1	L_2	L_3	L_4	L_5	k_1	k_2	k_3
750	40.5	120	85.42969	85.42969	0.01	0.01	0.003	2.54E-05	0.003	401	401	401
750	43.5	120	98.55469	98.55469	0.01	0.01	0.003	2.54E-05	0.003	401	401	401
750	46	120	110.2083	110.2083	0.01	0.01	0.003	2.54E-05	0.003	401	401	401
750	49.2	120	126.075	126.075	0.01	0.01	0.003	2.54E-05	0.003	401	401	401
750	52.6	120	144.1021	144.1021	0.01	0.01	0.003	2.54E-05	0.003	401	401	401
750	55	120	157.5521	157.5521	0.01	0.01	0.003	2.54E-05	0.003	401	401	401
750	58.1	120	175.813	175.813	0.01	0.01	0.003	2.54E-05	0.003	401	401	401
750	61.4	120	196.3521	196.3521	0.01	0.01	0.003	2.54E-05	0.003	401	401	401
750	64.2	120	214.6688	214.6688	0.01	0.01	0.003	2.54E-05	0.003	401	401	401
750	67.1	120	234.5005	234.5005	0.01	0.01	0.003	2.54E-05	0.003	401	401	401
750	70.6	120	259.6021	259.6021	0.01	0.01	0.003	2.54E-05	0.003	401	401	401
750	73.5	120	281.3672	281.3672	0.01	0.01	0.003	2.54E-05	0.003	401	401	401
750	76.1	120	301.6255	301.6255	0.01	0.01	0.003	2.54E-05	0.003	401	401	401
750	79.2	120	326.7	326.7	0.01	0.01	0.003	2.54E-05	0.003	401	401	401
750	82.4	120	353.6333	353.6333	0.01	0.01	0.003	2.54E-05	0.003	401	401	401
750	85.1	120	377.188	377.188	0.01	0.01	0.003	2.54E-05	0.003	401	401	401

Appendix A: (continued)

Table D: (continued)

0.3% wt Nanofluid (cont)												
k_4	k_5	A_1	R_1	R_2	R_3	R_4	$R_{5\ comsol}$	$q_{\ reminder}$	T_1	T_2	T_3	$T_{1\ cal}$
8.89	401	0.000113	0.220497	0.220497	0.066149	0.025263	0.111444	17.83605	150.636	144.744	140.465	150.4836
8.89	401	0.000113	0.220497	0.220497	0.066149	0.025263	0.111444	21.27827	170.57	163.56	158.522	170.4176
8.89	401	0.000113	0.220497	0.220497	0.066149	0.025263	0.111437	24.52094	181.893	174.635	168.882	181.7406
8.89	401	0.000113	0.220497	0.220497	0.066149	0.025263	0.111432	29.22938	196.191	188.0362	181.245	196.0386
8.89	401	0.000113	0.220497	0.220497	0.066149	0.025263	0.111429	34.94283	211.898	202.909	194.858	211.7456
8.89	401	0.000113	0.220497	0.220497	0.066149	0.025263	0.111426	38.54832	224.876	215.082	206.236	224.7236
8.89	401	0.000113	0.220497	0.220497	0.066149	0.025263	0.111424	45.45997	243.91	233.738	223.368	243.7576
8.89	401	0.000113	0.220497	0.220497	0.066149	0.025263	0.111423	52.17207	259.474	248.487	236.637	259.3216
8.89	401	0.000113	0.220497	0.220497	0.066149	0.025263	0.111555	65.69605	271.517	260.585	245.753	271.3646
8.89	401	0.000113	0.220497	0.220497	0.066149	0.025263	0.111536	73.98186	282.45	270.901	254.242	282.2976
8.89	401	0.000113	0.220497	0.220497	0.066149	0.025263	0.111528	79.12932	298.173	285.217	267.423	298.0206
8.89	401	0.000113	0.220497	0.220497	0.066149	0.025263	0.111521	83.94117	311.141	297.387	278.532	310.9886
8.89	401	0.000113	0.220497	0.220497	0.066149	0.025263	0.111521	85.93212	322.084	308.142	288.848	321.9316
8.89	401	0.000113	0.220497	0.220497	0.066149	0.025263	0.111545	72.01358	353.177	333.19	316.965	353.0246
8.89	401	0.000113	0.220497	0.220497	0.066149	0.025263	0.111536	75.13834	369.327	349.409	332.495	369.1746
8.89	401	0.000113	0.220497	0.220497	0.066149	0.025263	0.111515	88.4673	386.551	366.062	346.209	386.3986

Appendix A: (continued)

Table D: (continued)

0.3% wt Nanofluid (cont)											
$T_{2\ cal}$	$T_{3\ cal}$	q_{1-2}	q_{2-3}	% q_{lost}	q_{3-4}	q_{4-5}	T_4	T_5	$q_{3\text{-surface}}$	A_2	$q''_{3\text{-surface}}$
144.3978	140.465	27.60034	17.83605	79.12196	17.83605	17.83605	139.2852	138.8346	17.83605	0.000314	56773.9
163.2138	158.522	32.6707	21.27827	78.40969	21.27827	21.27827	157.1145	156.5769	21.27827	0.000314	67730.82
174.2888	168.882	33.79543	24.52094	77.75038	24.52094	24.52094	167.26	166.6405	24.52094	0.000314	78052.56
187.69	181.245	37.8626	29.22938	76.81588	29.22938	29.22938	179.3115	178.5731	29.22938	0.000314	93040.02
202.5628	194.858	41.64586	34.94283	75.75133	34.94283	34.94283	192.5466	191.6638	34.94283	0.000314	111226.5
214.7358	206.236	45.2967	38.54832	75.53297	38.54832	38.54832	203.6861	202.7122	38.54832	0.000314	122703.1
233.3918	223.368	47.01101	45.45997	74.143	45.45997	45.45997	220.3609	219.2124	45.45997	0.000314	144703.6
248.1408	236.637	50.7072	52.17207	73.42933	52.17207	52.17207	233.1859	231.8679	52.17207	0.000314	166068.9
260.2388	245.753	50.45776	65.69605	69.39655	65.69605	65.69605	241.4073	239.7476	65.69605	0.000314	209117
270.5548	254.242	53.25598	73.98186	68.4513	73.98186	73.98186	249.3482	247.4792	73.98186	0.000314	235491.6
284.8708	267.423	59.63701	79.12932	69.519	79.12932	79.12932	262.1887	260.1896	79.12932	0.000314	251876.4
297.0408	278.532	63.25611	83.94117	70.16668	83.94117	83.94117	272.9794	270.8588	83.94117	0.000314	267193
307.7958	288.848	64.10872	85.93212	71.51033	85.93212	85.93212	283.1637	280.9928	85.93212	0.000314	273530.4
332.8438	316.965	91.52403	72.01358	77.95727	72.01358	72.01358	312.2014	310.3821	72.01358	0.000314	229226.4
349.0628	332.495	91.2111	75.13834	78.75247	75.13834	75.13834	327.5247	325.6265	75.13834	0.000314	239172.8
365.7158	346.209	93.8007	88.4673	76.54557	88.4673	88.4673	340.357	338.122	88.4673	0.000314	281600.2

Appendix A: (continued)

Table D: (continued)

0.3% wt Nanofluid (cont)		
$T_{surface}$	Δ_{excess}	$h_{boiling}$
136.8469	36.84686	1540.807
154.2056	54.20558	1249.518
163.908	63.90796	1221.328
175.316	75.316	1235.329
187.7702	87.77018	1267.247
198.4169	98.41694	1246.768
214.1471	114.1471	1267.694
226.0547	126.0547	1317.435
232.4189	132.4189	1579.209
239.2276	139.2276	1691.415
251.3645	151.3645	1664.039
261.4976	161.4976	1654.471
271.4096	171.4096	1595.771
302.3494	202.3494	1132.825
317.2458	217.2458	1100.931
328.2566	228.2566	1233.7

Appendix A: (continued)

Table E: 0.4% wt Nanofluid Data Calculations

0.4% wt Nanofluid												
P_R	V_A	V_R	P_A	q	L_1	L_2	L_3	L_4	L_5	k_1	k_2	k_3
750	40.2	120	84.16875	84.16875	0.01	0.01	0.003	2.54E-05	0.003	401	401	401
750	43.2	120	97.2	97.2	0.01	0.01	0.003	2.54E-05	0.003	401	401	401
750	46.2	120	111.1688	111.1688	0.01	0.01	0.003	2.54E-05	0.003	401	401	401
750	49.5	120	127.6172	127.6172	0.01	0.01	0.003	2.54E-05	0.003	401	401	401
750	52.2	120	141.9188	141.9188	0.01	0.01	0.003	2.54E-05	0.003	401	401	401
750	55.3	120	159.2755	159.2755	0.01	0.01	0.003	2.54E-05	0.003	401	401	401
750	58.4	120	177.6333	177.6333	0.01	0.01	0.003	2.54E-05	0.003	401	401	401
750	61.2	120	195.075	195.075	0.01	0.01	0.003	2.54E-05	0.003	401	401	401
750	64.5	120	216.6797	216.6797	0.01	0.01	0.003	2.54E-05	0.003	401	401	401
750	67.2	120	235.2	235.2	0.01	0.01	0.003	2.54E-05	0.003	401	401	401
750	70.4	120	258.1333	258.1333	0.01	0.01	0.003	2.54E-05	0.003	401	401	401
750	73.3	120	279.838	279.838	0.01	0.01	0.003	2.54E-05	0.003	401	401	401
750	76.1	120	301.6255	301.6255	0.01	0.01	0.003	2.54E-05	0.003	401	401	401
750	79.3	120	327.5255	327.5255	0.01	0.01	0.003	2.54E-05	0.003	401	401	401
750	82.5	120	354.4922	354.4922	0.01	0.01	0.003	2.54E-05	0.003	401	401	401
750	84.7	120	373.6505	373.6505	0.01	0.01	0.003	2.54E-05	0.003	401	401	401

Appendix A: (continued)

Table E: (continued)

0.4% wt Nanofluid (cont)											
k_4	k_5	A_1	R_1	R_2	R_3	R_4	$R_{5\ comsol}$	T_1	T_2	T_3	$T_{1\ cal}$
8.89	401	0.000113	0.220497	0.220497	0.066149	0.025263	0.111444	150.548	144.058	139.515	150.3956
8.89	401	0.000113	0.220497	0.220497	0.066149	0.025263	0.111437	164.284	157.003	151.5	164.1316
8.89	401	0.000113	0.220497	0.220497	0.066149	0.025263	0.111437	176.578	168.009	161.65	176.4256
8.89	401	0.000113	0.220497	0.220497	0.066149	0.025263	0.111432	188.91	179.232	171.814	188.7576
8.89	401	0.000113	0.220497	0.220497	0.066149	0.025263	0.111426	201.054	190.413	181.574	200.9016
8.89	401	0.000113	0.220497	0.220497	0.066149	0.025263	0.111424	215.128	202.945	193.043	214.9756
8.89	401	0.000113	0.220497	0.220497	0.066149	0.025263	0.111423	228.182	214.589	203.299	228.0296
8.89	401	0.000113	0.220497	0.220497	0.066149	0.025263	0.111421	238.029	223.187	210.947	237.8766
8.89	401	0.000113	0.220497	0.220497	0.066149	0.025263	0.111568	251.414	235.169	221.412	251.2616
8.89	401	0.000113	0.220497	0.220497	0.066149	0.025263	0.111545	260.422	243.037	227.54	260.2696
8.89	401	0.000113	0.220497	0.220497	0.066149	0.025263	0.111536	270.998	252.314	235.938	270.8456
8.89	401	0.000113	0.220497	0.220497	0.066149	0.025263	0.111528	281.727	262.596	244.412	281.5746
8.89	401	0.000113	0.220497	0.220497	0.066149	0.025263	0.111521	292.662	270.761	252.191	292.5096
8.89	401	0.000113	0.220497	0.220497	0.066149	0.025263	0.111515	305.729	282.831	262.524	305.5766
8.89	401	0.000113	0.220497	0.220497	0.066149	0.025263	0.111509	320.105	295.097	273.744	319.9526
8.89	401	0.000113	0.220497	0.220497	0.066149	0.025263	0.111504	330.776	305.424	282.77	330.6236

Appendix A: (continued)

Table E: (continued)

0.4% wt Nanofluid (cont)											
$T_{2\ cal}$	$T_{3\ cal}$	q_{1-2}	q_{2-3}	% q_{lost}	q_{3-4}	q_{4-5}	T_4	T_5	$q_{3\text{-surface}}$	A_2	$q''_{3\text{-surface}}$
143.7118	139.515	30.31239	19.03334	77.38669	19.03334	19.03334	138.256	137.7751	19.03334	0.000314	60585
156.6568	151.5	33.89974	23.38714	75.93916	23.38714	23.38714	149.953	149.3621	23.38714	0.000314	74443.56
167.6628	161.65	39.74108	27.26927	75.47038	27.26927	27.26927	159.8462	159.1573	27.26927	0.000314	86800.78
178.8858	171.814	44.77062	32.07205	74.86855	32.07205	32.07205	169.6925	168.8822	32.07205	0.000314	102088.5
190.0668	181.574	49.13802	38.51657	72.86012	38.51657	38.51657	179.0262	178.0531	38.51657	0.000314	122602.1
202.5988	193.043	56.1313	43.33749	72.79086	43.33749	43.33749	190.1763	189.0814	43.33749	0.000314	137947.5
214.2428	203.299	62.52594	49.63236	72.0591	49.63236	49.63236	200.0159	198.762	49.63236	0.000314	157984.7
222.8408	210.947	68.19041	53.9408	72.34869	53.9408	53.9408	207.3789	206.0162	53.9408	0.000314	171698.9
234.8228	221.412	74.5533	60.8207	71.93059	60.8207	60.8207	217.3888	215.8523	60.8207	0.000314	193598.3
242.6908	227.54	79.72343	68.71196	70.78573	68.71196	68.71196	222.9948	221.2589	68.71196	0.000314	218716.9
251.9678	235.938	85.61466	72.6984	71.83688	72.6984	72.6984	231.1291	229.2925	72.6984	0.000314	231406.2
262.2498	244.412	87.64189	80.89805	71.09112	80.89805	80.89805	239.0607	237.017	80.89805	0.000314	257506.5
270.4148	252.191	100.2044	82.64864	72.59892	82.64864	82.64864	246.7239	244.6359	82.64864	0.000314	263078.8
282.4848	262.524	104.726	90.52628	72.36054	90.52628	90.52628	256.5358	254.2488	90.52628	0.000314	288154.1
294.7508	273.744	114.2953	95.27011	73.12491	95.27011	95.27011	267.442	265.0352	95.27011	0.000314	303254.2
305.0778	282.77	115.8554	101.1704	72.92379	101.1704	101.1704	276.0777	273.5218	101.1704	0.000314	322035.4

Appendix A: (continued)

Table E: (continued)

0.4% wt Nanofluid (cont)		
$T_{surface}$	Δ_{excess}	$h_{boiling}$
135.654	35.65398	1699.25
146.756	46.75595	1592.173
156.1185	56.11847	1546.742
165.3084	65.30838	1563.176
173.7614	73.76137	1662.144
184.2526	84.25259	1637.309
193.2318	93.23185	1694.536
200.006	100.006	1716.886
209.0666	109.0666	1775.046
213.5944	113.5944	1925.419
221.184	121.184	1909.544
227.9946	127.9946	2011.855
235.4189	135.4189	1942.704
244.1538	144.1538	1998.935
254.4117	154.4117	1963.932
262.2409	162.2409	1984.921

Appendix B: Heat Flux Uncertainty Analysis Calculations

Table F: De-Ionized Water Heat Flux Error Bar Calculations

De-ionized Water												
UA	A	UA/A	UT_1	UT_2	UΔT	ΔT	UΔT/ΔT	UL	L	UL/L	Uk	k
1.57E-07	0.000314	0.0005	0.621131	0.6034	0.865965	4.07814	0.212343	0.000005	0.006025	0.00083	0	401
1.57E-07	0.000314	0.0005	0.690583	0.669572	0.96189	4.832365	0.199052	0.000005	0.006025	0.00083	0	401
1.57E-07	0.000314	0.0005	0.744143	0.719736	1.035263	5.61328	0.184431	0.000005	0.006025	0.00083	0	401
1.57E-07	0.000314	0.0005	0.799667	0.77148	1.111148	6.482622	0.171404	0.000005	0.006025	0.00083	0	401
1.57E-07	0.000314	0.0005	0.858795	0.8278	1.192804	7.1283	0.167334	0.000005	0.006025	0.00083	0	401
1.57E-07	0.000314	0.0005	0.909879	0.875464	1.262663	7.914736	0.159533	0.000005	0.006025	0.00083	0	401
1.57E-07	0.000314	0.0005	0.960991	0.923272	1.332642	8.674499	0.153628	0.000005	0.006025	0.00083	0	401
1.57E-07	0.000314	0.0005	1.019435	0.978112	1.412781	9.503331	0.148662	0.000005	0.006025	0.00083	0	401
1.57E-07	0.000314	0.0005	1.068951	1.025268	1.481159	10.046	0.147438	0.000005	0.006025	0.00083	0	401
1.57E-07	0.000314	0.0005	1.132595	1.086572	1.569526	10.58413	0.14829	0.000005	0.006025	0.00083	0	401
1.57E-07	0.000314	0.0005	1.181603	1.131068	1.635696	11.6217	0.140745	0.000005	0.006025	0.00083	0	401
1.57E-07	0.000314	0.0005	1.216875	1.163764	1.683785	12.22292	0.137756	0.000005	0.006025	0.00083	0	401
1.57E-07	0.000314	0.0005	1.262919	1.205532	1.74593	13.2062	0.132205	0.000005	0.006025	0.00083	0	401
1.57E-07	0.000314	0.0005	1.307795	1.241252	1.803063	15.31174	0.117757	0.000005	0.006025	0.00083	0	401
1.57E-07	0.000314	0.0005	1.352935	1.284428	1.865526	15.76304	0.118348	0.000005	0.006025	0.00083	0	401
1.57E-07	0.000314	0.0005	1.394647	1.322296	1.92185	16.64752	0.115444	0.000005	0.006025	0.00083	0	401

Appendix B: (continued)

Table F: (continued)

De-ionized Water (cont)								
Uk/k	R_{th}	UR_{th}	UR_{th}/R_{th}	q"	Uq"	Uq" +	Uq" -	% $Uq"_{error}$
0	0.202856	0.000197	0.000969	63991.9	13588.42	77580.32	50403.48	21.2345958
0	0.202849	0.000197	0.000969	75829.42	15094.19	90923.61	60735.23	19.9054547
0	0.202844	0.000197	0.000969	88085.58	16246	104331.6	71839.59	18.4434213
0	0.202844	0.000197	0.000969	101727.6	17436.88	119164.5	84290.73	17.1407518
0	0.202841	0.000197	0.000969	111861.7	18718.62	130580.3	93143.06	16.7337176
0	0.202838	0.000197	0.000969	124204.5	19815.19	144019.6	104389.3	15.9536888
0	0.202836	0.000197	0.000969	136128.6	20913.63	157042.2	115215	15.3631446
0	0.202836	0.000197	0.000969	149135.4	22171.32	171306.8	126964.1	14.8665701
0	0.202834	0.000197	0.000969	157652.7	23244.59	180897.3	134408.1	14.7441752
0	0.202834	0.000197	0.000969	166097.7	24631.36	190729.1	141466.4	14.8294411
0	0.202833	0.000197	0.000969	182381.5	25670.05	208051.6	156711.5	14.0749157
0	0.202979	0.000197	0.000969	191678.3	26405.73	218084.1	165272.6	13.7760657
0	0.202967	0.000197	0.000969	207110.4	27382.04	234492.4	179728.4	13.2209875
0	0.202948	0.000197	0.000969	240154.4	28281.05	268435.5	211873.4	11.7761936
0	0.20294	0.000197	0.000969	247242.5	29261.93	276504.4	217980.6	11.8353157
0	0.20294	0.000197	0.000969	261115.5	30145.46	291260.9	230970	11.544878

Appendix B: (continued)

Table G: 0.1% wt Nanofluid Heat Flux Error Bar Calculations

0.1% wt Nanofluid												
UA	A	UA/A	UT_1	UT_2	UΔT	ΔT	UΔT/ΔT	UL	L	UL/L	Uk	k
1.57E-07	0.000314	0.0005	0.675335	0.65092	0.937963	5.61512	0.167042	0.000005	0.006025	0.00083	0	401
1.57E-07	0.000314	0.0005	0.737735	0.709732	1.023705	6.440304	0.158953	0.000005	0.006025	0.00083	0	401
1.57E-07	0.000314	0.0005	0.798127	0.76598	1.106224	7.393238	0.149627	0.000005	0.006025	0.00083	0	401
1.57E-07	0.000314	0.0005	0.860203	0.822024	1.189821	8.780287	0.13551	0.000005	0.006025	0.00083	0	401
1.57E-07	0.000314	0.0005	0.914271	0.8713	1.262955	9.882254	0.1278	0.000005	0.006025	0.00083	0	401
1.57E-07	0.000314	0.0005	0.964207	0.914912	1.329195	11.33654	0.117249	0.000005	0.006025	0.00083	0	401
1.57E-07	0.000314	0.0005	1.031171	0.969048	1.415051	14.29533	0.098987	0.000005	0.006025	0.00083	0	401
1.57E-07	0.000314	0.0005	1.095039	1.024836	1.4998	16.15328	0.092848	0.000005	0.006025	0.00083	0	401
1.57E-07	0.000314	0.0005	1.140575	1.060872	1.557678	18.33797	0.084943	0.000005	0.006025	0.00083	0	401
1.57E-07	0.000314	0.0005	1.184983	1.096528	1.614484	20.35055	0.079334	0.000005	0.006025	0.00083	0	401
1.57E-07	0.000314	0.0005	1.235567	1.16366	1.697272	16.54536	0.102583	0.000005	0.006025	0.00083	0	401
1.57E-07	0.000314	0.0005	1.293475	1.223648	1.78056	16.06676	0.110823	0.000005	0.006025	0.00083	0	401
1.57E-07	0.000314	0.0005	1.352203	1.284656	1.865153	15.54276	0.120001	0.000005	0.006025	0.00083	0	401
1.57E-07	0.000314	0.0005	1.418755	1.344848	1.954861	17.00496	0.114958	0.000005	0.006025	0.00083	0	401
1.57E-07	0.000314	0.0005	1.480499	1.402172	2.039109	18.02138	0.113149	0.000005	0.006025	0.00083	0	401
1.57E-07	0.000314	0.0005	1.546783	1.463952	2.129717	19.05713	0.111754	0.000005	0.006025	0.00083	0	401

Appendix B: (continued)

Table G: (continued)

0.1% wt Nanofluid (cont)								
Uk/k	R_{th}	UR_{th}	UR_{th}/R_{th}	q"	Uq"	Uq" +	Uq" -	% $Uq"_{error}$
0	0.202844	0.000197	0.000969	88114.46	14719.16	102833.6	73395.3	16.70459322
0	0.202844	0.000197	0.000969	101063.5	16064.73	117128.3	84998.82	15.89566884
0	0.202841	0.000197	0.000969	116019.2	17360.02	133379.3	98659.23	14.96304829
0	0.202836	0.000197	0.000969	137788.7	18672.42	156461.1	119116.3	13.5514821
0	0.202834	0.000197	0.000969	155083.1	19820.38	174903.4	135262.7	12.78049509
0	0.202833	0.000197	0.000969	177906.4	20860.21	198766.6	157046.2	11.72538379
0	0.202957	0.000197	0.000969	224202.6	22194.48	246397.1	202008.2	9.899293748
0	0.20294	0.000197	0.000969	253363.3	23525.91	276889.3	229837.4	9.285441751
0	0.202926	0.000197	0.000969	287648.8	24435.71	312084.6	263213.1	8.494979719
0	0.202916	0.000197	0.000969	319234.8	25328.47	344563.3	293906.3	7.9341192
0	0.20294	0.000197	0.000969	259513.1	26623.12	286136.2	232890	10.25887457
0	0.20294	0.000197	0.000969	252006.4	27929.34	279935.7	224077	11.08279068
0	0.202948	0.000197	0.000969	243777.8	29254.88	273032.7	214523	12.00063309
0	0.202933	0.000197	0.000969	266731.1	30664.34	297395.4	236066.7	11.49634975
0	0.202926	0.000197	0.000969	282682.9	31986.89	314669.8	250696	11.31546852
0	0.202921	0.000197	0.000969	298937.8	33409.19	332347	265528.6	11.17596761

Appendix B: (continued)

Table H: 0.2% wt Nanofluid Heat Flux Error Bar Calculations

0.2% wt Nanofluid												
UA	A	UA/A	UT_1	UT_2	UΔT	ΔT	UΔT/ΔT	UL	L	UL/L	Uk	k
1.57E-07	0.000314	0.0005	0.641051	0.608908	0.884147	7.392318	0.119603	0.000005	0.006025	0.00083	0	401
1.57E-07	0.000314	0.0005	0.701675	0.663952	0.966013	8.675419	0.111351	0.000005	0.006025	0.00083	0	401
1.57E-07	0.000314	0.0005	0.759703	0.716816	1.044497	9.862937	0.105901	0.000005	0.006025	0.00083	0	401
1.57E-07	0.000314	0.0005	0.811027	0.760816	1.112028	11.54719	0.096303	0.000005	0.006025	0.00083	0	401
1.57E-07	0.000314	0.0005	0.873843	0.816176	1.19572	13.27063	0.090103	0.000005	0.006025	0.00083	0	401
1.57E-07	0.000314	0.0005	0.928267	0.867388	1.27045	14.00907	0.090688	0.000005	0.006025	0.00083	0	401
1.57E-07	0.000314	0.0005	0.988407	0.92078	1.350846	15.56117	0.086809	0.000005	0.006025	0.00083	0	401
1.57E-07	0.000314	0.0005	1.058667	0.984572	1.445738	17.04821	0.084803	0.000005	0.006025	0.00083	0	401
1.57E-07	0.000314	0.0005	1.131107	1.039944	1.536518	20.97309	0.073261	0.000005	0.006025	0.00083	0	401
1.57E-07	0.000314	0.0005	1.171107	1.076784	1.590898	21.70009	0.073313	0.000005	0.006025	0.00083	0	401
1.57E-07	0.000314	0.0005	1.237567	1.134208	1.67869	23.77799	0.070598	0.000005	0.006025	0.00083	0	401
1.57E-07	0.000314	0.0005	1.309223	1.198464	1.774931	25.49162	0.069628	0.000005	0.006025	0.00083	0	401
1.57E-07	0.000314	0.0005	1.370439	1.254096	1.857649	26.77592	0.069378	0.000005	0.006025	0.00083	0	401
1.57E-07	0.000314	0.0005	1.437095	1.318632	1.950393	27.26301	0.07154	0.000005	0.006025	0.00083	0	401
1.57E-07	0.000314	0.0005	1.495319	1.414592	2.05841	18.57357	0.110825	0.000005	0.006025	0.00083	0	401
1.57E-07	0.000314	0.0005	1.537659	1.448084	2.112189	20.60822	0.102493	0.000005	0.006025	0.00083	0	401

Appendix B: (continued)

Table H: (continued)

0.2% wt Nanofluid (cont)								
Uk/k	R_{th}	UR_{th}	UR_{th}/R_{th}	q"	Uq"	Uq" +	Uq" -	% $Uq"_{error}$
0	0.202841	0.000197	0.000969	116004.8	13875.15	129880	102129.7	11.9608431
0	0.202836	0.000197	0.000969	136143	15160.33	151303.4	120982.7	11.13558842
0	0.202834	0.000197	0.000969	154779.9	16392.25	171172.2	138387.7	10.59068379
0	0.202833	0.000197	0.000969	181212.2	17452.38	198664.6	163759.8	9.630905683
0	0.202967	0.000197	0.000969	208120.9	18753.63	226874.6	189367.3	9.010928221
0	0.202957	0.000197	0.000969	219713	19926.7	239639.7	199786.3	9.069421495
0	0.202948	0.000197	0.000969	244066.6	21188.79	265255.4	222877.8	8.681561411
0	0.202933	0.000197	0.000969	267409.6	22678.98	290088.6	244730.6	8.48099193
0	0.202911	0.000197	0.000969	329008	24106.25	353114.2	304901.7	7.3269491
0	0.202911	0.000197	0.000969	340412.4	24959.41	365371.8	315453	7.33210752
0	0.202903	0.000197	0.000969	373023.4	26338.02	399361.4	346685.3	7.060689896
0	0.202993	0.000197	0.000969	399730	27835.82	427565.8	371894.1	6.963656108
0	0.202986	0.000197	0.000969	419882.6	29134.04	449016.6	390748.6	6.938615765
0	0.20298	0.000197	0.000969	427533.7	30589.27	458123	396944.4	7.154821204
0	0.202926	0.000197	0.000969	291344.5	32289.72	323634.2	259054.7	11.08300505
0	0.202916	0.000197	0.000969	323276.9	33135.35	356412.2	290141.5	10.24983589

Appendix B: (continued)

Table I: 0.3% wt Nanofluid Heat Flux Error Bar Calculations

0.3% wt Nanofluid												
UA	A	UA/A	UT_1	UT_2	UΔT	ΔT	UΔT/ΔT	UL	L	UL/L	Uk	k
1.57E-07	0.000314	0.0005	0.577591	0.56186	0.80579	3.618144	0.222708	0.000005	0.006025	0.00083	0	401
1.57E-07	0.000314	0.0005	0.652855	0.634088	0.910103	4.316418	0.210847	0.000005	0.006025	0.00083	0	401
1.57E-07	0.000314	0.0005	0.697155	0.675528	0.970754	4.974038	0.195164	0.000005	0.006025	0.00083	0	401
1.57E-07	0.000314	0.0005	0.75076	0.72498	1.043665	5.929003	0.176027	0.000005	0.006025	0.00083	0	401
1.57E-07	0.000314	0.0005	0.810251	0.779432	1.124287	7.087823	0.158622	0.000005	0.006025	0.00083	0	401
1.57E-07	0.000314	0.0005	0.858943	0.824944	1.190931	7.819065	0.152311	0.000005	0.006025	0.00083	0	401
1.57E-07	0.000314	0.0005	0.933567	0.893472	1.292223	9.220921	0.14014	0.000005	0.006025	0.00083	0	401
1.57E-07	0.000314	0.0005	0.992563	0.946548	1.371545	10.58229	0.129607	0.000005	0.006025	0.00083	0	401
1.57E-07	0.000314	0.0005	1.040955	0.983012	1.431747	13.33415	0.107375	0.000005	0.006025	0.00083	0	401
1.57E-07	0.000314	0.0005	1.082219	1.016968	1.485066	15.01445	0.098909	0.000005	0.006025	0.00083	0	401
1.57E-07	0.000314	0.0005	1.139483	1.069692	1.562902	16.05848	0.097326	0.000005	0.006025	0.00083	0	401
1.57E-07	0.000314	0.0005	1.188163	1.114128	1.628807	17.03441	0.095619	0.000005	0.006025	0.00083	0	401
1.57E-07	0.000314	0.0005	1.231183	1.155392	1.688414	17.43844	0.096821	0.000005	0.006025	0.00083	0	401
1.57E-07	0.000314	0.0005	1.331375	1.26786	1.838485	14.61564	0.125789	0.000005	0.006025	0.00083	0	401
1.57E-07	0.000314	0.0005	1.396251	1.32998	1.928306	15.24915	0.126453	0.000005	0.006025	0.00083	0	401
1.57E-07	0.000314	0.0005	1.462863	1.384836	2.014383	17.95235	0.112207	0.000005	0.006025	0.00083	0	401

Appendix B: (continued)

Table I: (continued)

0.3% wt Nanofluid (cont)								
Uk/k	R_{th}	UR_{th}	UR_{th}/R_{th}	q"	Uq"	Uq" +	Uq" -	% Uq" $_{error}$
0	0.202856	0.000197	0.000969	56773.9	12644.17	69418.07	44129.734	22.27109087
0	0.202856	0.000197	0.000969	67730.82	14281.02	82011.85	53449.804	21.08496572
0	0.202849	0.000197	0.000969	78052.56	15233.3	93285.87	62819.263	19.51672142
0	0.202844	0.000197	0.000969	93040.02	16377.88	109417.9	76662.144	17.60304447
0	0.202841	0.000197	0.000969	111226.5	17643.42	128869.9	93583.072	15.86260677
0	0.202838	0.000197	0.000969	122703.1	18689.53	141392.6	104013.58	15.2315049
0	0.202836	0.000197	0.000969	144703.6	20279.42	164983	124424.16	14.01445678
0	0.202834	0.000197	0.000969	166068.9	21524.53	187593.4	144544.33	12.96120762
0	0.202967	0.000197	0.000969	209117	22454.99	231572	186662.02	10.73800404
0	0.202948	0.000197	0.000969	235491.6	23293.69	258785.3	212197.89	9.891518253
0	0.20294	0.000197	0.000969	251876.4	24515.58	276392	227360.86	9.733176055
0	0.202933	0.000197	0.000969	267193	25550.3	292743.3	241642.73	9.562488245
0	0.202933	0.000197	0.000969	273530.4	26485.29	300015.7	247045.15	9.682756573
0	0.202957	0.000197	0.000969	229226.4	28835.21	258061.6	200391.15	12.57936107
0	0.202948	0.000197	0.000969	239172.8	30245.32	269418.1	208927.44	12.64580457
0	0.202926	0.000197	0.000969	281600.2	31599.05	313199.2	250001.11	11.22124818

Appendix B: (continued)

Table J: 0.4% wt Nanofluid Heat Flux Error Bar Calculations

0.4% wt Nanofluid												
UA	A	UA/A	UT_1	UT_2	UΔT	ΔT	UΔT/ΔT	UL	L	UL/L	Uk	k
1.57E-07	0.000314	0.0005	0.574847	0.55806	0.801174	3.861022	0.207503	0.000005	0.006025	0.00083	0	401
1.57E-07	0.000314	0.0005	0.626627	0.606	0.871721	4.744048	0.18375	0.000005	0.006025	0.00083	0	401
1.57E-07	0.000314	0.0005	0.670651	0.6466	0.931593	5.531534	0.168415	0.000005	0.006025	0.00083	0	401
1.57E-07	0.000314	0.0005	0.715543	0.687256	0.99213	6.50562	0.152504	0.000005	0.006025	0.00083	0	401
1.57E-07	0.000314	0.0005	0.760267	0.726296	1.051433	7.812625	0.134581	0.000005	0.006025	0.00083	0	401
1.57E-07	0.000314	0.0005	0.810395	0.772172	1.11937	8.790406	0.12734	0.000005	0.006025	0.00083	0	401
1.57E-07	0.000314	0.0005	0.856971	0.813196	1.181392	10.06715	0.117351	0.000005	0.006025	0.00083	0	401
1.57E-07	0.000314	0.0005	0.891363	0.843788	1.227398	10.94098	0.112184	0.000005	0.006025	0.00083	0	401
1.57E-07	0.000314	0.0005	0.939291	0.885648	1.290984	12.34536	0.104572	0.000005	0.006025	0.00083	0	401
1.57E-07	0.000314	0.0005	0.970763	0.91016	1.330704	13.94556	0.095421	0.000005	0.006025	0.00083	0	401
1.57E-07	0.000314	0.0005	1.007871	0.943752	1.380751	14.75397	0.093585	0.000005	0.006025	0.00083	0	401
1.57E-07	0.000314	0.0005	1.048999	0.977648	1.433944	16.41743	0.087343	0.000005	0.006025	0.00083	0	401
1.57E-07	0.000314	0.0005	1.081659	1.008764	1.479051	16.77211	0.088185	0.000005	0.006025	0.00083	0	401
1.57E-07	0.000314	0.0005	1.129939	1.050096	1.542551	18.37018	0.08397	0.000005	0.006025	0.00083	0	401
1.57E-07	0.000314	0.0005	1.179003	1.094976	1.609044	19.33229	0.083231	0.000005	0.006025	0.00083	0	401
1.57E-07	0.000314	0.0005	1.220311	1.13108	1.663881	20.52908	0.08105	0.000005	0.006025	0.00083	0	401

Appendix B: (continued)

Table J: (continued)

0.4% wt Nanofluid (cont)								
Uk/k	R_{th}	UR_{th}	UR_{th}/R_{th}	q"	Uq"	Uq" +	Uq" -	% $Uq"_{error}$
0	0.202856	0.000197	0.000969	60585	12571.76	73156.76	48013.25	20.75060499
0	0.202849	0.000197	0.000969	74443.56	13679.28	88122.84	60764.28	18.37536951
0	0.202849	0.000197	0.000969	86800.78	14618.85	101419.6	72181.93	16.8418386
0	0.202844	0.000197	0.000969	102088.5	15569.26	117657.8	86519.24	15.2507495
0	0.202838	0.000197	0.000969	122602.1	16500.49	139102.5	106101.6	13.45857235
0	0.202836	0.000197	0.000969	137947.5	17566.88	155514.4	120380.6	12.7344667
0	0.202834	0.000197	0.000969	157984.7	18540.49	176525.2	139444.2	11.73562254
0	0.202833	0.000197	0.000969	171698.9	19262.7	190961.6	152436.2	11.21888265
0	0.202979	0.000197	0.000969	193598.3	20246.15	213844.5	173352.2	10.45781499
0	0.202957	0.000197	0.000969	218716.9	20871.63	239588.6	197845.3	9.542757701
0	0.202948	0.000197	0.000969	231406.2	21657.62	253063.8	209748.6	9.359137059
0	0.20294	0.000197	0.000969	257506.5	22493.09	279999.6	235013.4	8.734959942
0	0.202933	0.000197	0.000969	263078.8	23201.41	286280.2	239877.4	8.819188275
0	0.202926	0.000197	0.000969	288154.1	24198.46	312352.6	263955.7	8.397748538
0	0.202921	0.000197	0.000969	303254.2	25242.27	328496.4	278011.9	8.323801406
0	0.202916	0.000197	0.000969	322035.4	26103.33	348138.7	295932.1	8.105732078

Appendix C: Heat Transfer Coefficient Uncertainty Analysis Calculations

Table K: De-Ionized Water Heat Transfer Coefficient Error Bar Calculations

De-ionized Water										
$U\Delta T_e$	ΔT_e	$U\Delta T_e/\Delta T_e$	UT_s	UT_{sat}	Uq"/q"	h	Uh	Uh +	Uh -	% Uh $_{error}$
0.6034	46.77186	0.01290092	0.6034	0	0.212346	1368.171	291.0613	1659.232	1077.11	21.27374899
0.669572	62.56064	0.01070277	0.669572	0	0.199055	1212.095	241.6215	1453.716	970.4733	19.93420731
0.719736	74.32072	0.00968419	0.719736	0	0.184434	1185.209	218.8942	1404.103	966.3148	18.46882847
0.77148	86.38738	0.00893047	0.77148	0	0.171408	1177.575	202.119	1379.694	975.4559	17.16400031
0.8278	99.8217	0.00829279	0.8278	0	0.167337	1120.615	187.7506	1308.365	932.8642	16.75425341
0.875464	110.9513	0.00789053	0.875464	0	0.159537	1119.451	178.812	1298.263	940.6386	15.97318971
0.923272	122.1435	0.00755891	0.923272	0	0.153631	1114.497	171.4289	1285.926	943.0683	15.38172891
0.978112	135.0247	0.00724395	0.978112	0	0.148666	1104.505	164.3968	1268.902	940.1082	14.88420826
1.025268	146.271	0.00700937	1.025268	0	0.147442	1077.812	159.094	1236.906	918.7182	14.76082703
1.086572	161.0589	0.00674643	1.086572	0	0.148294	1031.286	153.0921	1184.378	878.1937	14.84477909
1.131068	171.1453	0.00660882	1.131068	0	0.140749	1065.653	150.155	1215.808	915.4982	14.09042291
1.163764	178.7181	0.00651173	1.163764	0	0.137761	1072.518	147.9157	1220.434	924.6021	13.79144713
1.205532	188.1768	0.00640638	1.205532	0	0.13221	1100.616	145.683	1246.299	954.933	13.23649978
1.241252	195.0013	0.00636535	1.241252	0	0.117762	1231.553	145.2418	1376.795	1086.311	11.7933843
1.284428	205.344	0.00625501	1.284428	0	0.118353	1204.041	142.7009	1346.742	1061.34	11.85183316
1.322296	213.9265	0.00618108	1.322296	0	0.115449	1220.585	141.1169	1361.702	1079.468	11.56141277

Appendix C: (continued)

Table L: 0.1% wt Nanofluid Heat Transfer Coefficient Error Bar Calculations

0.1% wt Nanofluid										
$U\Delta T_e$	ΔT_e	$U\Delta T_e/\Delta T_e$	UT_s	UT_{sat}	Uq"/q"	h	Uh	Uh +	Uh -	% Uh_{error}
0.65092	57.11488	0.01139668	0.65092	0	0.167046	1542.758	258.3106	1801.069	1284.448	16.74342491
0.709732	70.9927	0.009997254	0.709732	0	0.158957	1423.577	226.7341	1650.311	1196.843	15.92707565
0.76598	84.10176	0.009107776	0.76598	0	0.14963	1379.51	206.7988	1586.309	1172.711	14.99074147
0.822024	96.72571	0.008498505	0.822024	0	0.135515	1424.531	193.4242	1617.955	1231.106	13.57810418
0.8713	107.9427	0.008071872	0.8713	0	0.127805	1436.716	183.9853	1620.701	1252.731	12.80595978
0.914912	117.3915	0.007793684	0.914912	0	0.117254	1515.497	178.0899	1693.587	1337.407	11.75125696
0.969048	127.9667	0.007572659	0.969048	0	0.098993	1752.039	173.9462	1925.985	1578.093	9.92821577
1.024836	140.0557	0.007317345	1.024836	0	0.092854	1809.018	168.4961	1977.514	1640.522	9.314229107
1.060872	146.88	0.007222711	1.060872	0	0.08495	1958.393	166.9653	2125.358	1791.428	8.525629356
1.096528	153.7815	0.007130431	1.096528	0	0.079341	2075.899	165.3681	2241.267	1910.531	7.966095524
1.16366	174.3696	0.006673524	1.16366	0	0.102589	1488.293	153.0048	1641.298	1335.288	10.2805577
1.223648	189.8452	0.006445503	1.223648	0	0.110828	1327.431	147.3649	1474.795	1180.066	11.10151766
1.284656	205.6212	0.006247681	1.284656	0	0.120006	1185.567	142.4683	1328.036	1043.099	12.0168852
1.344848	219.207	0.006135058	1.344848	0	0.114963	1216.8	140.0866	1356.886	1076.713	11.51270807
1.402172	232.5216	0.006030287	1.402172	0	0.113155	1215.727	137.7604	1353.488	1077.967	11.33152555
1.463952	246.9309	0.00592859	1.463952	0	0.11176	1210.613	135.488	1346.101	1075.125	11.19168145

Appendix C: (continued)

Table M: 0.2% wt Nanofluid Heat Transfer Coefficient Error Bar Calculations

0.2% wt Nanofluid										
$U\Delta T_e$	ΔT_e	$U\Delta T_e/\Delta T_e$	UT_s	UT_{sat}	Uq"/q"	h	Uh	Uh +	Uh -	% Uh_{error}
0.608908	44.83468	0.013581	0.608908	0	0.119608	2587.39	311.4623	2898.852	2275.928	12.03770131
0.663952	57.31258	0.011585	0.663952	0	0.111356	2375.448	265.9477	2641.395	2109.5	11.1956864
0.716816	69.34106	0.010338	0.716816	0	0.105907	2232.154	237.5238	2469.677	1994.63	10.64101642
0.760816	78.65681	0.009673	0.760816	0	0.096309	2303.834	222.9963	2526.83	2080.838	9.679356207
0.816176	90.77337	0.008991	0.816176	0	0.090109	2292.753	207.6243	2500.377	2085.129	9.055676279
0.867388	102.8379	0.008435	0.867388	0	0.090694	2136.498	194.6041	2331.102	1941.894	9.108557325
0.92078	114.6338	0.008032	0.92078	0	0.086816	2129.097	185.6283	2314.725	1943.469	8.718640739
0.984572	129.0948	0.007627	0.984572	0	0.08481	2071.42	176.3859	2247.806	1895.034	8.515215516
1.039944	139.0129	0.007481	1.039944	0	0.073269	2366.744	174.3117	2541.056	2192.433	7.365040685
1.076784	147.4959	0.0073	1.076784	0	0.073321	2307.945	170.0577	2478.003	2137.887	7.368362361
1.134208	159.774	0.007099	1.134208	0	0.070607	2334.694	165.6765	2500.37	2169.017	7.096286015
1.198464	174.1244	0.006883	1.198464	0	0.069637	2295.658	160.6407	2456.298	2135.017	6.997587894
1.254096	186.7481	0.006715	1.254096	0	0.069386	2248.391	156.7361	2405.127	2091.654	6.971037257
1.318632	202.395	0.006515	1.318632	0	0.071548	2112.373	151.7618	2264.135	1960.611	7.184423229
1.414592	235.0744	0.006018	1.414592	0	0.11083	1239.371	137.5619	1376.933	1101.809	11.09932972
1.448084	241.4128	0.005998	1.448084	0	0.102498	1339.104	137.4908	1476.595	1201.613	10.26737262

Appendix C: (continued)

Table N: 0.3% wt Nanofluid Heat Transfer Coefficient Error Bar Calculations

0.3% wt Nanofluid										
$U\Delta T_e$	ΔT_e	$U\Delta T_e/\Delta T_e$	UT_s	UT_{sat}	Uq"/q"	h	Uh	Uh +	Uh -	% Uh_{error}
0.56186	36.84686	0.015248519	0.56186	0	0.222711	1540.807	343.958	1884.765	1196.849	22.32323144
0.634088	54.20558	0.011697836	0.634088	0	0.21085	1249.518	263.8655	1513.383	985.652	21.1173903
0.675528	63.90796	0.010570326	0.675528	0	0.195167	1221.328	238.7125	1460.04	982.6152	19.54532509
0.72498	75.316	0.009625843	0.72498	0	0.17603	1235.329	217.7804	1453.109	1017.548	17.62934325
0.779432	87.77018	0.008880374	0.779432	0	0.158626	1267.247	201.3332	1468.58	1065.914	15.88744485
0.824944	98.41694	0.008382135	0.824944	0	0.152315	1246.768	190.1889	1436.957	1056.579	15.25455156
0.893472	114.1471	0.007827375	0.893472	0	0.140145	1267.694	177.9373	1445.631	1089.757	14.03629855
0.946548	126.0547	0.007509026	0.946548	0	0.129612	1317.435	171.0418	1488.477	1146.393	12.98294103
0.983012	132.4189	0.007423505	0.983012	0	0.10738	1579.209	169.9802	1749.189	1409.228	10.76363391
1.016968	139.2276	0.007304359	1.016968	0	0.098915	1691.415	167.7622	1859.177	1523.653	9.918450984
1.069692	151.3645	0.007066993	1.069692	0	0.097332	1664.039	162.3902	1826.429	1501.649	9.758798083
1.114128	161.4976	0.006898728	1.114128	0	0.095625	1654.471	158.6197	1813.09	1495.851	9.587340921
1.155392	171.4096	0.006740534	1.155392	0	0.096828	1595.771	154.8886	1750.66	1440.883	9.706189924
1.26786	202.3494	0.006265698	1.26786	0	0.125794	1132.825	142.6788	1275.504	990.146	12.59495592
1.32998	217.2458	0.006122004	1.32998	0	0.126458	1100.931	139.3847	1240.316	961.5467	12.66061463
1.384836	228.2566	0.006067013	1.384836	0	0.112212	1233.7	138.6387	1372.338	1095.061	11.23763753

Appendix C: (continued)

Table O: 0.4% wt Nanofluid Heat Transfer Coefficient Error Bar Calculations

0.4% wt Nanofluid										
$U\Delta T_e$	ΔT_e	$U\Delta T_e/\Delta T_e$	UT_s	UT_{sat}	Uq"/q"	h	Uh	Uh +	Uh -	% Uh_{error}
0.55806	35.65398	0.015652	0.55806	0	0.207506	1699.25	353.6062	2052.856	1345.643	20.80955293
0.606	46.75595	0.012961	0.606	0	0.183754	1592.173	293.2945	1885.468	1298.878	18.42102218
0.6466	56.11847	0.011522	0.6466	0	0.168418	1546.742	261.1087	1807.851	1285.633	16.88120567
0.687256	65.30838	0.010523	0.687256	0	0.152507	1563.176	238.9629	1802.139	1324.213	15.28701236
0.726296	73.76137	0.009847	0.726296	0	0.134586	1662.144	224.2988	1886.443	1437.846	13.49454399
0.772172	84.25259	0.009165	0.772172	0	0.127345	1637.309	209.0419	1846.351	1428.267	12.76740411
0.813196	93.23185	0.008722	0.813196	0	0.117356	1694.536	199.4128	1893.949	1495.123	11.76799139
0.843788	100.006	0.008437	0.843788	0	0.112189	1716.886	193.1593	1910.045	1523.726	11.25056534
0.885648	109.0666	0.00812	0.885648	0	0.104578	1775.046	186.1898	1961.236	1588.856	10.48929351
0.91016	113.5944	0.008012	0.91016	0	0.095428	1925.419	184.3846	2109.804	1741.035	9.576335638
0.943752	121.184	0.007788	0.943752	0	0.093591	1909.544	179.3345	2088.878	1730.209	9.391482224
0.977648	127.9946	0.007638	0.977648	0	0.08735	2011.855	176.4053	2188.26	1835.449	8.76829208
1.008764	135.4189	0.007449	1.008764	0	0.088192	1942.704	171.9408	2114.644	1770.763	8.850592601
1.050096	144.1538	0.007285	1.050096	0	0.083977	1998.935	168.4959	2167.431	1830.439	8.429283924
1.094976	154.4117	0.007091	1.094976	0	0.083238	1963.932	164.066	2127.998	1799.866	8.353953062
1.13108	162.2409	0.006972	1.13108	0	0.081057	1984.921	161.4864	2146.407	1823.435	8.135657662

Appendix D: Surface Roughness Images

Figure A: Copper Hat after 0.1% wt Nanofluid Experiment

Appendix D: (continued)

Figure B: Copper Hat after 0.2% wt Nanofluid Experiment

Appendix D: (continued)

Figure C: Copper Hat after 0.3% wt Nanofluid Experiment

Appendix D: (continued)

Figure D: Copper Hat after 0.4% wt Nanofluid Experiment

Appendix E: COMSOL Thermal Resistance Data

Table P: Thermal Resistance Data from COMSOL

A_{COMSOL}	q	q"	$top_{boundary\ \int}$	$bottom_{boundary\ \int}$	A_{top}	A_{bottom}	T_{top}	T_{bottom}	$R_{th\ COMSOL}$
0.000113	15	132629.1192	0.100247	0.036278	0.000314	0.000113	319.0961	320.7679	0.111455617
0.000113	20	176838.8257	0.102247	0.037061	0.000314	0.000113	325.4623	327.6912	0.111443828
0.000113	25	221048.5321	0.104247	0.037844	0.000314	0.000113	331.8285	334.6144	0.111436754
0.000113	30	265258.2385	0.106247	0.038627	0.000314	0.000113	338.1947	341.5377	0.111432039
0.000113	35	309467.9449	0.108247	0.03941	0.000314	0.000113	344.5609	348.4609	0.11142867
0.000113	40	353677.6513	0.110247	0.040193	0.000314	0.000113	350.9271	355.3841	0.111426144
0.000113	45	397887.3577	0.112247	0.040976	0.000314	0.000113	357.2933	362.3074	0.111424179
0.000113	50	442097.0641	0.114247	0.041759	0.000314	0.000113	363.6595	369.2306	0.111422607
0.000113	55	486306.7706	0.116247	0.042542	0.000314	0.000113	370.0257	376.1539	0.111421321
0.000113	60	530516.477	0.118247	0.043326	0.000314	0.000113	376.3919	383.0859	0.111567615
0.000113	65	574726.1834	0.120247	0.044109	0.000314	0.000113	382.7581	390.0092	0.111555372
0.000113	70	618935.8898	0.122247	0.044892	0.000314	0.000113	389.1243	396.9324	0.111544879
0.000113	75	663145.5962	0.124247	0.045675	0.000314	0.000113	395.4905	403.8557	0.111535784
0.000113	80	707355.3026	0.126247	0.046458	0.000314	0.000113	401.8567	410.7789	0.111527826
0.000113	85	751565.009	0.128247	0.047241	0.000314	0.000113	408.2229	417.7021	0.111520805
0.000113	90	795774.7155	0.130247	0.048024	0.000314	0.000113	414.5891	424.6254	0.111514563
0.000113	95	839984.4219	0.132247	0.048807	0.000314	0.000113	420.9553	431.5486	0.111508979
0.000113	100	884194.1283	0.134247	0.04959	0.000314	0.000113	427.3215	438.4719	0.111503953

Appendix E: (continued)

Table P: (continued)

A_{COMSOL}	q	q"	$top_{boundary\ \int}$	$bottom_{boundary\ \int}$	A_{top}	A_{bottom}	T_{top}	T_{bottom}	$R_{th\ COMSOL}$
0.000113	105	928403.8347	0.136247	0.050373	0.000314	0.000113	433.6877	445.3951	0.111499406
0.000113	110	972613.5411	0.138247	0.051156	0.000314	0.000113	440.0539	452.3183	0.111495272
0.000113	115	1016823.248	0.140247	0.051939	0.000314	0.000113	446.4201	459.2416	0.111491498
0.000113	120	1061032.954	0.142247	0.052723	0.000314	0.000113	452.7863	466.1737	0.11156172
0.000113	125	1105242.66	0.144246	0.053506	0.000314	0.000113	459.1493	473.0969	0.111581055
0.000113	130	1149452.367	0.146246	0.054289	0.000314	0.000113	465.5155	480.0202	0.111574417
0.000113	135	1193662.073	0.148246	0.055072	0.000314	0.000113	471.8817	486.9434	0.11156827
0.000113	140	1237871.78	0.150246	0.055855	0.000314	0.000113	478.2479	493.8666	0.111562563
0.000113	145	1282081.486	0.152246	0.056638	0.000314	0.000113	484.6141	500.7899	0.111557249
0.000113	150	1326291.192	0.154246	0.057421	0.000314	0.000113	490.9803	507.7131	0.111552289

Appendix F: Heat Flux Curves for All Data Points

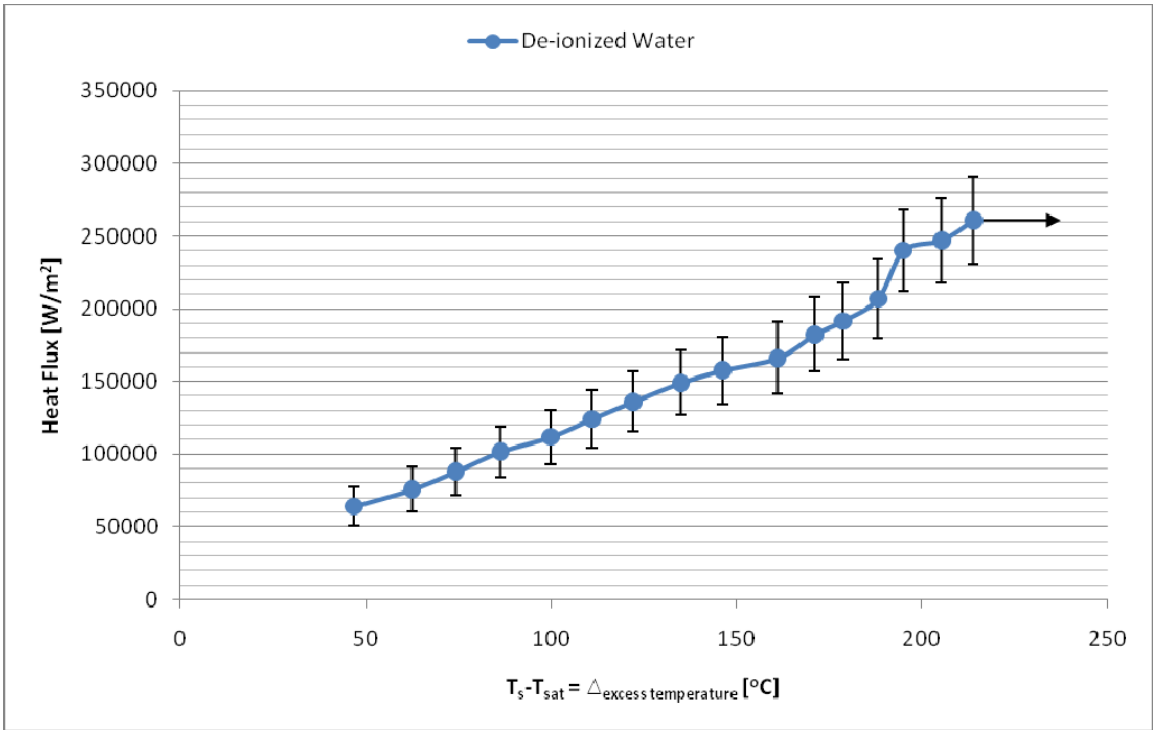

Figure E: Heat Flux De-Ionized Water All Data Points

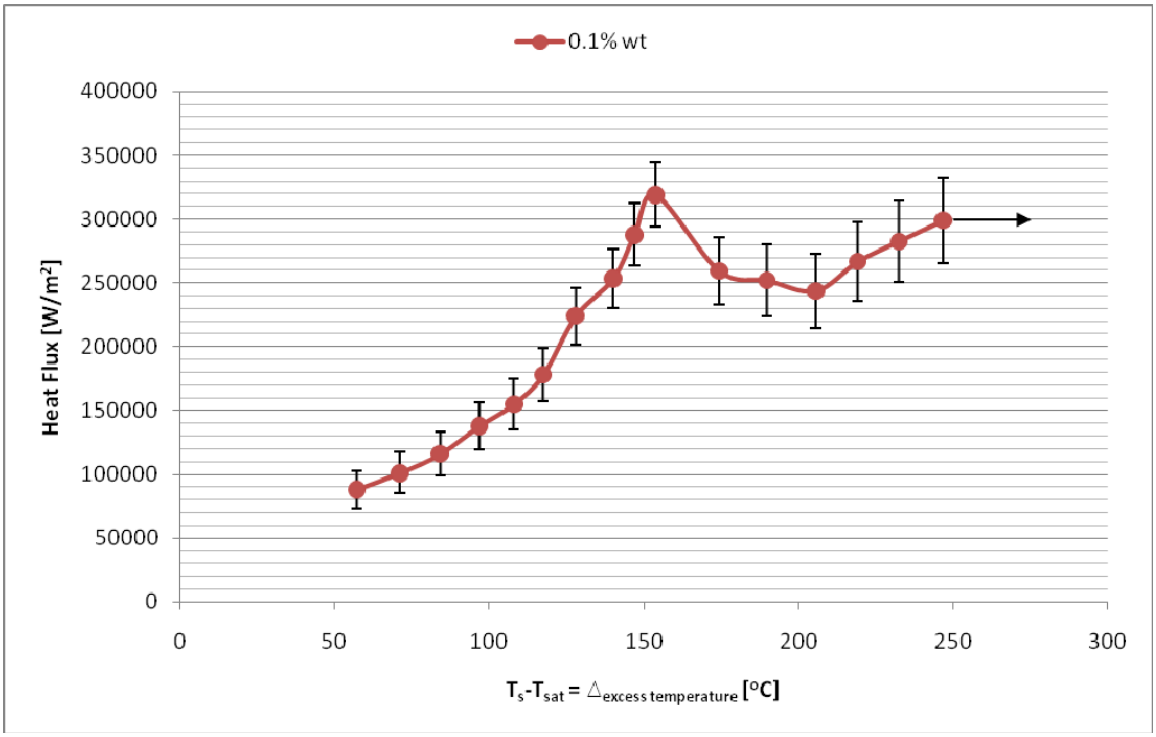

Figure F: Heat Flux 0.1% wt Nanofluid All Data Points

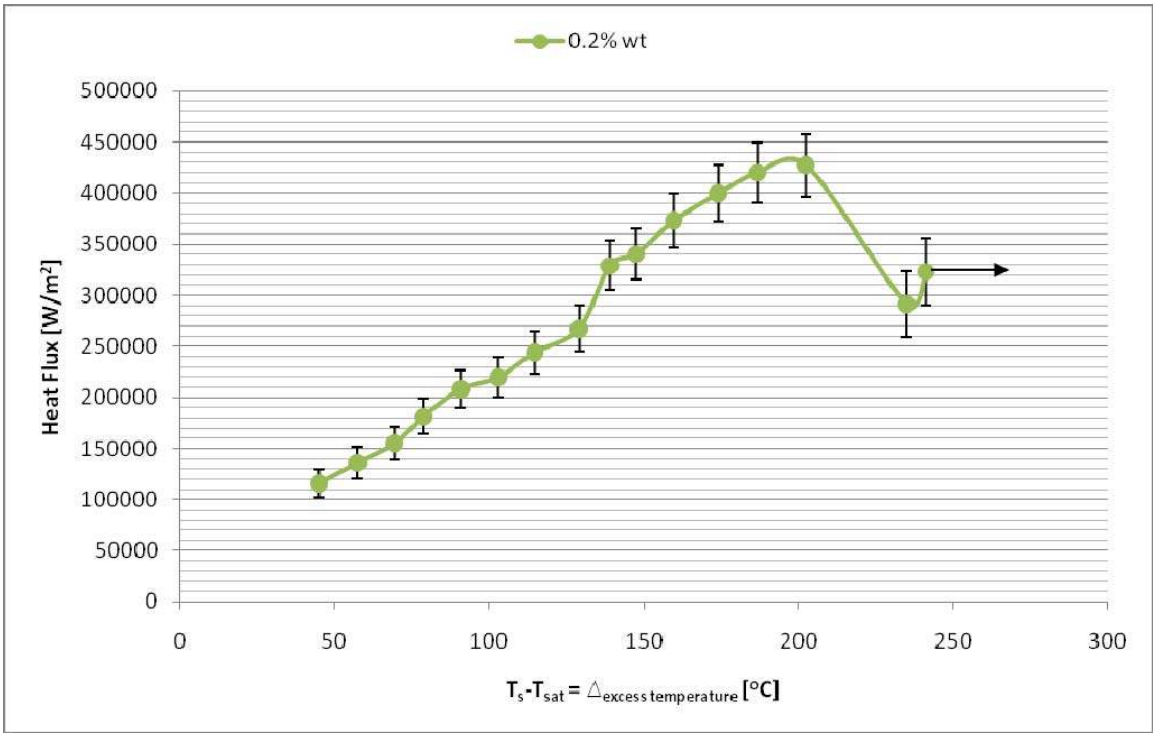

Figure G: Heat Flux 0.2% wt Nanofluid All Data Points

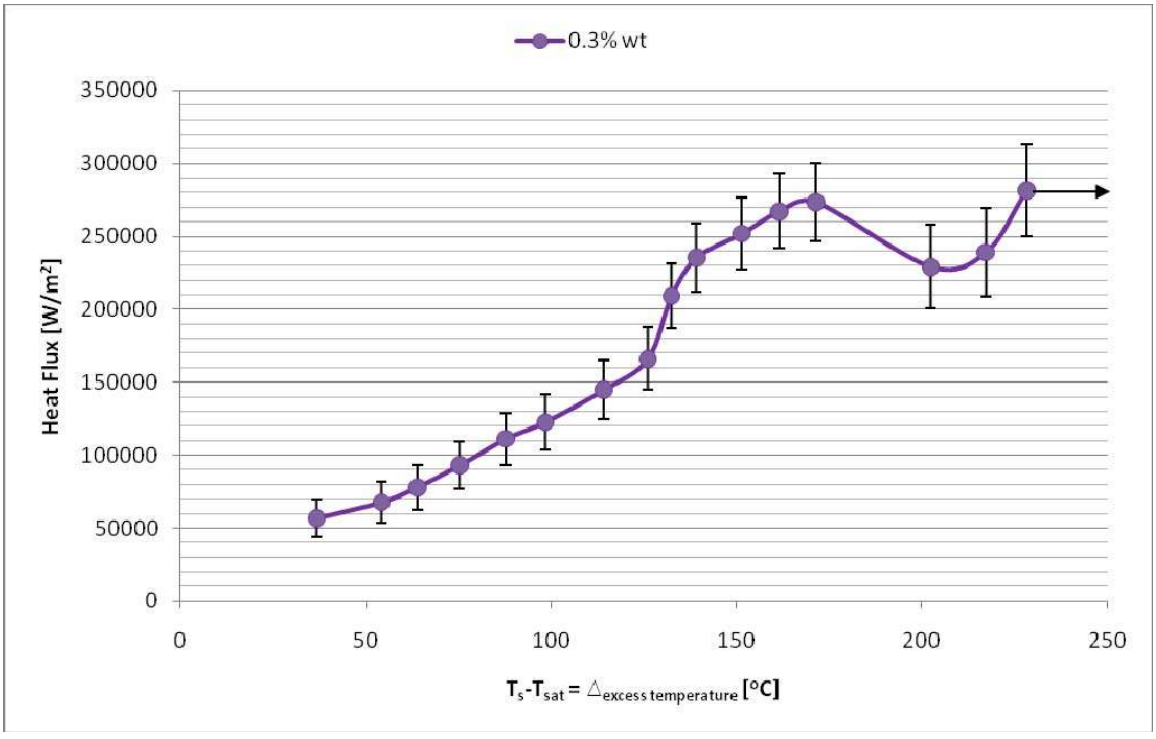

Figure H: Heat Flux 0.3% wt Nanofluid All Data Points

Appendix F: (continued)

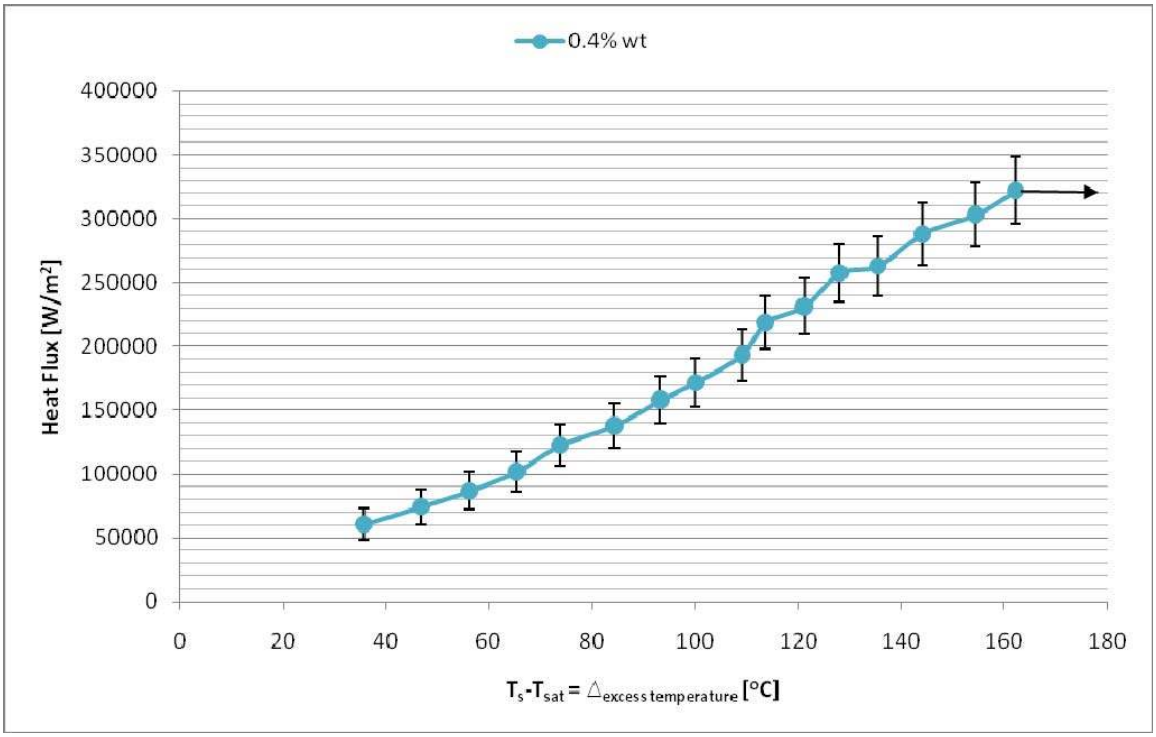

Figure I: Heat Flux 0.4% wt Nanofluid All Data Points

Appendix G: Heat Transfer Coefficient Curves for All Data Points

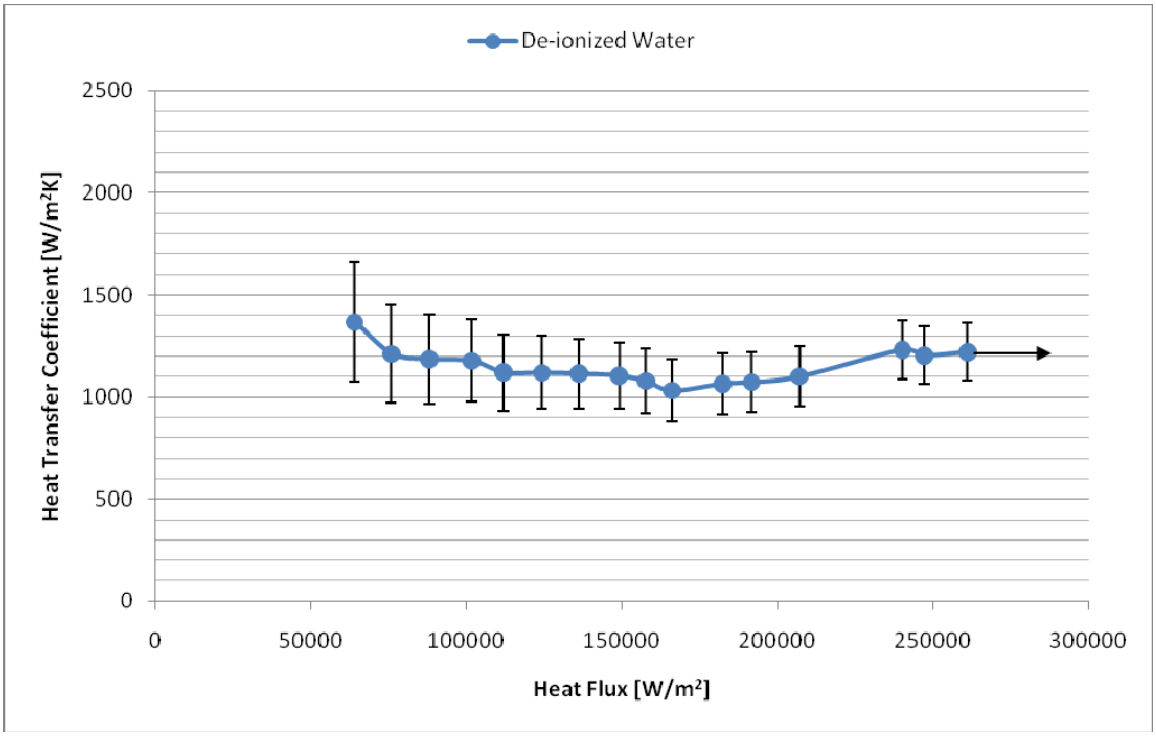

Figure J: Heat Transfer Coefficient De-Ionized Water All Data Points

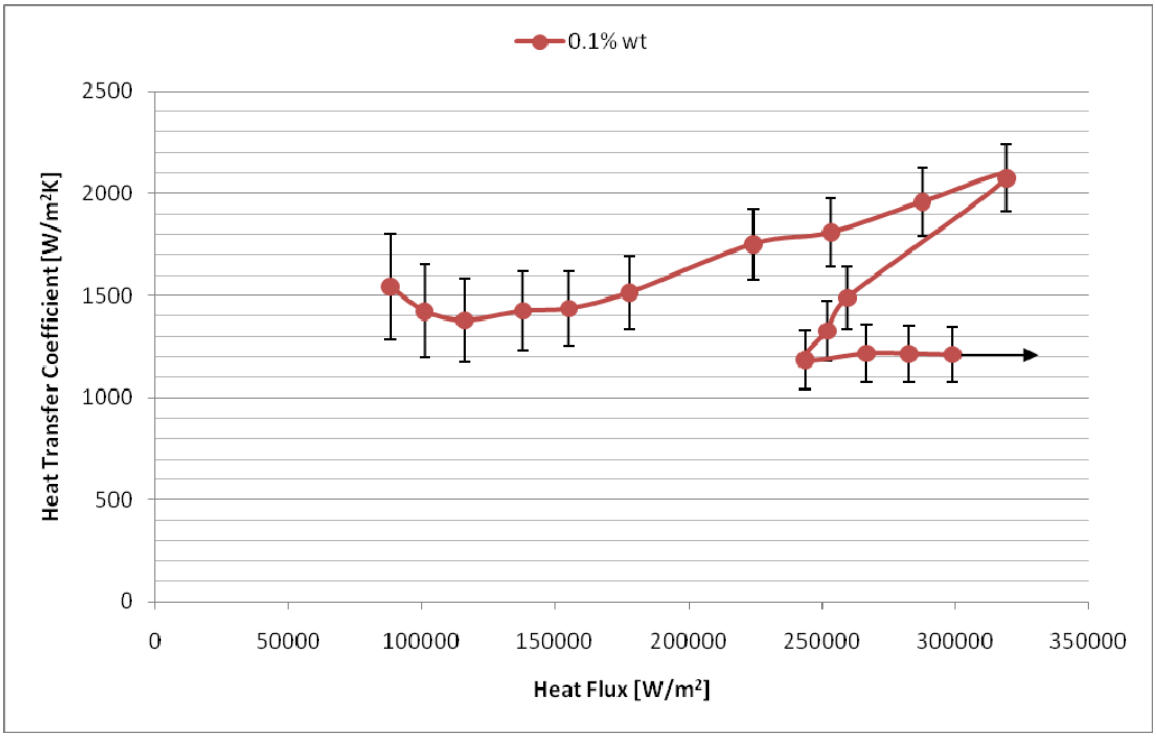

Figure K: Heat Transfer Coefficient 0.1% wt Nanofluid All Data Points

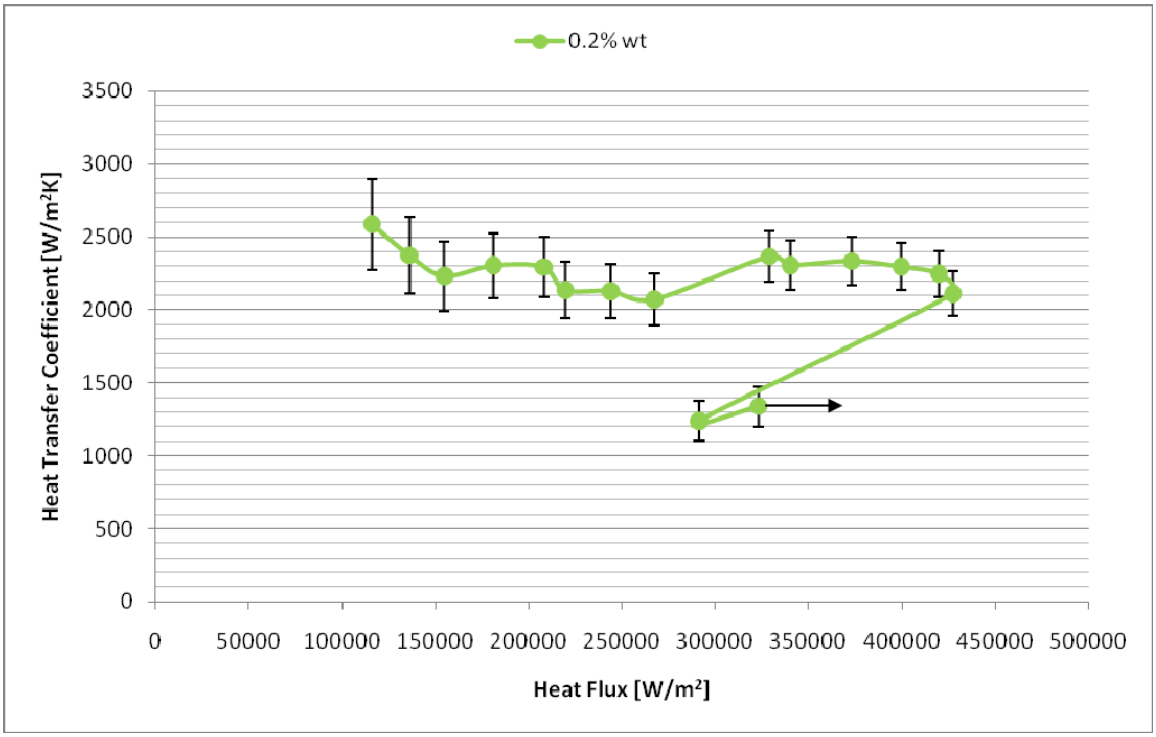

Figure L: Heat Transfer Coefficient 0.2% wt Nanofluid All Data Points

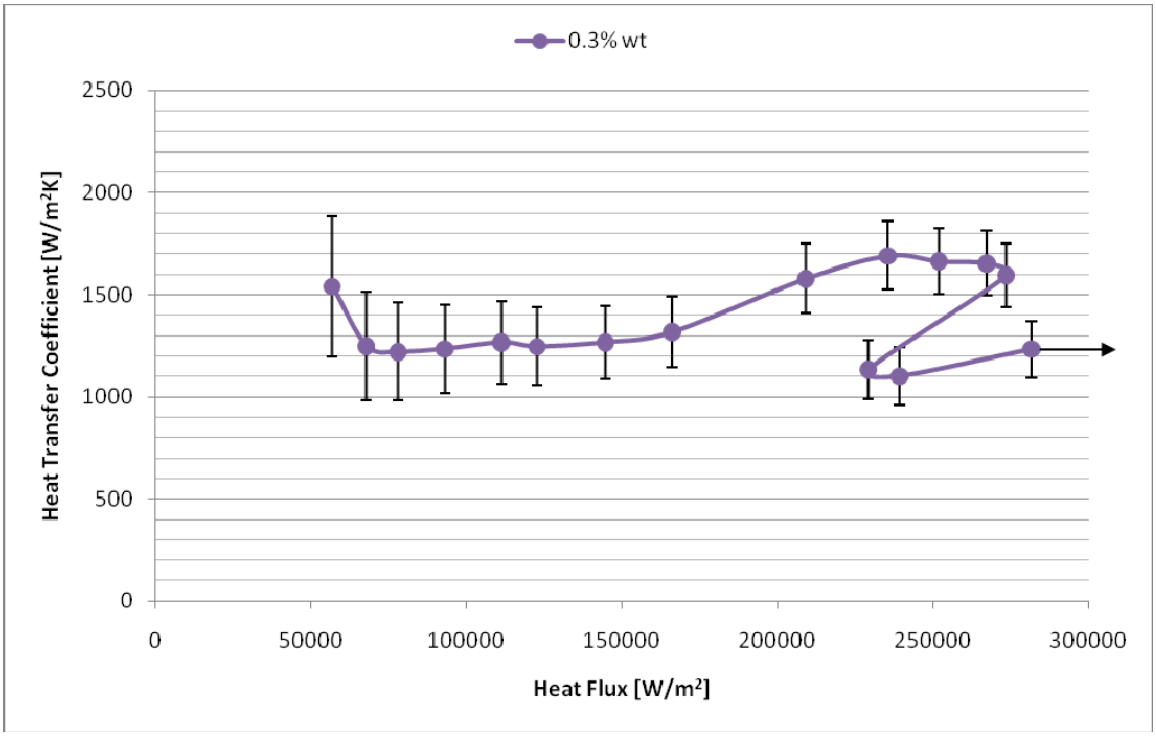

Figure M: Heat Transfer Coefficient 0.3% wt Nanofluid All Data Points

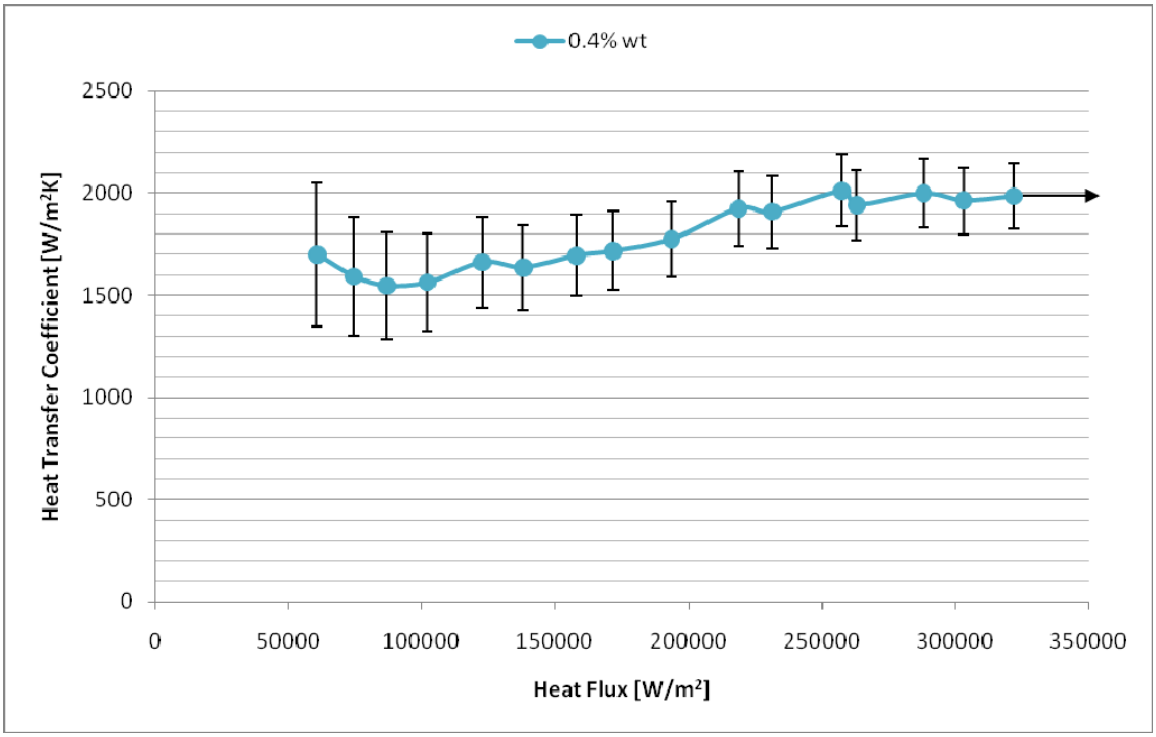

Figure N: Heat Transfer Coefficient 0.4% wt Nanofluid All Data Points